Effects of Nonnormality on Turing-Like Pattern Formation

Muolo, Riccardo

Link to publication

Università degli Studi di Firenze

DEPARTMENT OF MATHEMATICS AND COMPUTER SCIENCE "ULISSE DINI"
School of Mathematical, Physical and Natural Sciences

MASTER DEGREE IN APPLIED MATHEMATICS
CORSO DI LAUREA MAGISTRALE IN MATEMATICA, CURRICULUM APPLICATIVO

Effects of Nonnormality on Turing-Like Pattern Formation

Effetti della Nonnormalità nella Formazione di "Patterns" à la Turing

Candidate:
Riccardo Muolo

Supervisor:
Prof. Timoteo Carletti

Co-Supervisors:
Prof. Duccio Fanelli
Dr. Malbor Asllani

Academic Year 2016-2017

Acknowledgements

My first acknowledgement goes to **Professor Timoteo Carletti** and **Professor Duccio Fanelli**, for making possible my research experience in Namur, for the time they have dedicated supervising me, for their many suggestions and their patience. Also I would like to acknowledge **Doctor Malbor Asllani** for the time he has spent teaching me how to program in Matlab, for hosting me into his office and for the many feedback and encouragements he gave me during the work. From Professor Carletti, Doctor Asllani and Professor Fanelli I have learned a lot; to them go my biggest thanks and all my gratitude.

I would like to thank **Universidad de Granada** and **Université de Namur** for having me as an Erasmus student and the Erasmus Office of the Faculty of Science of Università di Firenze, in particular **Camilla Cosi**, **Professor Anna Maria Papini** and **Professor Angiolo Farina**; thanks to the **European Union** and to the **Erasmus Main Office** of Università di Firenze for funding my two Erasmus semesters and to the **Department of Mathematics** of Université de Namur for funding my conferences.
Also thanks to the secretaries of Mathematics, in particular to **Elisabetta Salvestrini**, who was always kind and helpful with all my administrative issues; thanks to all my professors in Firenze and Granada, in particular to **Professor Luigi Barletti**, **Professor María José Gálvez Ruiz** and **Professor Stefania Bellavia** for the extra tutoring time.

Finally I would like to thank the many friends I have had in Firenze, Granada and Namur for making these two and a half years special. In particular **my friends at Dini**: I thank you for all the great time we have spent together; getting to know you has been one of the highlights of this journey and I will always carry you in my memories wherever I will go.

Last but not least, I thank my family, in particular my grandparents **Aura** and **Luciano** and my parents **Roberta** and **Cesare**, for all they have done for me.

Contents

Abstract (in Italian)

Nel 1952 il matematico britannico Alan Turing descrisse il processo di instabilità responsabile della formazione spontanea di motivi regolari, o "patterns", in modelli di reazione e diffusione, sistemi spazialmente estesi i cui costituenti elementari possono interagire localmente e diffondere nel dominio nel quale sono confinati. Il meccanismo di formazione dei patterns, noto come instabilità di Turing, risiede nella perturbazione non omogenea di un punto fisso omogeneo e stabile che, sotto certe condizioni, dette condizioni di Turing, guida il sistema verso una nuova configurazione stazionaria e non omogenea, ovvero un pattern. Il suddetto processo, inizialmente concepito nel campo della morfogenesi, trova applicazione in svariati ambiti disciplinari, dalla chimica delle reazioni oscillanti alla biologia delle popolazioni e, negli ultimi anni, anche in neuroscienze, poiché studiato come processo di dinamica su rete, grazie ad una sua recente estensione su supporto discreto. Nel caso di reti complesse il meccanismo di Turing diventa ancora più interessante in quanto l'operatore di diffusione discreto riflette la topologia del supporto e questo può avere effetti sulla dinamica; per esempio, mentre su rete indiretta le condizioni di Turing sono le stesse del caso su supporto continuo, a meno di effetti di taglia finita dovuti all'operatore di diffusione discreto, su rete diretta la zona di Turing viene estesa rispetto al caso classico.

In questo lavoro di tesi abbiamo esplorato possibili estensioni della teoria di Turing studiando gli effetti sulle dinamiche di reazione e diffusione di matrici nonnormali, ovvero di matrici che non sono diagonalizzabili a mezzo di trasformazioni unitarie. Nel primo capitolo abbiamo introdotto la teoria classica di Turing arrivando alle condizioni per la formazione di patterns, abbiamo svolto delle simulazioni numeriche per il modello del Brussellatore riproducendo risultati già noti in letteratura e abbiamo studiato il caso particolare di un sistema a cui viene applicata una corrente esterna, responsabile di un allargamento della regione di Turing. Nel secondo capitolo abbiamo introdotto il concetto di rete complessa, i principali algoritmi per la generazione di reti e i processi di diffusione su rete; nel terzo capitolo, invece, abbiamo rivisitato la teoria di Turing su rete simmetrica e la sua estensione su rete asimmetrica, riproducendo, sempre relativamente al Brussellatore, dei risultati già noti. Nel quarto capitolo abbiamo introdotto il concetto di nonnormalità e i suoi effetti sulla dinamica lineare, per poi passare al caso nonlineare; lì abbiamo visto che la nonnormalità del sistema è una condizione necessaria per avere instabilità di Turing e che tale nonnormalità è responsabile di un nuovo tipo di patterns à la Turing, ai bordi della regione di Turing, che trascende il meccanismo classico; tali

patterns possono essere sia transienti che stazionari. L'ultima parte di questo lavoro, comprendente i capitoli cinque e sei, contiene i risultati originali del lavoro di tesi. Nel capitolo cinque abbiamo introdotto le reti nonnormali, ovvero reti la cui matrice di adiacenza è nonnormale, e studiato le dinamiche di reazione e diffusione su tale supporto, osservando un'ulteriore estensione della regione di Turing dovuta a questo nuovo meccanismo à la Turing, sia per quanto riguarda i patterns stazionari, che quelli transienti. Sorprendentemente questo allargamento della regione di Turing, causato dalla formazione di patterns à la Turing, non è dovuto ad una maggiore nonnormalità del sistema su rete nonnormale ma, come spieghiamo in dettaglio nel capitolo sei, alla maggiore sensibilità delle matrici nonnormali rispetto alle perturbazioni spettrali.

La teoria da noi sviluppata potrebbe avere applicazioni in ecologia, neuroscienze, epidemiologia e persino in sicurezza informatica, gestione dei trasporti e diffusione delle fake news.

Parole Chiave: "Patterns" di Turing; dinamica su rete; matrici nonnormali.

Introduction

Napoleon: In your book "Exposition du système du monde"
you did not mention the work God, why?
Laplace: Sir, I have not needed that hypothesis

Patterns are ubiquitous in Nature. Just by contemplating any glimpse of Nature, it is clear that we are surrounded by a variety of patterns, forms, colors and shapes. These facts and the impossibility to bear a rational explanation have brought mankind to wonder "who made this?". Of course the answer was to look for a supernatural power. In the XVIII century, the English clergyman William Paley (1743-1805) used an argument in defense of divine creation, that today may appear naif, but for those times was more than enough: if you find a clock in the ground, you can figure by the details and its functioning that someone has to be the creator of it; hence, when you observe the patterns and shapes in Nature, it is obvious that there must be a creator [Girotto et al. 2008]. There were many scientists who did not need an external architect to describe Nature[1], however they were a minority.

Fortunately, at the end of the XIX century and at the beginning of the XX century, took form a new branch of physics that studied systems of small constituents in mutual interaction from a global point of view and a statistical approach, what is now called statistical mechanics [Bellone 2004]. In such studies, collective behavior and self-organization phenomena were predicted theoretically and observed experimentally. Times were mature to understand that Nature itself is capable to conceive regular and organized structures and scientists have to find mathematical and physical laws able to describe such phenomena.

Between the 1940s and the 1950s, biology was starting to become a quantitative science, motivated by the inputs of several mathematicians and physicists, such as the Austrian Erwin Schrödinger (1887-1961) [Schrödinger 1944]. One of the studied topics was that of a growing hembrio in morphogenesis; the idea on how to approach such problem mathematically came from a lonely genius, whose biography is as interesting as his great contributions to modern science: Alan Turing (1912-1954). In his seminal paper *The Chemical Basis of Morphogenesis* [Turing 1952] he proposed that a reaction-diffusion system of two species, in an homogeneous steady state, could become unstable due to diffusion after an inhomogeneous perturbation and such instability would guide the system to another steady state, but inhomo-

---

[1]One example is the French mathematician and physicist Pierre Simone Laplace (1749-1827), as can be understood by the citation at the beginning of the introduction, taken from [Boncinelli 2012].
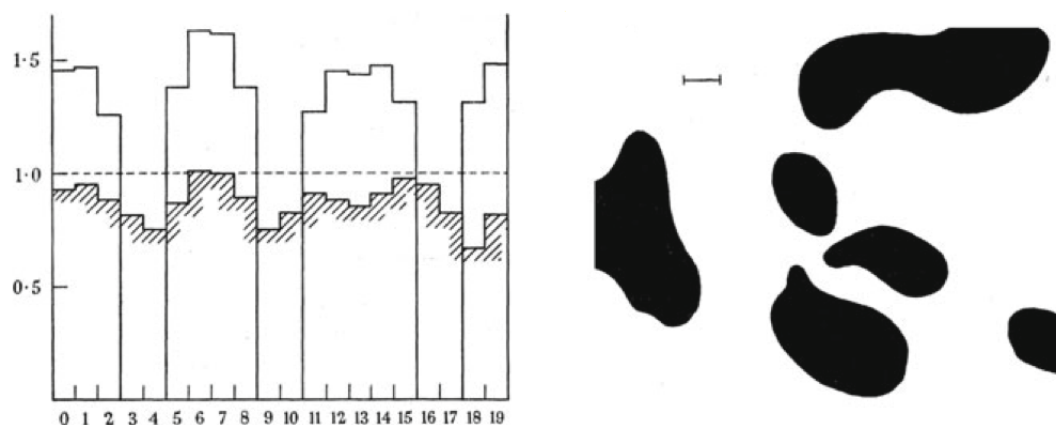
Figure 1: Patterns obtained by Turing himself in his seminal paper [Turing 1952].

geneous, that is a pattern. In figure 1 we show an example of patterns obtained by Turing in his original paper. Such idea of diffusion-driven instability, ingenious but counterintuitive, since the diffusion usually homogenizes a system, is at the base of several studies of pattern formation, particularly in biology [Koch-Meinhardt 1994], but also in many other fields of research [Woolley et al. 2017].

A pattern is a non trivial structure that is spatially extended and stable; however, in popular culture, Turing patterns, i.e., patterns that emerge with Turing's mechanism, are predominantly known for being the best explanation of the animals' coats. One of the first scientists to propose such connection was the mathematician James Murray who showed, in a paper for the common public [Murray 1988], how numerical simulations of Turing patterns were comparable to patterns observed in felines' coats.

Self-organization and Turing instability are enough to explain the variety of patterns and shapes found in Nature? Partially. In Nature we witness much more patterns than those allowed by classical Turing theory. A striking example, which comes from population ecology, where we have a pattern when two or more interacting species coexist in a certain domain, is that of the *plankton paradox* [Hutchinson 1961]: how do we have coexistence between several species of plankton, while, according to the *exclusion principle* [Hardin 1960], they should compete for resources until only one of them survives?

In fact Turing mechanism is a mathematical idealization and it does not explain properly the phenomena observed. Moreover, Turing patterns emerge if the interacting species considered in the process are one activator and one inhibitor and there has to be a significant difference between their diffusion coefficients, fact that is quite difficult to recreate experimentally [Castets et al. 1990]. Therefore, it is fundamental to find less restrictive conditions for Turing instability to arise in reaction-diffusion systems and for such patterns to be robust, meaning that by varying very little the parameters of the model the system should remain in the Turing regime [Maini et al. 2012].

One attempt to broaden the region where to find Turing patterns was to study models with intrinsic noise, i.e., stochastic differential equations. It was shown that, in such case, a system is more likely to allow Turing instability [Biancalani et al. 2010], fact that should reassure us about the validity of the theory, since stochastic phenomena play a role of paramount importance in biology [Murray 1989]. In literature there are many other examples of procedures designed to extend the Turing region: growing domain [Woolley et al. 2017], delay [Maini et al. 2012], external drift [Rovinsky-Menzinger 1992], reactivity with noise [Biancalani et al. 2017] or without noise [Neubert et al. 2002]; this last approach is the one that will be mostly used in this work.

This work, which is structured in six chapters, goes in this direction: the aim is to extend the Turing region and achieve Turing patterns in settings that classical Turing theory would not predict. However, unlike the works we have cited above, we will investigate systems whose support is discrete and modeled through a network, such as neural networks, food webs or metabolic networks, just to make a few examples [Newman 2010]. Turing's theory for reaction-diffusion systems on symmetric networks was first proposed by Othmer and Scriven [Othmer-Scriven 1971] and then by Nakao and Mikhailov [Nakao-Mikhailov 2010]. Later on, such theory was extended by Asllani and colleagues on asymmetric networks [Asllani et al. 2014], where it was shown that, due to the directionality within the spatial support, the Turing region was enlarged. Starting from this last work, we will show that, if the network is not only asymmetric, but also nonnormal, meaning that its adjacency matrix is not diagonalizable by a unitary similarity transformation, one can seed a further extension of the Turing region.

In the first chapter, we will present the basics of Turing theory from his seminal paper [Turing 1952] revised by the mathematician James Murray [Murray 1989]. We will reproduce the calculations leading to Turing instability and show that, for reaction-diffusion systems of two species, patterns can be only stationary. Then, we will perform a numerical study of the Brussellator model [Nicolis- Prigogine 1977] on a one-dimensional lattice ring, first for an isolated system and then for a system subject to an external drift [Rovinsky-Menzinger 1992], showing that, in the latter case, the Turing region is broader.
In Chapter 2, we will introduce mathematically the notion of network, illustrating basic definitions and the main algorithms and methods used to generate networks computationally. Then, we will study the processes of diffusion on discrete support, introducing the discrete Laplacian, for which some important properties will be presented.
In the third chapter, we will review the Turing theory of pattern formation on networks. First, we will reproduce the calculations of the work by Nakao and Mikhailov [Nakao-Mikhailov 2010] and perform some numerical simulations for the Brussellator. We will show that the Turing instability region is, analytically, equivalent to the case on continuum support; however, due to the discreteness of the diffusion operator, we may have situations in which the Turing region is narrower for

networked reaction-diffusion systems. Then, we will change the topology of the support, studying systems on directed networks, i.e., networks whose adjacency matrix is asymmetric. We will obtain that, for certain directed networks, the Turing region is remarkably enlarged [Asllani et al. 2014]. Moreover, in such settings we may find Turing wave patterns, that cannot emerge for reaction-diffusion systems of two species on continuum support or undirected networks.

In the fourth chapter, we will introduce the concept of nonnormality [Trefethen-Embree 2005] through the definition of nonnormal matrix, that is a matrix which cannot be diagonalized by a unitary similarity transformation, i.e., its eigenvectors are not orthogonal. We will review the effects of nonnormality on linear dynamics, that is a transient growth before decaying if the matrix is stable but its Hermitian part is unstable. Then we will study its effects on nonlinear dynamics and Turing pattern formation, following the work of Neubert and colleagues [Neubert et al. 2002], where it is shown that nonnormality is necessary to obtain Turing patterns; hence the models studied must be intrinsically nonnormal. Moreover, we will observe that transient Turing-like patterns, predicted in the latter work, may stabilize when the system is networked and the nonnormality is significant. However, we will argue that the setting in which such new patterns emerge, may not be suitable for applications.

In Chapter 5, we will present nonnormal networks, that are networks whose adjacency matrix is nonnormal, and show intuitively their effects on linear dynamics, intuition that is the core of an algorithm through which nonnormal networks can be generated. Then, we will study reaction-diffusion systems on such networks and observe that they yield Turing-like patterns in a setting that may be interesting for applications. Moreover, the Turing region is enlarged as the nonnormality of the networks increases. Our new results, which are a straightforward extension of the work on directed networks, may find application in many disciplinary fields, such as neuroscience or epidemiology, but also in, cybersecurity and the spreading of fake news, just to make a few examples.

Lastly, in the sixth chapter, we will introduce the notion of pseudospectrum [Trefethen-Embree 2005], which constitutes a fundamental theoretical tools to explain our numerical results. In fact, nonnormal matrices are more sensible to spectral perturbations if compared to their normal analogous, hence, the pseudospectrum, or perturbed spectrum, of a nonnormal matrix is bigger the more nonnormal is the matrix; in this manner, a system that should not go unstable after a perturbation, i.e., we would not have Turing patterns, may still reach the unstable state due to the degree of underlying nonnormality, which is the result of the intrinsic nonnormality of the model and the nonnormality of the network.

1 Turing Theory on Continuum Support

In 1952 the British mathematician and war hero Alan Turing, see figures 1.1, published a paper on "Philosophical Transactions of the Royal Society of London" titled *The chemical basis of Morphogenesis* [Turing 1952] in which for the first time a real progress was made in the understanding of a complex biological phenomenon from a quantitative point of view. Turing's idea, as we will see soon, is the following: we start with a reaction-diffusion system involving at least two species with different diffusion coefficients, admitting a stable homogeneous state; under certain conditions, that we will determine analytically later on, if such state is perturbed inhomogeneously, the system leaves the initial stable equilibrium, which turns thus to be unstable, and reaches a new inhomogeneous state, i.e., patterns are formed. The value of this pioneering work was not completely understood at that time, as for most of Turing's works, among which we can cite the *Turing Test*, the *Turing Machine* and the solutions of the *Entscheidungsproblem* just for what regards theoretical computer science [Hodges 1986]. About two decades later, when the study of oscillating chemical reaction[1], which can be cast in the formalism proposed by Turing, gained interest, Turing's work was re-discovered and it earned the respect it deserves.

Up to today, Turing mechanism of patterns formation has a wide range of applications from chemistry [Lengyel-Epstein 1992], [Lengyel-Epstein 1993], to biology [Economou et al. 2012], [Kondo-Miura 2010], to neuroscience [Bressloff et al. 2002] and even in social sciences [Helbing 2009], just to make some examples.
In this chapter we will go through Turing theory, reformulated in a more modern way, up to the conditions under which Turing instability arises. Then we will test numerically our theoretical results with a model, the Brussellator, which schematizes a chemical reaction. At the end we will study a well know phenomenon, that is the enlargement of the Turing instability region when the systems is subject to an external drift [Rovinsky-Menzinger 1992]; however, we have reformulated it in an original way, which allows us to compare the results with the ones obtained in the case without drift.

---

[1]The most famous and studied among the oscillating reaction is the Belousov-Zhabotinsky reaction [Murray 1989], which can yield Turing patterns, as shown in figure 1.2.

Figure 1.1: Left: Alan Turing (1912-1954), *alanturing.net.* Right: Statue of Alan Turing at Bletchley Park, *wikimedia.org.*
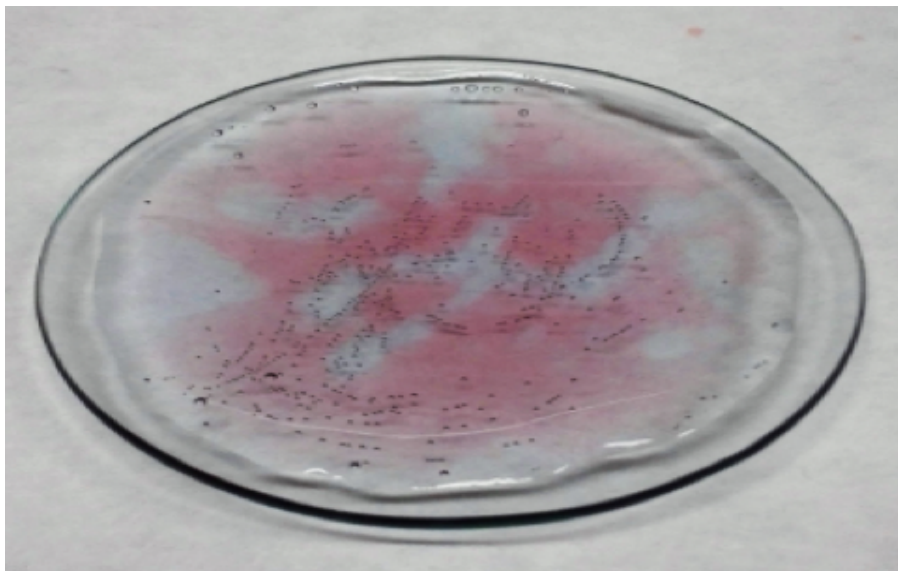

Figure 1.2: Turing Patterns obtained experimentally for the Belousov-Zhabotinsky reaction: sulfuric acid $[H_2SO_4]$, malonic acid $[CH_2(COOH)_2]$, potassium bromate $[KBrO_3]$, cerium(IV) sulfate $[Ce(SO_4)_2]$ and ferroin $[C_{36}H_{24}FeN_6^{2+}]$, [López-Muolo 2016].

1.1 Classical Turing Instability

Let us consider a system of parabolic PDEs describing a two species reaction-diffusion system[2], i.e., a system of diffusion equations with a source/sink term describing the interactions between two species

$$
\begin{cases}
\dfrac{\partial}{\partial t}\varphi(\underline{x},t) = f(\varphi,\psi) + D_\varphi \nabla^2 \varphi(\underline{x},t) \\[2mm]
\dfrac{\partial}{\partial t}\psi(\underline{x},t) = g(\varphi,\psi) + D_\psi \nabla^2 \psi(\underline{x},t)
\end{cases}
\quad \text{with} \quad
\begin{cases}
\underline{x} \in \Omega \subseteq \mathbb{R}^n \\
t \in \mathbb{R}^+
\end{cases}
\tag{1.1}
$$

where $\Omega \neq \emptyset$ is an open subset of $\mathbb{R}^n$ bounded by a smooth surface Σ, $\varphi, \psi : \Omega \times \mathbb{R}^+ \to \mathbb{R}^+$ are the species concentrations[3], $f, g : \mathbb{R}^+ \times \mathbb{R}^+ \to \mathbb{R}$ are **nonlinear** functions, that are at least C^2, describing the reaction dynamics and $D_\varphi, D_\psi \in \mathbb{R}^+$ are the *diffusion coefficients*[4].

Remark   For the theory developed in this chapter, the minimum requirement for f and g is to be C^1, in light of the fact that we will need to perform a linear analysis and compute the Jacobian matrix, in which appear the first derivatives. However, in the last chapter, we will need a nonlinear analysis up to the second order, meaning that we will compute the Hessian matrices of f and g, which we will need to be C^2. Hence, we will assume f, g to be C^2 from the beginning.

In general, but not always, such systems are studied with periodic boundary conditions (as we will see in the next section) or with Neumann's boundary conditions, i.e., the system is isolated, which are expressed as

$$
\begin{cases}
\hat{n} \cdot \underline{\nabla}\varphi(\underline{x},t) = 0 \\
\hat{n} \cdot \underline{\nabla}\psi(\underline{x},t) = 0
\end{cases}
$$

where $\hat{n}$ stands for the unit vector orthogonal the smooth surface Σ which bounds the domain Ω.

Remark   The power of this approach, as for most of applied mathematics, relies in its universality: in fact system (1.1) can describe the interactions between chemical reactants, healthy and infected individuals in a epidemiological model, as well as animals competing to survive in an ecological model.

As we have already said, Turing's idea is to start from an homogeneous stable fixed point and then to introduce a small and spatially inhomogeneous perturbation, so that a spontaneous instability arises (symmetry breaking), which asymptotically

---

[2]The derivation of such equations can be found in Appendix A

[3]The concentrations should have their unity measures, namely $[mol/V]$ using the International System. However, throughout this work we will not use unity measures.

[4]Regarding the unity measures, $[m^2/s]$, see the previous note.

results in a stationary and spatially inhomogeneous pattern. Using a terminology that comes from ecology, we will denote with φ the activator species' concentration and with ψ the inhibitor's one. Before determining the calculations that lead to the conditions of existence of such patterns, let us illustrate the physics of the process by using a descriptive, though qualitative, example conceived by the mathematician James Murray in [Murray 1989]:

> "*Consider a field of dry grass in which there is a large number of grasshoppers which can generate a lot of moisture by sweating if they get warm. Now suppose the grass is set alight at some point and a flame front starts to propagate. We can think of the grasshopper as an inhibitor and the fire as an activator. If there were no moisture to quench the flames the fire would simply spread over the whole field which would result in a uniform charred area. Suppose, however, that when the grasshoppers get warm enough they can generate enough moisture to dampen the grass so that when the flames reach such a pre-moistened area the grass will not burn. The scenario for spatial pattern is then as follows. The fire starts to spread-it is one of the reactants, the activator, with a diffusion coefficient Df say. When the grasshoppers, the inhibitor reactant, ahead of the flame front feel it coming they move quickly well ahead of it; that is, they have a diffusion coefficient, Dg say, which is much larger than Df. The grasshoppers then sweat profusely and generate enough moisture to prevent the fire spreading into the moistened area. In this way the charred area is restricted to a finite domain which depends on the diffusion coefficients of the reactants-fire and grasshoppers-and various reaction parameters. If, instead of a single initial fire, there were a random scattering of them we can see how this process would result in a final spatially heterogeneous steady state distribution of charred and uncharred regions in the field and a spatial distribution of grasshoppers, since around each fire the above scenario would take place. If the grasshoppers and flame front diffused at the same speed no such spatial pattern could evolve.*"

As Murray clearly explains, a necessary condition to observe such patterns is that the inhibitor (for us ψ) diffuses faster than the activator (for us φ); we will see the mathematical proof of such condition at the end of this section.

Let us return to the formal approach and let us consider a homogeneous (i.e., spatially constant) solution (φ^*, ψ^*), so that

$$\nabla^2 \varphi^* = \nabla^2 \psi^* = 0$$

and let us assume that is a fixed point for the nonspatial system

$$\exists (\varphi^*, \psi^*) \text{ s.t. } \begin{cases} \dot{\varphi}(t) = f(\varphi^*, \psi^*) = 0 \\ \dot{\psi}(t) = g(\varphi^*, \psi^*) = 0 \end{cases}$$

Let us define the Jacobian matrix of the system in the fixed point

$$J_0 = \begin{bmatrix} f_\varphi & f_\psi \\ g_\varphi & g_\psi \end{bmatrix}$$

where we have used for the partial derivatives the following notation

$$f_\varphi = \left.\frac{\partial f}{\partial \varphi}\right|_{(\varphi,\psi)=(\varphi^*,\psi^*)}$$

It is known[5] that the fixed point is stable if and only if

$$tr J_0 < 0, \text{ i.e., } f_\varphi + g_\psi < 0 \tag{1.2}$$

$$det J_0 > 0, \text{ i.e., } f_\varphi g_\psi - g_\varphi f_\psi > 0 \tag{1.3}$$

If such conditions stand and we do not perturb the system, it will perpetrate in its equilibrium state.

Now, let us perturb our system lying in the steady state with a spatially inhomogeneous perturbation

$$\begin{cases} \varphi(\underline{x},t) = \varphi^* + \delta\varphi(\underline{x},t) \\ \psi(\underline{x},t) = \psi^* + \delta\psi(\underline{x},t) \end{cases}$$

We are interested in linear stability analysis because it allows us to determine the local behavior of nonlinear systems, as we explain in details in Appendix B. Therefore, let us perform a Taylor expansion of f, g close to the fixed point, halting at the first order, to obtain

$$\begin{cases} f(\varphi^* + \delta\varphi, \psi^* + \delta\psi) \simeq f(\varphi^*, \psi^*) + \left.\frac{\partial f}{\partial \varphi}\right|_{(\varphi^*,\psi^*)} \delta\varphi + \left.\frac{\partial f}{\partial \psi}\right|_{(\varphi^*,\psi^*)} \delta\psi \\ \\ g(\varphi^* + \delta\varphi, \psi^* + \delta\psi) \simeq g(\varphi^*, \psi^*) + \left.\frac{\partial g}{\partial \varphi}\right|_{(\varphi^*,\psi^*)} \delta\varphi + \left.\frac{\partial g}{\partial \psi}\right|_{(\varphi^*,\psi^*)} \delta\psi \end{cases}$$

Hence, for what we have stated previously

$$\begin{cases} f(\varphi^* + \delta\varphi, \psi^* + \delta\psi) = f_\varphi \delta\varphi + f_\psi \delta\psi \\ g(\varphi^* + \delta\varphi, \psi^* + \delta\psi) = g_\varphi \delta\varphi + g_\psi \delta\psi \end{cases}$$

and the system of equations becomes

$$\begin{cases} \dfrac{\partial}{\partial t}\delta\varphi = f_\varphi \delta\varphi + f_\psi \delta\psi + D_\varphi \nabla^2 \delta\varphi \\ \\ \dfrac{\partial}{\partial t}\delta\psi = g_\varphi \delta\varphi + g_\psi \delta\psi + D_\psi \nabla^2 \delta\psi \end{cases}$$

---

[5]For further details see Appendix B and [Strogatz 1994].

Now, defining $\underline{\mu} = \begin{bmatrix} \delta\varphi \\ \delta\psi \end{bmatrix}$ **perturbation vector**, $D = \begin{bmatrix} D_\varphi & 0 \\ 0 & D_\psi \end{bmatrix}$ **diffusion matrix** and J_0 as previously, we can rewrite our system in a compact form

$$\dot{\underline{\mu}} = J_0\underline{\mu} + D\nabla^2\underline{\mu}. \tag{1.4}$$

This last equation describes the evolving of the perturbation $\underline{\mu}$ in the linear regime, i.e., for small t.

There are two equivalent ways to solve system (1.4): we could perform the Fourier transform and work in the conjugate space, or we could expand the perturbation on the orthornormal base generated by the Laplacian's eigenfunctions. We will go with the first method, leaving the latter in a further section when we will study reaction diffusion systems on a network.
Let us Fourier transform system (1.4) to obtain

$$\frac{\partial}{\partial t}\underline{\mu_k} = J_0\underline{\mu_k} - k^2 D\underline{\mu_k} \tag{1.5}$$

where k stands for the wave number's modulus in the conjugate space[6].

Introducing the **extendend Jacobian** matrix[7]

$$\tilde{J}(k) = \tilde{J} = J_0 - k^2 D = \begin{bmatrix} f_\varphi - k^2 D_\varphi & f_\psi \\ g_\varphi & g_\psi - k^2 D_\psi \end{bmatrix}$$

our system becomes

$$\frac{\partial}{\partial t}\underline{\mu_k} = \tilde{J}\underline{\mu_k} \tag{1.6}$$

Remark Let us observe that if we set $k = 0$ we obtain J_0, which describes the homogeneous (hence nonspatial) system, the mode $k = 0$ being associated to the spatial average state.

The system (1.6) is linear and its solutions are exponential whose growth (or decay) rate is determined by $\tilde{J}$'s eigenvalues $\lambda_1(k)$ and $\lambda_2(k)$. Namely, the system will be unstable after the inhomogeneous perturbation if and only if $max\{\Re(\lambda_1), \Re(\lambda_2)\} > 0$ for some $k \in \mathbb{R}$ [8]; if such condition is not satisfied, we will not observe an instability. In fig 1.3 (b) we can observe the discrimination between

---

[6]The $-k^2$ comes out from one of Fourier Transform's properties, namely $FT\{\frac{d^n f(x)}{dx^n}\}(k) = (ik)^n FT\{f(x)\}(k)$; for us $n = 2$.

[7]The extended Jacobian matrix for continuous spatial systems may be indicated as $\tilde{J}_k$ or simply J_k to distinguish it from the one related to networked systems that we will see in the next chapter, namely $\tilde{J}_\alpha$; we will stick to $\tilde{J}$ for both cases unless there might be ambiguity.

[8]Let us point out that the values of k are discrete, since we are studying a system with boundary conditions; we say that the set of possible k is a countably infinite set.

these two cases, varying with $d = \frac{D_\psi}{D_\varphi}$: if $d > d_c$, there exists a finite interval of k^2 for which $\Re(\lambda) > 0$, therefore the corresponding modes will activate guiding the exponential instability.

Thus, let us compute $\tilde{J}$'s eigenvalues

$$
\begin{aligned}
det(\tilde{J} - \lambda I) = 0 &\Leftrightarrow \lambda^2 - tr\tilde{J}\lambda + det\tilde{J} = 0 \\
\Longleftrightarrow \quad &\lambda^2 + (f_\varphi + g_\psi - k^2 D_\varphi - k^2 D_\psi)\lambda + [(f_\varphi - k^2 D_\varphi)(g_\psi - k^2 D_\psi) - f_\psi g_\varphi] = 0 \\
\Longleftrightarrow \quad &\lambda^2 - (tr J_0 - [D_\varphi + D_\psi]k^2)\lambda + D_\varphi D_\psi k^4 - k^2(D_\varphi g_\psi + D_\psi f_\varphi) + det J_0 = 0
\end{aligned}
$$

Defining
$$
h(k^2) = D_\varphi D_\psi k^4 - k^2(D_\varphi g_\psi + D_\psi f_\varphi) + det J_0
$$

we have at last

$$
\lambda_{1,2} = \frac{1}{2}\left\{ (tr J_0 - [D_\varphi + D_\psi]k^2) \pm \left[(tr J_0 - [D_\varphi + D_\psi]k^2)^2 - 4h(k^2) \right]^{\frac{1}{2}} \right\} \qquad (1.7)
$$

So, for what already discussed, if we want to observe an instability, we have to impose the conditions such that $max\{\Re(\lambda_1), \Re(\lambda_2)\} > 0$.

Looking at equation (1.7), being that $(tr J_0 - [D_\varphi + D_\psi]k^2) < 0$, we can assert that the smallest root, i.e., the one with the minus sign in front of the square root term, will be surely negative and thus we can neglect it; hence to have instability we must impose the condition $h(k^2) < 0$. Moreover we cannot have oscillatory instability, as the term under square root has to be positive[9]; we will see in Chapter 3 that the topology of the spatial support can, in certain cases, lead to oscillatory patterns for two species reaction-diffusion systems.

Hence, we have that

$$
max\{\Re(\lambda_1), \Re(\lambda_2)\} > 0 \Longleftrightarrow h(k^2) < 0
$$

Being that $D_\varphi D_\psi > 0$, $h(k^2) = 0$ is a parabola in k^2 with upward concavity, hence, in order to have $h(k^2) < 0$ for at least a finite interval of k^2, it is sufficient imposing to its minimum to be negative, as we can notice from figure 1.3.
Let $y = k^2$, thus we have

$$
D_\varphi D_\psi y^2 - (D_\varphi g_\psi + D_\psi f_\varphi)y + det J_0 = 0.
$$

whose minimum is placed in $y = y_{min}$ s.t.

$$
y_{min} = \frac{D_\varphi g_\psi + D_\psi f_\varphi}{D_\varphi D_\psi} = k^2_{min} > 0.
$$

Since the denominator is positive, we have to impose the following condition

$$
D_\varphi g_\psi + D_\psi f_\varphi > 0 \qquad (1.8)
$$
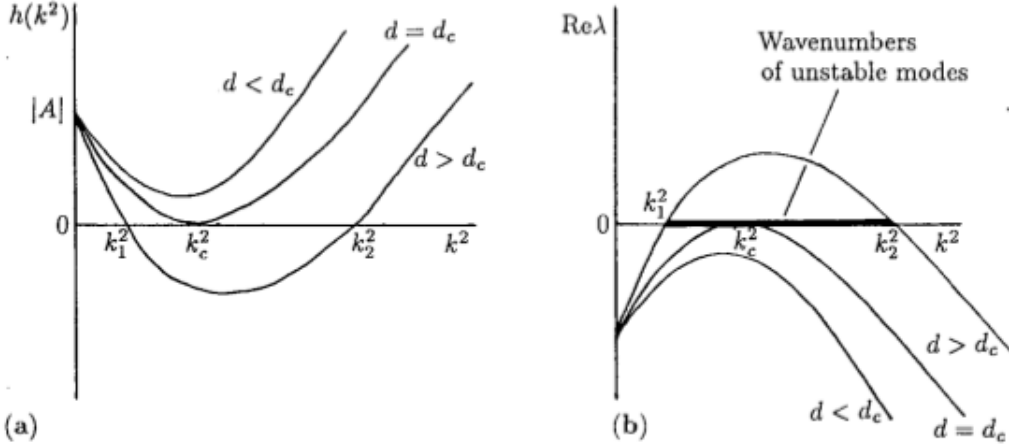
Figure 1.3: When $h(k^2) < 0$ (a) we have that $\Re(\lambda) > 0$ (b), here $d = \frac{D_\psi}{D_\varphi}$, [Murray 1989]

Now let us substitute $y_{min} = k_{min}^2$ in $h(k^2)$ and impose the negativity

$$h_{k_{min}^2} = D_\varphi D_\psi \frac{(D_\varphi g_\psi + D_\psi f_\varphi)^2}{4D_\varphi^2 D_\psi^2} - \frac{(D_\varphi g_\psi + D_\psi f_\varphi)^2}{2D_\varphi D_\psi} + det J_0 < 0$$

After some calculations and with the explicit form of $det J_0$, we obtain our last condition

$$(f_\varphi g_\psi - f_\psi g_\varphi) - \frac{1}{4} \frac{(D_\varphi g_\psi + D_\psi f_\varphi)^2}{D_\varphi D_\psi} < 0 \tag{1.9}$$

To conclude, we have found four conditions. The first two (1.2 and 1.3) to have a stable fixed point, while the others (1.8 and 1.9) to have an unstable state after a spatially inhomogeneous perturbation, i.e., we have proved the following theorem:

Theorem (Turing Instability) The following conditions are necessary and sufficient for the raising of Turing Istability from a homogeneous stable fixed point when inhomogeneously perturbed

$$\begin{cases} f_\varphi + g_\psi < 0 & \text{I} \\ f_\varphi g_\psi - f_\psi g_\varphi > 0 & \text{II} \\ D_\varphi g_\psi + D_\psi f_\varphi > 0 & \text{III} \\ (f_\varphi g_\psi - f_\psi g_\varphi) - \frac{1}{4} \frac{(D_\varphi g_\psi + D_\psi f_\varphi)^2}{D_\varphi D_\psi} < 0 & \text{IV} \end{cases} \tag{1.10}$$

As a last thing, we can prove the fact qualitatively explained by Murray, in the form of a corollary.

---

[9]However we can have oscillations that lead the system back to its equilibrium point, thus having a *stable spiral* phase portrait (figure B4 in Appendix B); to observe an oscillatory instability we need at least three interacting species [Zhabotinsky et al. 1995].

Corollary   The raising of Turing Instability, i.e., conditions (1.10), implies that the activator species must diffuse slower than the inhibitor species, namely $D_\varphi < D_\psi$.

Proof   From (1.10 I and III) we have that $f_\varphi g_\psi < 0$. ψ being the inhibitor, we have $g_\psi < 0$, hence $f_\varphi > 0$
From (1.10 I) we obtain that

$$f_\varphi < |g_\psi|$$

At last, from (1.10 III) we can conclude our proof

$$D_\psi f_\varphi > D_\varphi |g_\psi| \Rightarrow D_\psi f_\varphi > D_\varphi |g_\psi| > D_\varphi f_\varphi \implies \frac{D_\psi}{D_\varphi} > 1$$

$$\square$$

Remark   As we will discuss in the next section, in order to have a large instability region in the parameters' space of the model, it is necessary that $D_\psi >> D_\varphi$; this qualitative inequality should actually be in many relevant cases of at least one order of magnitude. Such a setting is quite difficult to reproduce experimentally and might explain the fact that, although Turing Instability was predicted in the '50s, its experimental proof was obtained only several years later [Castets et al. 1990], [Dulos et al. 1996].

1.2   The Brussellator Model

Let us now consider a nonlinear model for reaction and diffusion known as *the Brussellator Model*, a portmanteau of Brussels and oscillator. Such model was proposed by the Nobel Prize laureate Ilya Prigogine while he was working at Université Libre de Bruxelles [Prigogine-Nicolis 1967], [Prigogine-Lefever 1968] and it describes an autocatalytic reaction[10]. There are several microscopic formulations of this model, we will adopt the description used by Boland ad colleagues [Boland et al. 2008]. The model consists of four chemical species, namely Φ, Ψ, X and Y, whose interactions are described by the following chemical equations

$$\begin{cases} X \xrightarrow{a} X + \Phi \\\\ \Phi + Y \xrightarrow{b} \Psi + Y \\\\ 2\Phi + \Psi \xrightarrow{c} 3\Phi \\\\ \Phi \xrightarrow{d} \emptyset \end{cases} \tag{1.11}$$

---
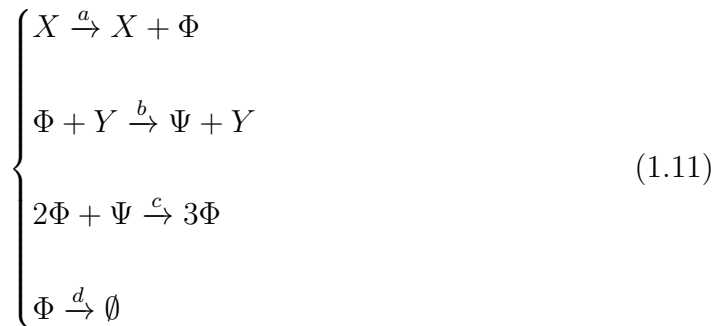
[10]An autocatalytic reaction is a reaction in which the presence of a given reactant acts to increase the rate of its own production; an example is the Belousov-Zhabotinsky reaction.

We can observe that the reactions (1.11) do not alter the number of constituents belonging to species X and Y; such species are called *enzyme activators*.

Let use name φ, ψ, x and y the concentrations of the species Φ, Ψ, X and Y. The reaction dynamics is described by the following ordinary differential equations

$$\begin{cases} \dot{\varphi} = f(\varphi, \psi) = ax - (by + d)\varphi + c\varphi^2\psi \\ \dot{\psi} = g(\varphi, \psi) = by\varphi - c\varphi^2\psi \end{cases}$$

The previous systems may be difficult to menage, however we can discard some variables. First of all, we can set $x = 1$ and $y = 1$, since those concentrations do not change due to the interactions. Moreover, by setting the reaction rates $a = d = 1$, we obtain the Brussellator model used in [Boland et al. 2008], which describes the dynamics of φ and ψ

$$\begin{cases} \dot{\varphi}(t) = f(\varphi(t), \psi(t)) = 1 - (b+1)\varphi(t) + c\varphi^2(t)\psi(t) \\ \dot{\psi}(t) = g(\varphi(t), \psi(t)) = b\varphi(t) - c\varphi^2(t)\psi(t) \end{cases} \tag{1.12}$$

f and g are polynomials, hence they are clearly C^2, as we request in order to develop our theory.

Finally, if we include the diffusion, we obtain the reaction-diffusion Brussellator model

$$\begin{cases} \dfrac{\partial}{\partial t}\varphi(\underline{x}, t) = 1 - (b+1)\varphi(\underline{x}, t) + c\varphi^2(\underline{x}, t)\psi(\underline{x}, t) + D_\varphi \nabla^2 \varphi(\underline{x}, t) \\[4mm] \dfrac{\partial}{\partial t}\psi(\underline{x}, t) = b\varphi(\underline{x}, t) - c\varphi^2(\underline{x}, t)\psi(\underline{x}, t) + D_\psi \nabla^2 \psi(\underline{x}, t) \end{cases} \tag{1.13}$$

where D_φ and D_ψ are the species' diffusion coefficients.

Let us consider the case of one dimensional support with periodic boundary conditions, i.e., $x \in \mathbb{S}^1$ and

$$\begin{cases} \varphi(x + L, t) = \varphi(x, t) \\ \\ \psi(x + L, t) = \psi(x, t) \end{cases} \qquad \begin{cases} \dfrac{\partial}{\partial x}\varphi(x + L, t) = \dfrac{\partial}{\partial x}\varphi(x, t) \\[4mm] \dfrac{\partial}{\partial x}\psi(x + L, t) = \dfrac{\partial}{\partial x}\psi(x, t) \end{cases}$$

where L is the spatial support's length, and let us assume that $D_\psi > D_\varphi$.

Now we can proceed as in the previous section:

- we look for the fixed point (φ^*, ψ^*) by imposing that $f(\varphi^*, \psi^*) = 0$ e $g(\varphi^*, \psi^*) = 0$, i.e.,

$$\begin{cases} 1 - (b+1)\varphi^* + c(\varphi^*)^2\psi^* = 0 \\ b\varphi^* - c(\varphi^*)^2\psi^* = 0 \end{cases}$$

$$\iff \begin{cases} \varphi^* = 1 \\ \psi^* = \frac{b}{c} \end{cases}$$

- we compute the Jacobian matrix J_0 in such fixed point, i.e.,

$$J_0 = \begin{bmatrix} b-1 & c \\ -b & -c \end{bmatrix}$$

- we impose conditions (1.10 I and II) in order to have a stable homogeneous equilibrium, i.e.,

$$\begin{cases} f_\varphi + g_\psi < 0 \\ f_\varphi g_\psi - f_\psi g_\varphi > 0 \end{cases}$$

$$\iff \begin{cases} c > b-1 \\ c > 0 \end{cases} \tag{1.14}$$

- we impose conditions (1.10 III and IV) so that Turing instability arises, i.e.,

$$\begin{cases} D_\varphi g_\psi + D_\psi f_\varphi > 0 \\ (f_\varphi g_\psi - f_\psi g_\varphi) - \dfrac{1}{4}\dfrac{(D_\varphi g_\psi + D_\psi f_\varphi)^2}{D_\varphi D_\psi} < 0 \end{cases}$$

$$\iff \begin{cases} \dfrac{D_\psi}{D_\varphi}(b-1) > c \\[2mm] -\dfrac{1}{4}\dfrac{D_\varphi}{D_\psi}c^2 + c\left[1 + \dfrac{1}{2}(b-1)\right] - \dfrac{1}{4}\dfrac{D_\psi}{D_\varphi}(b-1)^2 < 0 \end{cases} \tag{1.15}$$

Results

In figure 1.4 we show the behavior of φ and ψ for the nonspatial Brussellator when the fixed point is stable, i.e., conditions (1.14) are satisfied. When such conditions are not satisfied, i.e., $c < b-1$, we have a stable limit cycle[11] [Nicolis-Prigogine 1977].

Putting together conditions (1.14) and (1.15) we obtain the Turing's region, showed in red in figure 1.5. We find such region above the curve

$$c = b - 1$$

which gives us the region where the fixed point is stable and below the curve

$$c = \frac{D_\psi}{D_\varphi}(b+1)\left\{ 1 - \sqrt{1 - \frac{(b-1)^2}{(b+1)^2}} \right\}$$

which gives us the region where the stable fixed point becomes unstable after an inhomogeneous perturbation, i.e., where the systems yields Turing instability.

---

[11]A limit cycle is an isolated closed trajectory in the phase space which can be stable, i.e., all the solutions are attracted by it, unstable, i.e., all the solutions are repulsed by it, or metastable, i.e., the inner part attracts (repulses) the solutions while the outer part repulses (attracts) the solutions.
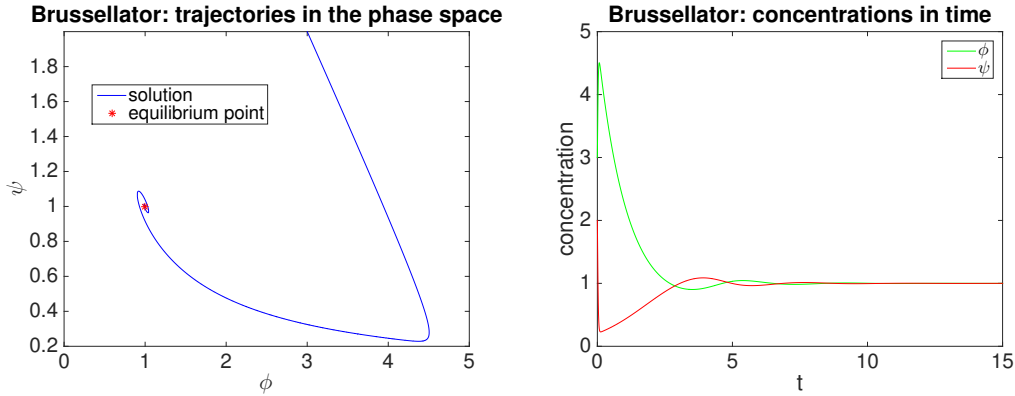
Figure 1.4: On the left we see the solution in the phase space, on the right the solutions in time; b=c=3.

We observe that the latter, that we will call $c = t(b)$, depends on the diffusion coefficients' ratio, while the former does not. We can clearly see in figure 1.6, that as the ratio between D_ψ and D_φ grows, so does Turing's region. Moreover we can notice that, when the diffusion coefficients are equal, we do not have a Turing's region, as we have demonstrated in the previous section.

For the instability to arise it is necessary that $\Re(\lambda) > 0$, as we show in figure 1.7, where we plot the dispersion relations with fixed D_ϕ, D_ψ and c, varying b.

In figures 1.8, 1.9, 1.10 and 1.11 we show the numerical integration[12] of equations (1.13) when we perturb the system with an inhomogeneous perturbation (more details can be found in Appendix C) and we have chosen parameters b and c such that conditions (1.14) and (1.15) are matched. Figures 1.8 and 1.9 show the behavior of the activator species, while figures 1.10 and 1.11 show the behavior of the inhibitor one. For all figures $D_\varphi = 0.07$, $D_\psi = 0.5$ and $b = c = 5$.

Remark   We can recall from the previous section that one of the ways to study the perturbation is to expand it on the basis formed by the Laplacian's eigenvectors, that are sines [Barletti 2013]. In fact, by looking at the spatial profile of the concentrations (left part of figures 1.8 and 1.10), we see that the final patterns have a sine-like shape, whose period is related to the dominant wavenumber k_*, i.e., the wave number such that the dispersion $\Re(\lambda)(k_*^2)$ is maximized.

Turing patterns for reaction-diffusion systems are also studied in 2-dimensional domains, see [Asllani 2015], and even in non-Euclidean geometries to try to reproduce patterns found in nature [Plaza et al. 2004], [Varea et al. 1999], such as felines' tails [Murray 1988] or shells, or even in animal-like shaped surfaces, as displayed in figure 1.12.

---

[12]For all our numerical simulation we have used the explicit fourth order Runge-Kutta method [Press et al. 1986].
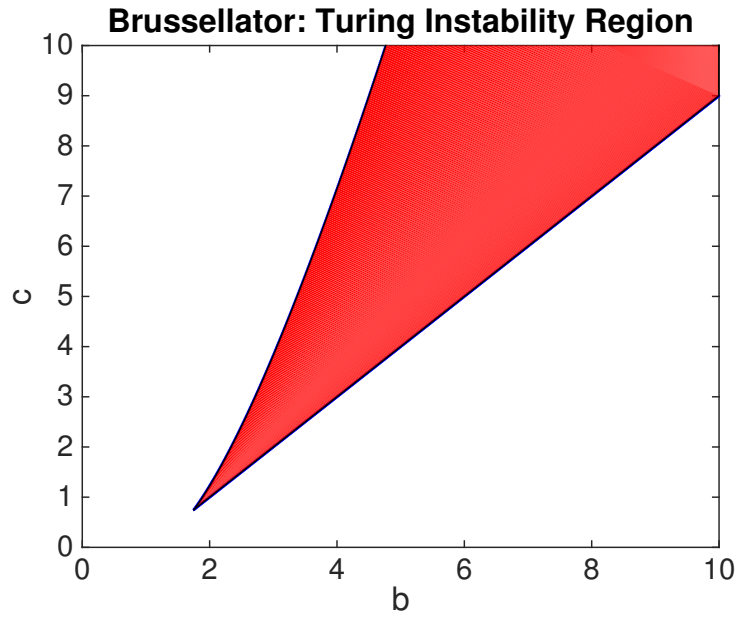
Figure 1.5: When $c > b - 1$ and $c < t(b)$ we have Turing instability; the region where it arises is in red; $D_\varphi = 0.07$, $D_\psi = 0.5$.
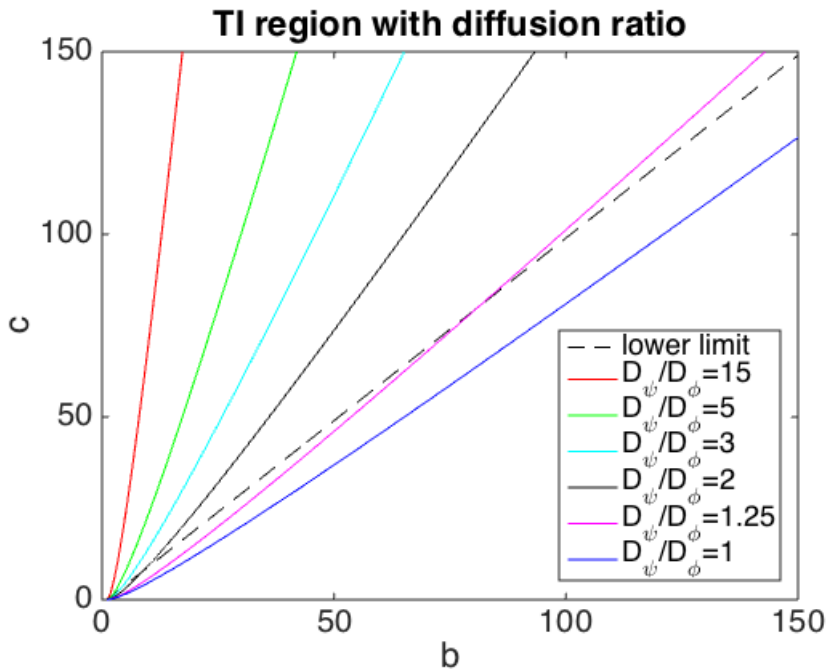
Figure 1.6: Curves $c = t(b)$ vary with the ratio between the diffusion coefficients; the dashed line is $c = b - 1$; we observe that when the ratio between the diffusion coefficients is 1 we do not have a Turing instability region.
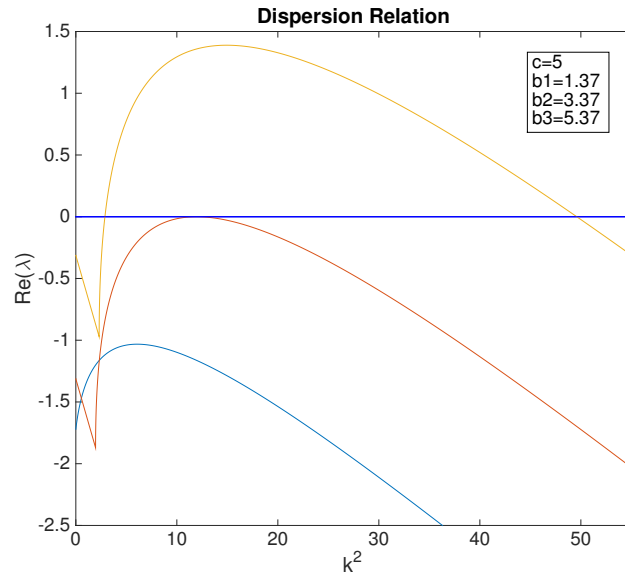
Figure 1.7: Dispersion Relation for the Brussellator model: with reference to figure 1.5, at fixed $c = 5$, $D_\varphi = 0.07$ and $D_\psi = 0.5$, we start outside the Turing Instability region $(b = 1.37)$, to move on the border $(b = 3.37)$ and finally inside the region $(b = 5.37)$.
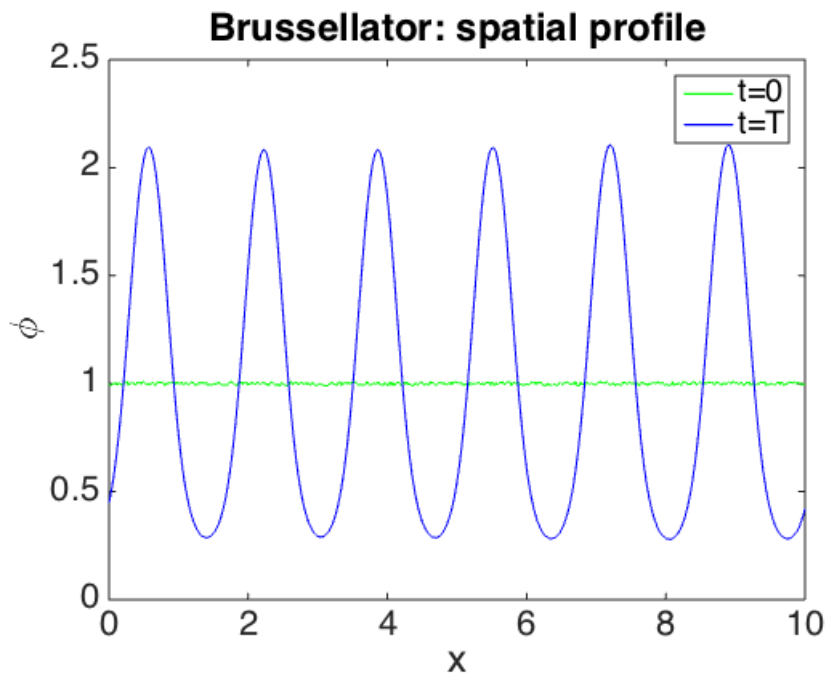
Figure 1.8: Activator species φ; we see the initial perturbation of the steady state $(t = 0)$ and the final spatial pattern $(t = T)$; $D_\varphi = 0.07$, $D_\psi = 0.5$ and $b = c = 5$.
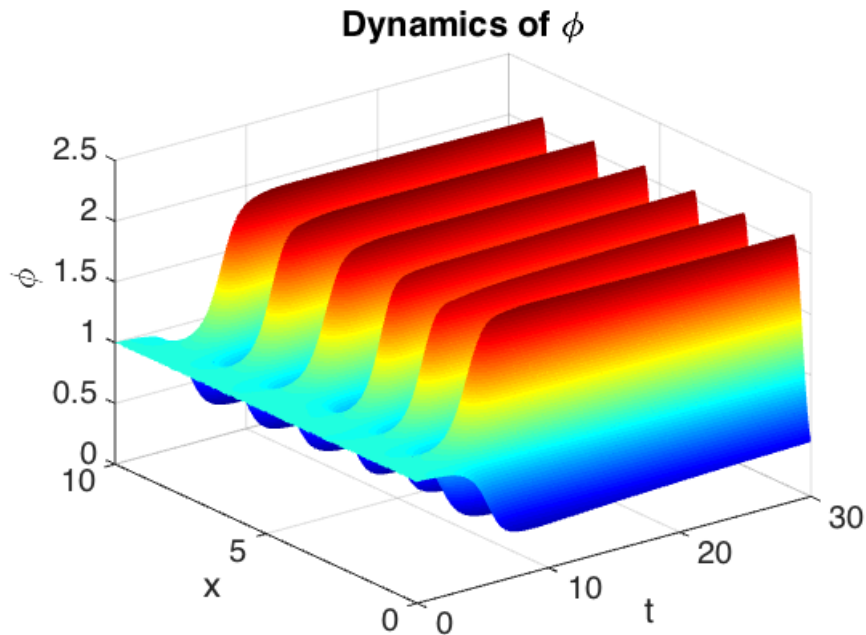
Figure 1.9: Dynamics of φ on a one-dimensional circular domain; we see that after the perturbation the system goes unstable and then stabilizes in a new ihomogeneous equilibrium, i.e., a pattern; $D_\varphi = 0.07$, $D_\psi = 0.5$ and $b = c = 5$.
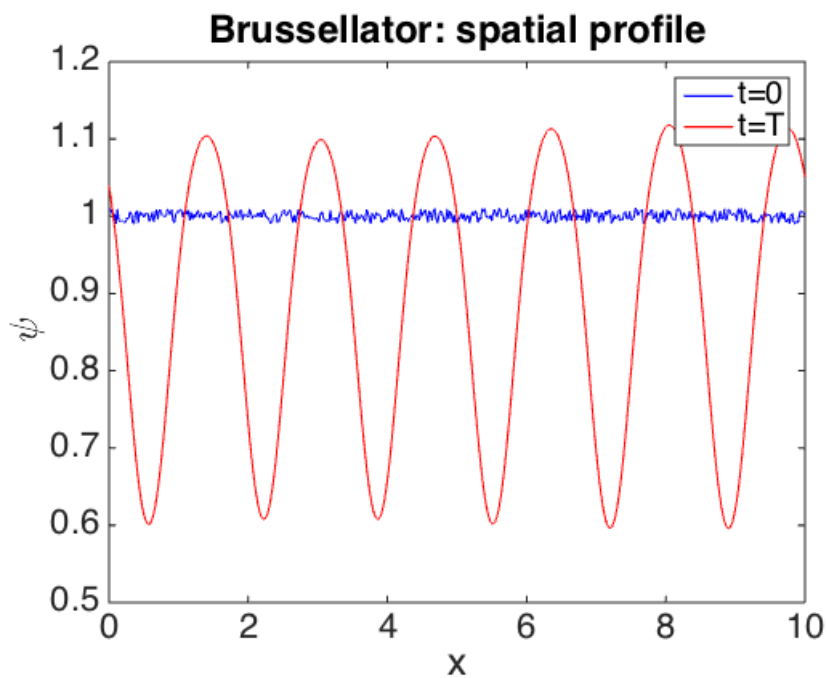
Figure 1.10: Inhibitor species ψ; we see the initial perturbation of the steady state ($t = 0$) and the final spatial pattern ($t = T$); $D_\varphi = 0.07$, $D_\psi = 0.5$ and $b = c = 5$.
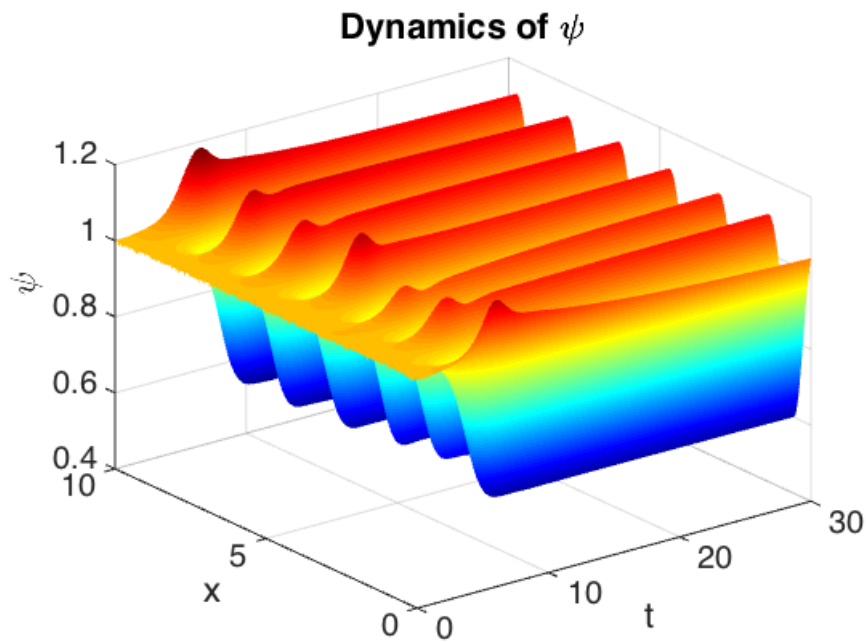
Figure 1.11: Dynamics of ψ on a one-dimensional circular domain; we see that after the perturbation the system goes unstable and then stabilizes in a new ihomogeneous equilibrium, i.e., a pattern; $D_\varphi = 0.07$, $D_\psi = 0.5$ and $b = c = 5$.
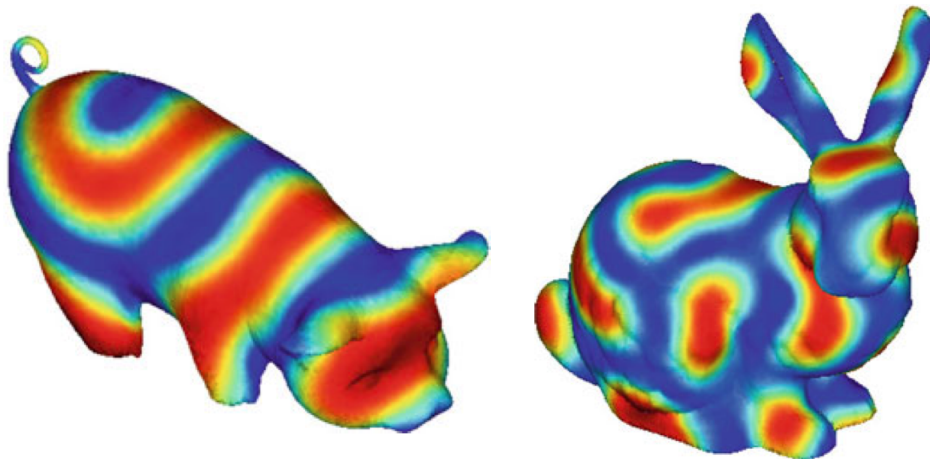
Figure 1.12: Turing patterns obtained numerically for reaction-diffusion systems on animal-like shaped surfaces, respectively a pig on the left and a rabbit on the right; [Macdonald-Ruuth 2009].

1.3 Turing Instability with Drift

In the Introduction, we have manifested the necessity to provide new frameworks in which it is easier to obtain Turing pattern formation. An interesting case is that of the system subject to a drift, that physically may arise, for example, due to an external electric field. In such case, the microscopic constituents of the system will have a certain velocity, which we will assume constant, in the given domain. We will see that, if different species are affected differently by the source of the drift, the Turing region is enlarged.

Therefore, let us now consider the following reaction diffusion system, analogous to that seen in the previous section, but subject to a drift

$$
\begin{cases}
\dfrac{\partial}{\partial t}\varphi(\underline{x},t) = f(\varphi,\psi) + D_\varphi \nabla^2 \varphi(\underline{x},t) + \underline{v_\varphi} \cdot \underline{\nabla}\varphi(\underline{x},t) \\[2mm]
\dfrac{\partial}{\partial t}\psi(\underline{x},t) = g(\varphi,\psi) + D_\psi \nabla^2 \psi(\underline{x},t) + \underline{v_\psi} \cdot \underline{\nabla}\psi(\underline{x},t)
\end{cases}
\qquad
\begin{cases}
\underline{x} \in \Omega \subseteq \mathbb{R}^n \\[2mm]
t \in \mathbb{R}^+
\end{cases}
\tag{1.16}
$$

where $\Omega \neq \emptyset$ is an open subset of $\mathbb{R}^n$ bounded by a smooth surface Σ, $\varphi, \psi : \Omega \times \mathbb{R}^+ \to \mathbb{R}^+$ are the species concentrations, $f, g : \mathbb{R}^+ \times \mathbb{R}^+ \to \mathbb{R}$ are non-linear functions describing the reaction dynamics, $D_\varphi, D_\psi \in \mathbb{R}^+$ are the diffusion coefficients and $\underline{v_\varphi}, \underline{v_\psi} \in \mathbb{R}^n$ are the velocities, uniform in time and space, of the two species driven from an external force field. Such equations can be derived from a microscopic framework, as we show in Appendix A.

Let us examine the simplest possible case, that is a one dimensional support with spatial periodic boundary conditions $\mathbb{S}^1$. System (1.16) then becomes

$$
\begin{cases}
\dfrac{\partial}{\partial t}\varphi(x,t) = f(\varphi,\psi) + D_\varphi \dfrac{\partial^2}{\partial x^2}\varphi(x,t) + v_\varphi \dfrac{\partial}{\partial x}\varphi(x,t) \\[2mm]
\dfrac{\partial}{\partial t}\psi(x,t) = g(\varphi,\psi) + D_\psi \dfrac{\partial^2}{\partial x^2}\psi(x,t) + v_\psi \dfrac{\partial}{\partial x}\psi(x,t)
\end{cases}
\qquad
\begin{cases}
x \in \mathbb{S}^1 \\[2mm]
t \in \mathbb{R}^+
\end{cases}
$$

with conditions

$$
\begin{cases}
\varphi(x+L,t) = \varphi(x,t) \\[2mm]
\psi(x+L,t) = \psi(x,t)
\end{cases}
\qquad
\begin{cases}
\dfrac{\partial}{\partial x}\varphi(x+L,t) = \dfrac{\partial}{\partial x}\varphi(x,t) \\[2mm]
\dfrac{\partial}{\partial x}\psi(x+L,t) = \dfrac{\partial}{\partial x}\psi(x,t)
\end{cases}
$$

where L is the length of the spatial support.

With these assumptions we can prove a first result

Proposition   The effects of the drift on systems (1.16) depends only on $\Delta v = |v_\varphi - v_\psi|$.

Proof   Let us introduce the *co-moving frame* for species φ, assuming $v_\varphi \neq 0$, therefore let us define the concentrations in the latter reference system

$$\begin{cases} \Phi(x,t) = \varphi(x - v_\varphi t, t) \\ \Psi(x,t) = \psi(x - v_\varphi t, t) \end{cases}$$

where Φ, Ψ are defined on the same domain as φ, ψ.
Then let us derive with respect of time and substitute equations (1.16) for variable Φ

$$\begin{aligned} \frac{\partial}{\partial t}\Phi(x,t) &= \frac{\partial}{\partial t}\varphi(x - v_\varphi t, t) - v_\varphi \frac{\partial}{\partial x}\varphi(x - v_\varphi t, t) = \\ &= f(\varphi(x - v_\varphi t, t), \psi(x - v_\varphi t, t)) + D_\varphi \frac{\partial^2}{\partial x^2}\varphi(x - v_\varphi t, t) + \\ &\quad + v_\varphi \frac{\partial}{\partial x}\varphi(x - v_\varphi t, t) - v_\varphi \frac{\partial}{\partial x}\varphi(x - v_\varphi t, t) = \\ &= f(\varphi(x - v_\varphi t, t), \psi(x - v_\varphi t, t)) + D_\varphi \frac{\partial^2}{\partial x^2}\varphi(x - v_\varphi t, t) = \\ &= f(\Phi(x,t), \Psi(x,t)) + D_\varphi \frac{\partial^2}{\partial x^2}\Phi(x,t) \end{aligned}$$

and for variable Ψ

$$\begin{aligned} \frac{\partial}{\partial t}\Psi(x,t) &= \frac{\partial}{\partial t}\psi(x - v_\varphi t, t) - v_\varphi \frac{\partial}{\partial x}\psi(x - v_\varphi t, t) = \\ &= g(\varphi(x - v_\varphi t, t), \psi(x - v_\varphi t, t)) + D_\psi \frac{\partial^2}{\partial x^2}\psi(x - v_\varphi t, t) + \\ &\quad + v_\psi \frac{\partial}{\partial x}\psi(x - v_\varphi t, t) - v_\varphi \frac{\partial}{\partial x}\psi(x - v_\varphi t, t) = \\ &= g(\varphi(x - v_\varphi t, t), \psi(x - v_\varphi t, t)) + D_\psi \frac{\partial^2}{\partial x^2}\psi(x - v_\varphi t, t) + \\ &\quad + (v_\psi - v_\varphi)\frac{\partial}{\partial x}\psi(x - v_\varphi t, t) = \\ &= g(\Phi(x,t), \Psi(x,t)) + D_\psi \frac{\partial^2}{\partial x^2}\Psi(x,t) - (v_\varphi - v_\psi)\frac{\partial}{\partial x}\Psi(x,t) \end{aligned}$$

So at the end we obtain

$$\begin{cases} \dfrac{\partial}{\partial t}\Phi(x,t) = f(\Phi, \Psi) + D_\varphi \dfrac{\partial^2}{\partial x^2}\Phi \\[4mm] \frac{\partial}{\partial t}\Psi(x,t) = g(\Phi, \Psi) + D_\psi \dfrac{\partial^2}{\partial x^2}\Psi - (v_\varphi - v_\psi)\dfrac{\partial}{\partial x}\Psi(x,t) \end{cases}$$

Otherwise, if we choose the *co-moving frame* of species ψ, with analogous calculations that we omit, we obtain

$$\begin{cases} \dfrac{\partial}{\partial t}\Phi(x,t) = f(\Phi,\Psi) + D_\varphi \dfrac{\partial^2}{\partial x^2}\Phi + (v_\varphi - v_\psi)\dfrac{\partial}{\partial x}\Phi(x,t) \\[2mm] \dfrac{\partial}{\partial t}\Psi(x,t) = g(\Phi,\Psi) + D_\psi \dfrac{\partial^2}{\partial x^2}\Psi \end{cases}$$

The space being isotropic there is no difference between $\pm(v_\varphi - v_\psi)$.
Observing in conclusion that, in our setting, the physics of the problem does not change if one species moves with respect to the other with the same velocity, we conclude our proof.

$$\square$$

Now we would like to obtain the conditions for the Turing Instability, as we have done for the system without drift.
In analogy to what we have done previously, let us assume that there exists a homogeneous fixed point for the nonspatial system, i.e., (φ^*, ψ^*) s.t. $f(\varphi^*, \psi^*) = g(\varphi^*, \psi^*) = 0$, and then let us impose that it is stable, i.e., after defining the Jacobian matrix

$$J_0 = \begin{bmatrix} f_\varphi & f_\psi \\ g_\varphi & g_\psi \end{bmatrix}$$

where we have used for the partial derivatives the following notation

$$f_\varphi = \left.\frac{\partial f}{\partial \varphi}\right|_{(\varphi,\psi)=(\varphi^*,\psi^*)}$$

we impose the conditions

$$tr J_0 < 0, \text{ i.e., } f_\varphi + g_\psi < 0$$

$$det J_0 > 0, \text{ i.e., } f_\varphi g_\psi - g_\varphi f_\psi > 0$$

Let us then perturb the system in the steady state with a spatial inhomogeneous perturbation and perform a Taylor expansion halted at the first order, to obtain

$$\frac{\partial}{\partial t}\underline{\mu} = J_0\underline{\mu} + D\frac{\partial^2}{\partial x^2}\underline{\mu} + V\frac{\partial}{\partial x}\underline{\mu}$$

where $V = \begin{bmatrix} \Delta v & 0 \\ 0 & 0 \end{bmatrix}$, J_0 as defined above and $\underline{\mu}, D$ as defined in the previous section.
If we perform a Fourier transform we obtain

$$\frac{\partial}{\partial t}\underline{\mu_k} = \tilde{J}\underline{\mu_k}$$

where $\underline{\mu_k}$, as previously defined, is the perturbation vector in the conjugate space and

$$\tilde{J}(k) = \tilde{J} = J_0 - k^2 D + ikV = \begin{bmatrix} f_\varphi - k^2 D_\varphi + ik\Delta v & f_\psi \\ g_\varphi & g_\psi - k^2 D_\psi \end{bmatrix}$$

is the **extended Jacobian** matrix for system (1.16) for which we omit the dependence on k for the sake of notation.

We have instability if the real part of at least one eigenvalue of $\tilde{J}$ is positive, but having $\tilde{J}$ an immaginary part, the calulations are not as simple as in the case without drift. Let us start by distinguish between real and immaginary part

$$\begin{cases} \Re(tr\tilde{J}) = \tilde{J}_1 = f_\varphi + g_\psi - k^2(D_\varphi + D_\psi) \\ \Im(tr\tilde{J}) = \tilde{J}_2 = k\Delta v \\ \Re(det\tilde{J}) = \tilde{J}_3 = k^4 D_\varphi D_\psi - k^2(f_\varphi D_\psi + g_\psi D_\varphi) + f_\varphi g_\psi - f_\psi g_\varphi \\ \Im(det\tilde{J}) = \tilde{J}_4 = -k^3 D_\psi \Delta v + k g_\psi \Delta v \end{cases} \tag{1.17}$$

so that

$$tr\tilde{J} = \tilde{J}_1 + i\tilde{J}_2 \quad , \quad det\tilde{J} = \tilde{J}_3 + i\tilde{J}_4$$

and

$$\lambda_{1,2} = \frac{1}{2}\left\{ tr\tilde{J} \pm \left[(tr\tilde{J})^2 - 4det\tilde{J} \right]^{\frac{1}{2}} \right\} = \frac{1}{2}\left\{ (\tilde{J}_1 + i\tilde{J}_2) \pm \left[(\tilde{J}_1 + i\tilde{J}_2)^2 - 4(\tilde{J}_3 + i\tilde{J}_4) \right]^{\frac{1}{2}} \right\}$$

To study such relation we can use a property of complex numbers:

Proposition   Let $z = x + iy$, with $x, y \in \mathbb{R}$, be a complex number. Then

$$\sqrt{z} = \pm \left(\sqrt{\frac{x + |z|}{2}} + i\sqrt{\frac{-x + |z|}{2}} sgn(y) \right) \tag{1.18}$$

So, using property (1.18) for $\lambda_{1,2}$, we obtain

$$\lambda = \frac{1}{2}\left(\tilde{J}_1 + \gamma \right) + \frac{1}{2}i\left(\tilde{J}_2 + \eta \right) \tag{1.19}$$

where

$$\gamma = \sqrt{\frac{A + \sqrt{A^2 + B^2}}{2}} \quad , \qquad \eta = \sqrt{\frac{-A + \sqrt{A^2 + B^2}}{2}}$$

and

$$A = \tilde{J}_1^2 - \tilde{J}_2^2 - 4\tilde{J}_3 \quad , \qquad B = 2\tilde{J}_1\tilde{J}_2 - 4\tilde{J}_4$$

We want $\Re(\lambda) > 0$, i.e.,

$$\tilde{J}_1 + \gamma > 0 \Longleftrightarrow \tilde{J}_1 + \sqrt{\frac{A + \sqrt{A^2 + B^2}}{2}} > 0 \Longleftrightarrow \sqrt{\frac{A + \sqrt{A^2 + B^2}}{2}} > -\tilde{J}_1$$

Since $\tilde{J}_1 < 0$, we can take the second power preserving the sign

$$\frac{A + \sqrt{A^2 + B^2}}{2} > \tilde{J}_1^2 \Longleftrightarrow \sqrt{A^2 + B^2} > 2\tilde{J}_1^2 - A \Longleftrightarrow \sqrt{A^2 + B^2} > \tilde{J}_1^2 + \tilde{J}_2^2 + 4\tilde{J}_3$$

Now we would like to take the second power of both terms in this last expression, in order to get rid of the square root. However we don't know whether the right

hand side term $\tilde{J}_1^2 + \tilde{J}_2^2 + 4\tilde{J}_3$ is positive or negative, hence by taking the second power we would lose information about the sign of the inequality.

To overcome this limitation we can turn the above inequality into an equation, obtaining

$$\sqrt{A^2 + B^2} = \tilde{J}_1^2 + \tilde{J}_2^2 + 4\tilde{J}_3$$

Now we can take the second power

$$A^2 + B^2 = (\tilde{J}_1^2 - \tilde{J}_2^2 - 4\tilde{J}_3)^2 \iff A^2 + B^2 = \tilde{J}_1^4 + \tilde{J}_2^4 + 16\tilde{J}_3^2 + 2\tilde{J}_1^2\tilde{J}_2^2 + 8\tilde{J}_3(\tilde{J}_2^2 + \tilde{J}_1^2) \iff$$

$$\tilde{J}_1^4 + \tilde{J}_2^4 + 16\tilde{J}_3^2 - 2\tilde{J}_1^2\tilde{J}_2^2 + 8\tilde{J}_3(\tilde{J}_2^2 - \tilde{J}_1^2) + 4\tilde{J}_1^2\tilde{J}_2^2 + 16\tilde{J}_4(\tilde{J}_4 - \tilde{J}_1\tilde{J}_2) =$$

$$= \tilde{J}_1^4 + \tilde{J}_2^4 + 16\tilde{J}_3^2 + 2\tilde{J}_1^2\tilde{J}_2^2 + 8\tilde{J}_3(\tilde{J}_2^2 + \tilde{J}_1^2)$$

and finally obtain

$$\tilde{J}_1^2\tilde{J}_3 - \tilde{J}_4(\tilde{J}_4 - \tilde{J}_1\tilde{J}_2) = 0 \tag{1.20}$$

The explicit formula of (1.20), if we substitute expressions (1.17), is rather cumbersome and difficult to study analytically.

However, we observed with the symbolic calculation on MATLAB® that equation (1.20) is a 4th degree polynomial in the variable k^2, i.e.,

$$\xi(k^2) = a_1 k^8 + a_2 k^6 + a_3 k^4 + a_4 k^2 + a_5$$

whose first and last coefficients are always positive, explicitly

$$a_1 = D_\varphi D_\psi (D_\varphi + D_\psi)^2 \quad , \quad a_5 = f_\varphi^2 g_\psi^2 (f_\varphi g_\psi - f_\psi g_\varphi)$$

being that $D_{\varphi,\psi} > 0$ and $f_\varphi g_\psi - f_\psi g_\varphi = det J_0 > 0$. Thus it always admits at least a negative minimum for appropriate values of the free parameters, i.e., the diffusion coefficients and the model parameters. As for the case without drift, the dispersion relation becomes positive, i.e., $\Re(\lambda) > 0$, for k^2 s.t. the polynomial (1.20) is negative, as we can see in figures 1.13 and 1.14 where we show an example using the Brussellator Model.

The case is in principle quite different from that of the previous section, $\xi(k^2)$ being of order four while $h(k^2)$ was of order two; however, due to the fact that two ξ's roots are negative (k_1^2 and k_2^2 with reference to figure 1.13), we consider only the other two roots which are positive (k_3^2 and k_4^2 with reference to figure 1.13). Now, remembering figure 1.3, we see that there are some similarities with figure 1.14 if we ignore the negative k^2 axis. Hence we have that, when $\xi(k^2) > 0$, $\Re(\lambda)$ is always negative (thus no instability occurs); vice versa, if $\xi(k^2) < 0$, $\Re(\lambda)$ becomes positive and we have Turing instability.

Moreover we have observed the k^2 for which $\Re(\lambda) > 0$ are the same k^2 s.t. $\xi(k^2) < 0$, therefore their roots coincide; this is exactly the case of figure 1.3 of last section. In conclusion, we have a perfect analogy between $h(k^2)$ and $\xi(k^2)$ if we ignore, as we must do for obvious reasons, negative values of k^2.
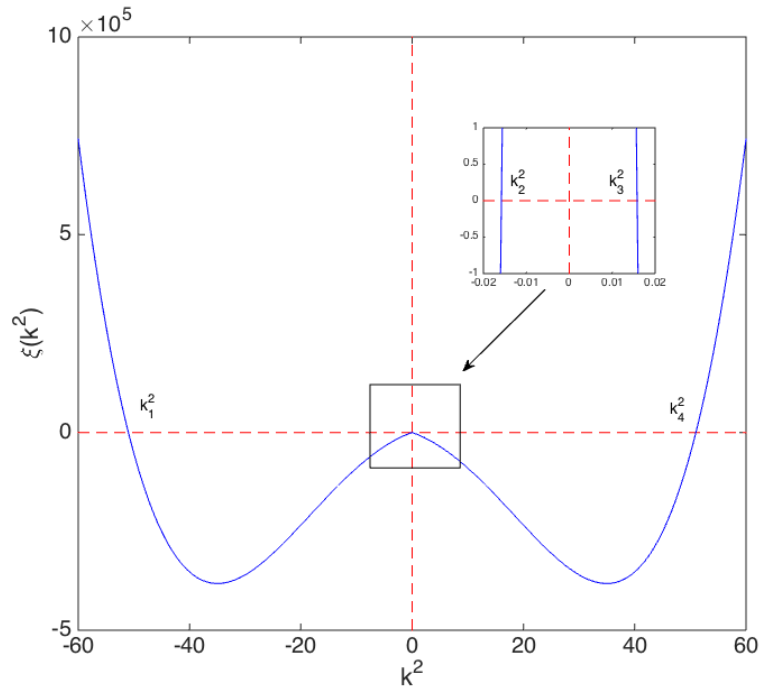
Figure 1.13: Plot of the 4th degree polynomial $\xi(k^2)$ for the Brussellator Model; when Turing's conditions are matched it has 4 roots, but we consider only the two that are positive; $v_\varphi = 1$, $v_\psi = 5$, $b = c = 5$, $D_\varphi = 0.07$, $D_\psi = 0.5$.
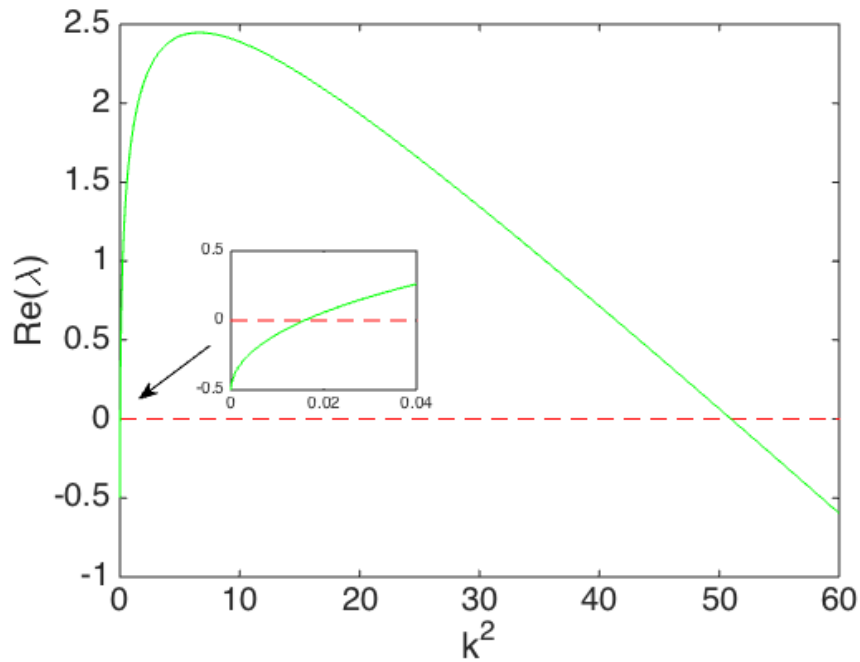
Figure 1.14: Dispersion relation for the Brussellator Model with drift; $v_\varphi = 1$, $v_\psi = 5$, $b = c = 5$, $D_\varphi = 0.07$, $D_\psi = 0.5$.

Equation (1.20) being unmanageable, we looked for the instability region numerically making use again of the Brussellator Model. We have found the instability region, i.e., where $\Re(\lambda) > 0$, as depicted in yellow in figures 1.15, where we see the numerical check of the dependence on Δv, that we have demonstrated analytically at the beginning of this section.

Summing up our outcomes we have here reproduced the results obtained by Rovinsky and Merzinger, who proved theoretically [Rovinsky-Menzinger 1992] and experimentally [Rovinsky-Menzinger 1993] that the drift enlarges the Turing region and that such enlargement depends on Δv.
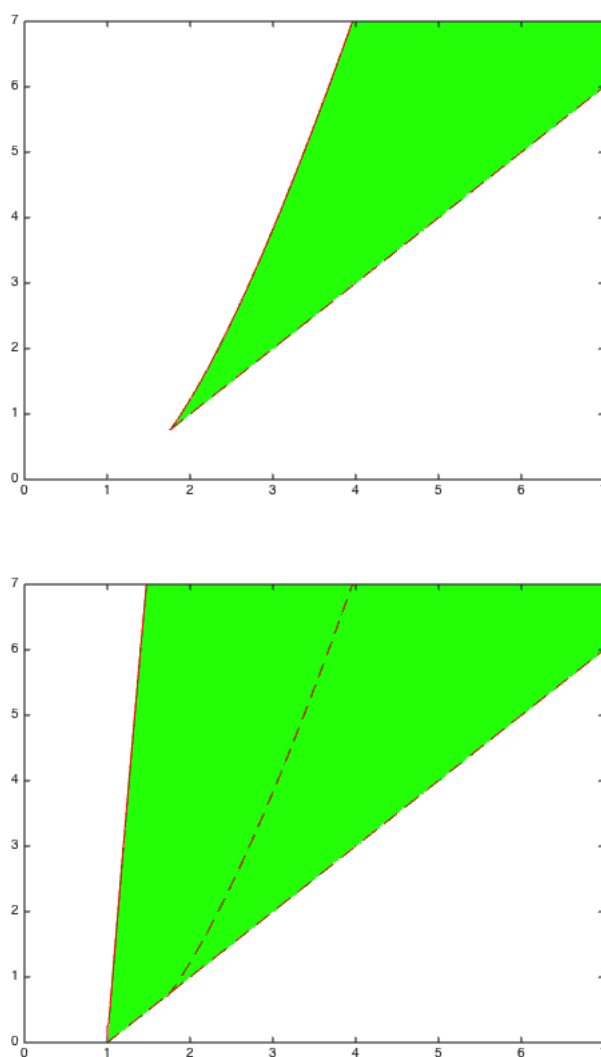
Figure 1.15: In the figure up we show the case with $\Delta v = 0$ and in the figure down the case with $\Delta v = 9$; we see that the Turing region (in green) is wider when there is a difference between the velocities, otherwise it is the same as for the case without drift (dashed red contour); Brussellator model with $D_\varphi = 0.07$ and $D_\psi = 0.5$.

2

Basic Tools of Network Theory

Recurrently in nature the topology on which the dynamics takes place is discrete. To model a discrete support we set to use the tools of **network science**, an interdisciplinary field combining mathematics, physics and computer science; as for most of modern sciences, its foundations rely in mathematics, namely in a branch that comes from algebra: graph theory. At first graph theory was seen as a hobby for intellectual circles and its first known result was the solution of a game, i.e., the Königsberg bridges' problem[1], by Leonard Euler (1707-1783) in 1736, figure 2.1. However, later on, it started gaining more and more respect from the mathematical community as some important mathematicians got into it, one for all Paul Erdős (1913-1996), and many notable results were obtained. Now graph theory is to all effects a well developed branch of pure and applied mathematics and, through network science, finds applications in many disciplinary fields.

   Mainly there are three approaches to graph theory: algebraic, combinatorial and spectral; usually in applications it is common to focus on the latter. In this chapter we will give some basic definitions in graph theory, then we will see some algorithms

---

[1]Euler demonstrated that it was not possible to start a walk that ended at the starting point, crossing only one time each bridge of Königsberg (now Kaliningrad). Such path would be possible only in a graph for which each point was connected to an even number of other points.

Figure 2.1: On the left Königsberg bridges, on the right its graph representation; [Newman 2010].

for generating computationally networks of interests in applications and at the end we will talk about the discrete Laplacian. All this without any claim of completeness; we will follow mostly the scheme of [Newman 2010][2], bringing to subject only what we are going to need throughout our work.

2.1 How to Build a Network

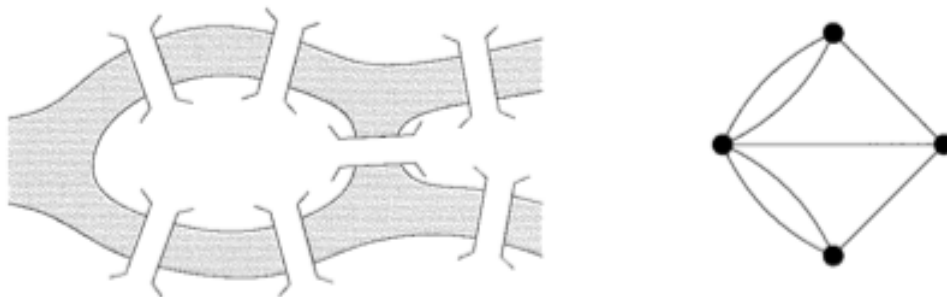A **network** is a mathematical object made of **nodes** connected by **links** and can be undirected if each link is walkable in both directions or directed if there is only one direction available for every link[3]. The **degree** of a node is the number of other nodes to which it connects when the network is undirected, while, if the network is directed, it is necessary to discriminate between the *in-degree*, i.e., the number of links incoming to the node, and the *out-degree*, i.e., the number of links outgoing from the node. An example of network is the human brain, with its 10^{10} neurons (which play the role of the nodes) and 10^{12} synapses (links) [Kandel et al. 2012].
The variety of networks is wide; in pure mathematics, for example, it is common to study networks with a certain regularity, such as *k*-regular graphs or bipartite graphs[4], for which it is possible to demonstrate interesting properties [Casolo-Fumagalli 2016]. However those kinds of networks are rarely found in applications, where the support does not often show any kind of regularity, even if there are ways to discriminate from one to another. We will describe only one regular graph, the 1D *regular lattice*, which will be useful to make comparisons with the others and it is the starting point in some algorithms to generate networks. Mainly we deal with two classes of networks: *random graphs* or Erdős-Rényi graphs and *small-world networks*. Another important class is that of *scale-free networks*; however in some recent and detailed studies has emerged that the latter type is not as common in natural and artificial systems as it was used to think [Broido-Clauset 2018] and they will not be considered during our work.
In this section, we will first describe some computational methods of network generation and, at the end, we will give some basic and rigorous definitions.

Regular Lattices   A 1D *k*-**regular lattice** is a network in which every node is connected to the same number of nodes, namely *k*, making a circular ring and that can be embedded in the Euclidean space $\mathbb{R}$. The simplest 1D regular lattice is nothing else but a discretized ring. There are several kinds of lattice graphs, however during this work we are going to deal only with 1D lattices; for more details on lattices one could refer to [Grätzer 2011].

Random Graphs   A **random graph**, or Erdős-Rényi network, is a model of network in which some specific set of parameters take fixed values, but the network

---

[2]For the algebraic and combinatorial points of view see [Casolo-Fumagalli 2016] and [Wilson 1996].

[3]We will give the rigorous mathematical definitions at the end of this section.

[4]A graph is said to be *k-regular* if every node has degree *k*, while it is called *bipartite* if the nodes are divided into two sets and nodes of the same set are never connected by a link.
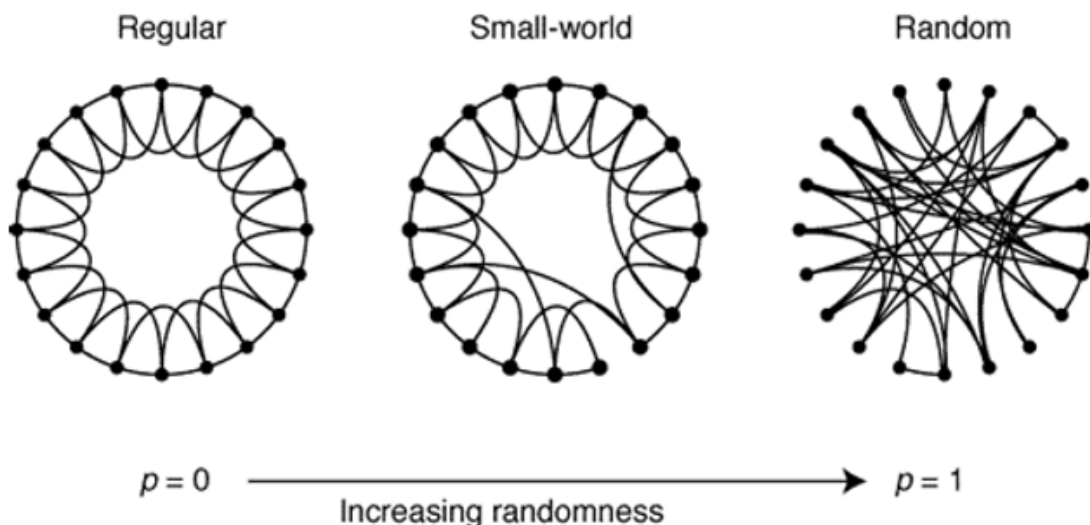
Figure 2.2: On the left we have a regular lattice, as the randomness increases we have a Small-World (center) and, on the right, a random graph; [Watts-Strogatz 1999].

is random in other respects. In general we talk about an *ensemble* of random graphs and there are different kinds of algorithms to generate such graphs, the most famous of which was first proposed by the mathematicians Paul Erdős and Alfred Rényi [Erdős-Rényi 1959]. The main trait of such networks is that they have a weak structure, meaning that some components may be disconnected or it is sufficient to remove a small percentage of links to disconnect them, but it is easy to reach every node in relatively short paths. The model we use here was designed by Edgar Nelson Gilbert [Gilbert 1959]; it consists on fixing the number of nodes n and a probability p: each couple of nodes is connected by a link with such probability. In such case, the degrees are distributed according to a Gaussian curve, thus deviations from the average degree are quite rare. For historical reasons, independently of the methods used to generate them, random graphs are always called Erdős-Rényi.

In the figures obtained from numerical simulations on Erdős-Rényi networks we will always specify the number of nodes n and the probability p of having a link between each couple of nodes.

Small-World Networks A network where every node can be easily reached through a relatively short path and has a strong structure, meaning that it is connected and a significant number of links must be removed in order to disconnect it[5], is called **Small-World**. Such name comes from social sciences and it is known in the mainstream culture as the "six grade of separation rule". The majority of the networks found in nature are Small-World, those networks being well connected but at the same time strong. The most important algorithm to generate Small-World

---

[5]The property of having strong structure is in comparison with a random graph with the same number of nodes and links; we will describe more rigorously such property at the end of this section.

networks is the Watts-Strogatz algorithm [Watts-Strogatz 1998]: we start from a 1D k-regular lattice and then we rewire some of the links with a probability p. The rewired links may produce *short cuts* or *long range links*, because they allow to jump to another area of the network. In weighted networks, such links are usually weak links and they are what makes the structure strong[6]. As we see in figure 2.2, with $p = 0$ the network is a 1D regular lattice, while with $p = 1$ it is a random graph; the Small-World structure lies in between and conserves the strong structure of the regular lattice but it easy to reach every node, as in the random graph. In the figures obtained from numerical simulations on Small-World network we will always specify the number of nodes n, the connectivity of the starting lattice k (that will be k^{out} if the network is directed) and the rewiring probability p.

Our work will follow mostly an informal setting; nevertheless let us now give some rigorous definitions of the concepts and structures we are dealing with.

Definition A **network** (or graph) is an ordered couple $\mathcal{G} = (V, E)$ where V is the **nodes**' set and E is the **links**' set[7]. A link between two nodes $u, v \in V$ is indicated as $\{u, v\} \in E$. Two nodes $u, v \in V$ are said to be **adjacents** ($u \sim v$) if $\{u, v\} \in E$.

Definition Let $\mathcal{G} = (V, E)$ be a network. $\mathcal{G}$ is said to be **undirected** (or *symmetric*) if $\forall u, v \in V$ we have that $u \sim v \implies v \sim u$, i.e., the relation of adjacency is *symmetric*. Conversely we say that a network is **directed** (or *asymmetric*) when $\forall u, v \in V$ s.t. $u \sim v \, \exists$ at least one couple $\hat{u}, \hat{v}$ s.t. $\hat{u} \sim \hat{v}$ but $\hat{v} \not\sim \hat{u}$. We denote the direct link from node u to node v as (u, v).

Given a network of n nodes, the most common way to represent it mathematically is by its **adjacency matrix**, a matrix A such that

$$A_{ij} = \begin{cases} 1 & \text{if } \{i, j\} \in E \\ 0 & \text{otherwise} \end{cases} \qquad \forall i, j = 1, ..., n \qquad (2.1)$$

if $\mathcal{G}$ is symmetric and

$$A_{ij} = \begin{cases} 1 & \text{if } (j, i) \in E \\ 0 & \text{otherwise} \end{cases} \qquad \forall i, j = 1, ..., n \qquad (2.2)$$

if $\mathcal{G}$ is asymmetric.

Remark The notation for the asymmetric adjacency matrix is not the same in every text book. It is possible to find an equivalent definition, that is $A_{ij} = 1$ if $(i, j) \in E$, as for example in [Newman 2010].

---

[6]In [Buchanan 2003] are given many examples of Small-World network and it is explained the importance of long range links and weak links for the structure.

[7]The fact that in algebraic graph theory the nodes are called *vertices* and the links are called *edges* explains the identification of the sets with V and E.

From equations (2.1) and (2.2) it is clear that A is a *square matrix* whose number of rows (or columns) is the nodes' number of the network it represents, i.e., if $|V| = n$ then $A \in \mathbb{R}^{n \times n}$.

When a graph does not have neither multilinks ($\{u, v\}$ is not unique) nor self-links (i.e., $A_{ii} > 0 \; \exists i$), we talk about a **simple network**; otherwise we have a **multinetwork**.

In some situations is necessary to represent links as having a strength, so that $A_{ij} \in \mathbb{R}^+$; in such cases we are dealing with a **weighted network**.

It is very important to know how many nodes are connected to node i. To that use, we define the **degree** of a node as

$$k_i = \sum_{j=1}^{n} A_{ij} \qquad \forall i = 1, ..., n$$

if the network is symmetric, while if it is asymmetric we need to discriminate between the links that exit the node and the ones entering it, i.e.,

$$\begin{cases} k_i^{out} = \sum_{j=1}^{n} A_{ji} \\[2em] k_i^{in} = \sum_{j=1}^{n} A_{ij} \end{cases} \qquad \forall i = 1, ..., n$$

Definition Let $\mathcal{G} = (V, E)$ a directed network with $|V| = n$. If $\mathcal{G}$ is s.t. $\forall i \in \{1, ..., n\}$ $k_i^{in} = k_i^{out}$, it is **balanced**, while if $\exists \; i \in \{1, ..., n\}$ s.t. $k_i^{in} \neq k_i^{out}$, it is **unbalanced**.

In applications it may be useful to know how "easy" is to reach each node and how "strong" is the network; to measure such properties we need two other definitions.

Definition The **geodesic path** g_{ij} between two nodes i and j ($i \neq j$) is the shortest nontrivial path connecting the two nodes. The *length* of a path between two nodes is the number of links crossed to reach one node from the other. The **characteristic path length** l_c is the average of all the geodesic paths

$$l_c = \frac{1}{n(n-1)} \sum_{i=1}^{n} \sum_{j \neq i, j=1}^{n} g_{ij}$$

Definition The *local clustering coefficient* for each node i is defined as the ratio between the number of triangles of which such node is part with the other adjacent nodes Δ_i and all the possible triangles it could be part of $k_i(k_i - 1)/2$

$$c_i = \frac{2\Delta_i}{k_i(k_i - 1)} \quad \forall \; i \in \{1, ..., n\}$$

and the **clustering coefficient** is the average of all the local coefficients c_i over the n nodes

$$C = \frac{1}{n} \sum_{i=1}^{n} c_i$$

It is clear that $0 \le c_i \le 1$ and $0 \le C \le 1$.

A network whose l_c is small will be well connected, while a $C \lesssim 1$ will indicate a strong structure[8]. It is straightforward to understand that a regular lattice has a high value of C due to its regular structure, but its l_c is big and grows as the number of node increases, while a random graph has a small value of l_c but a weak structure, C being small. What makes Small-World structures interesting is the fact that they conserve the C of the starting regular lattice, while gaining a small l_c[9] if compared to an Erdős-Rényi network with the same number of nodes and links.

2.2   Diffusion on Networks

The process of diffusion on networks is a fundamental process for systems whose support is discrete: for instance let us think about the spreading of an idea in a community of people, the diffusing current in an electric network, the exchange of information in the world wide web or the flow of energy in a food web[10]. As for the continuum case, instead of studying the motion of every single unity, we look for a general approach which takes into account the average motion of the unities considered.

Remark   In the description below we are going to consider the most simple case of undirected network whose links are all simple and weighted 1. Such approach, as we will see at the end of this subsection, is easily generalized.

Let us consider an undirected simple graph $\mathcal{G} = (V, E)$, $|V| = n$ and a given concentration ψ of a certain substance in the $j-$th node, which is moving towards the node i along the link $\{i, j\}$, with a rate $\mathcal{D}(\psi_j - \psi_i)$ where $\mathcal{D}$ is the *diffusivity*. In a small interval of time dt, the substance that goes from node j to node i is $\mathcal{D}(\psi_j - \psi_i)dt$, hence the rate at which ψ_i varies is given by the discrete version of Fick's law of diffusion [Newman 2010]

$$\dot{\psi}_i = \mathcal{D} \sum_{j=1}^{n} A_{ij}(\psi_j - \psi_i) = \mathcal{D} \sum_{j=1}^{n} A_{ij}\psi_j - \mathcal{D}\psi_i \sum_{j=1}^{n} A_{ij} = \mathcal{D} \sum_{j=1}^{n} A_{ij}\psi_j - \mathcal{D}\psi_i k_i$$

therefore

$$\dot{\psi}_i = \mathcal{D} \sum_{j=1}^{n} (A_{ij} - \delta_{ij}k_i)\psi_j$$

---

[8]Another measure of the strength is given by the *connectivity*, which will not take into account in this work; for more details see [Casolo-Fumagalli 2016] and [Newman 2010].

[9]It has been shown that usually $l_c < 7$ for Small-World networks of interest, [Buchanan 2003].

[10]Of course all these processes are different from a physical point of view; for instance, the energy in a food web is conserved, while a person can spread his/her idea without losing it.

If we rewrite the above equation in matrix form we obtain

$$\dot{\underline{\psi}} = \mathcal{D}(A - P)\underline{\psi}$$

with $\underline{\psi}$ vector whose components are ψ_i, A adjacency matrix and P is a diagonal matrix whose entries are the nodes' degree, i.e., $P = diag(k_1, ...k_n)$. Calling $L = A - P$, we can write it in a more compact form

$$\dot{\underline{\psi}} - \mathcal{D}L\underline{\psi} = 0 \quad \Longleftrightarrow \quad \dot{\underline{\psi}} = \mathcal{D}L\underline{\psi} \tag{2.3}$$

Definition   Equation (2.3) is a *discrete diffusion equation*. Hence the matrix L, whose entries are

$$L_{ij} = \begin{cases} -k_i \text{ if } i = j \\ 1 \text{ if } \{i, j\} \in E \\ 0 \text{ otherwise} \end{cases} \quad \Longleftrightarrow \quad L_{ij} = A_{ij} - \delta_{ij}k_i$$

is the **discrete Laplacian**. L is symmetric, A being symmetric.

Let us now demonstrate one important property of the discrete Laplacian L on a symmetric network.

Property 1   Let L be the discrete Laplacian matrix of an undirected simple network of n nodes, whose entries are $L_{ij} = A_{ij} - \delta_{ij}k_i$. Then

- L is *negative semidefinite*;

- L has n real eigenvalues, to which correspond n orthonormal eigenvectors.

Before giving the proof, let us point out that in some textbooks the Laplacian is defined in a different way, i.e., $L_{ij} = \delta_{ij}k_i - A_{ij}$, and of course, if defined in this way, it is a positive semidefinite matrix. Our notation follows the work of Nakao and Mikhailov [Nakao-Mikhailov 2010], while the book [Newman 2010], from where the following proof is taken, uses the other; this explains the change of sign that we must do in order to demonstrate that L is negative semidefinite.

Proof   Let $\mathbb{L}$ be a symmetric matrix whose entries are $\mathbb{L}_{ij} = \delta_{ij}k_i - A_{ij}$, i.e., $\mathbb{L}_{ij} = -L_{ij}$ where L is the discrete Laplacian matrix.
Let us consider an undirected graph $\mathcal{G} = (V, E)$ with $|V| = n$ and $|E| = m$ and let us name, arbitrarily, γ one end of every link and ω the other one. Now, let us define the *incidence matrix* $B \in \mathbb{R}^{m \times n}$ s.t.

$$B_{ij} = \begin{cases} +1 \text{ if } \gamma_i \text{ is connected to the j-th node} \\ -1 \text{ if } \omega_i \text{ is connected to the j-th node} \\ 0 \text{ otherwise} \end{cases}$$

Let us consider the following expression

$$\sum_{s=1}^{m} B_{si} B_{sj}$$

If $i \neq j$ we have that

$$B_{si} B_{sj} = \begin{cases} -1 \text{ if the s-th link is } \{i, j\} \\ 0 \text{ otherwise} \end{cases}$$

$\mathcal{G}$ being a simple network, we can have at most one link between two nodes, hence

$$\sum_{s=1}^{m} B_{si} B_{sj} = \begin{cases} -1 \text{ if } \{i, j\} \in E \\ 0 \text{ otherwise} \end{cases}$$

If $i = j$ we have that

$$B_{si}^2 = \begin{cases} 1 \text{ if the s-th link goes into the i-th node} \\ 0 \text{ otherwise} \end{cases}$$

therefore

$$\sum_{s=1}^{m} B_{si}^2 = k_i$$

Putting all together we obtain

$$B^t B = \mathbb{L}$$

Let $\underline{v}_i$ a normalized eigenvector of $\mathbb{L}$ which related eigenvalue is λ_i. Therefore

$$\underline{v}_i^t B^t B \underline{v}_i = \underline{v}_i^t \mathbb{L} \underline{v}_i = \lambda_i \underline{v}_i^t \underline{v}_i = \lambda_i$$

Let us notice that

$$\underline{v}_i^t B^t B \underline{v}_i = |B \underline{v}_i|^2 \geq 0$$

hence the eigenvalue $\lambda_i \geq 0$, i.e., $\mathbb{L}$ is a positive semidefinite matrix.

Remembering that $\mathbb{L} = -L$, we have obtained that L, besides the fact that it is symmetric, it is negative semidefinite, i.e., its n eigenvalues are zero or negative. From the *Spectral Theorem* we know that such eigenvalues are real and related to n orthonormal eigenvectors.

$\square$

Other properties, that we will not demonstrate, are

Property 2 Let $\{\lambda_i\}_{i=1,...,n} = \sigma(L)$, then $\lambda_i = 0 \; \exists \; i \in \{1, ..., n\}$, $\lambda_j \leq \lambda_i \; \forall \; j \neq i$ and it corresponds to the constant eigenvector $\underline{1} = (1, ..., 1)$. If the network is connected, 0 is simple, i.e., $\lambda_j < \lambda_i \; \forall \; j \neq i$.

Property 3 L is singular, i.e., $\nexists\, L^{-1}$.

Property 4 L is a *diagonally dominant* matrix, i.e., $|L_{ii}| \geq \sum_{j \neq i} |L_{ij}| \quad \forall\; i \in \{1, ..., n\}$.

If the network is *directed*, A is asymmetric, L is asymmetric. Therefore $\sigma(L) \subseteq \mathbb{C}^-$, but we can still estimate the eigenvalues from the following theorem [Varga 2004]:

Geršgorin Circle Theorem Let $A \in \mathbb{C}^{n \times n}$, whose elements are a_{ij}. Let

$$R_i = \sum_{j \neq i, j=1}^{n} |a_{ij}| \quad \text{and} \quad C_i = \sum_{j \neq i, j=1}^{n} |a_{ji}|$$

Then

$$\sigma(A) \subseteq \left[\bigcup_{i=1}^{n} D_{a_{ii}}(R_i) \right] \cap \left[\bigcup_{i=1}^{n} D_{a_{ii}}(C_i) \right]$$

where $D_x(y)$ is a disk centered in x, whose radius is y.

So L's eigenvalues are contained in a disk $D_\vartheta(\varrho)$, where

- $\vartheta = -(max_{i=1,...,n}\{k_i^{out}\}) \in \mathbb{R}^- \setminus \{0\}$

- $\varrho = min\left(max_{i=1,...,n}\{k_i^{out}\}, max_{i=1,...,n}\{k_i^{in}\} \right) \in \mathbb{R}^+ \setminus \{0\}$

Remark When L is asymmetric, in general, $L \neq L^*$ and it is called **nonnormal**. We will give more details on this subject in Chapters 4 and 6. For now, let us focus only on the fact the L's spectrum is complex, that, as we will show in Section 3.2, is what matters (as long as L is diagonalizable).

Let us conclude this section with an observation about the dynamics that will come useful in Chapter 4. As we have seen in Chapter 1, to develop the theory for Turing instability, we need to start from an homogeneous fixed point. For the theory on discrete support, when the network is unbalanced a problem arises.
In fact, let $\underline{x}^*$ be a homogeneous point:

$$\dot{\underline{x}}^* = \sum_{j=1}^{n} L_{ij}\underline{x}^* = \left(\sum_{j=1}^{n} A_{ij} - \sum_{j=1}^{n} k_i^{out}\delta_{ij} \right)\underline{x}^* = (k_i^{in} - k_i^{out})\underline{x}^* \neq 0$$

Hence, to develop our theory, we need another definition of the Laplacian, namely

$$\mathcal{L}_{ij} = A_{ji} - k_i^{out}\delta_{ij} \tag{2.4}$$

Recalling equation (2.3), we have changed the coupling from

$$\dot{\underline{\psi}}_i = \mathcal{D} \sum_{j=1}^{n} A_{ij}(\psi_j - \psi_i) = \mathcal{D} \sum_{j=1}^{n} L_{ij}\psi_j$$

to

$$\dot{\underline{\psi}}_i = \mathcal{D} \sum_{j=1}^{n} A_{ji}(\psi_j - \psi_i) = \mathcal{D} \sum_{j=1}^{n} \mathcal{L}_{ij}\psi_j$$

When the network is unbalanced, such operator has a homogeneous fixed point

$$\dot{\underline{x}}^* = \sum_{j=1}^{n} \mathcal{L}_{ij}\underline{x}^* = \left(\sum_{j=1}^{n} A_{ji} - \sum_{j=1}^{n} k_i^{out}\delta_{ij} \right)\underline{x}^* = (k_i^{out} - k_i^{out})\underline{x}^* = 0$$

but it does not conserve the mass

$$
\begin{aligned}
\sum_{i=1}^{n} \dot{x}_i \ &= \sum_{i=1}^{n}\sum_{j=1}^{n} \mathcal{L}_{ij}x_j = \sum_{i=1}^{n}\sum_{j=1}^{n}\left(A_{ji} - k_i^{out} \right)x_j \\
&= \sum_{i=1}^{n}\sum_{j=1}^{n} A_{ji}x_j - \sum_{i=1}^{n} k_i^{out}x_i = \sum_{j=1}^{n} k_j^{in}x_j - \sum_{i=1}^{n} k_i^{out}x_i \neq 0
\end{aligned}
$$

while of course L does

$$
\begin{aligned}
\sum_{i=1}^{n} \dot{x}_i \ &= \sum_{i=1}^{n}\sum_{j=1}^{n} L_{ij}x_j = \sum_{i=1}^{n}\sum_{j=1}^{n}\left(A_{ij} - k_i^{out} \right)x_j = \\
&= \sum_{i=1}^{n}\sum_{j=1}^{n} A_{ij}x_j - \sum_{i=1}^{n} k_i^{out}x_i = \sum_{j=1}^{n} k_j^{out}x_j - \sum_{i=1}^{n} k_i^{out}x_i = 0
\end{aligned}
$$

For this reason $\mathcal{L}$ is suitable for processes that do not require a conservation law, e.g., electricity flowing in an electric grid (that is partially disperse due to Joules effect) or spreading of an idea in a community of people.
We can say that $\mathcal{L}$ is a *diffusion-like* operator and it is mostly used in control problems [Asllani et al. 2014].

Remark When the network is balanced both L and $\mathcal{L}$ conserve the mass an have an homogeneous fixed point. For this reason we will set to use the operator $\mathcal{L}$ only in Chapter 5, where we will use unbalanced networks.

3

Turing Theory on Discrete Support

The modern and interdisciplinary version of graph theory, network science[1], is crucial in the understanding of many phenomena of different domains of studies, from social sciences to biology, when the support can be modeled as discrete (e.g. social networks, metabolic and ecological networks) [Caldarelli-Catanzaro 2012]. To study the dynamics on such support is fundamental in applications: just to make some examples, it has been used to predict cascade failures in electric grids [Yang et al. 2017] and to characterize the connectivity of the brain in neural networks [Burioni et al. 2014].

In this direction goes the study of pattern formation on discrete support and in particular Turing pattern formation on networks, that is what we will focus on. Such field was first explored by Othmer and Scriven [Othmer-Scriven 1971], but it has become popular since the work of Nakao and Mikhailov [Nakao-Mikhailov 2010], that is a direct generalization of the theory on continuum support seen in Chapter 1, the support being symmetric; the analysis was recently extended on asymmetric support by Asllani and colleagues [Asllani et al. 2014].

In this chapter we will study Turing theory on symmetric networks and its extension on asymmetric networks, reproducing theoretically and numerically the results obtained in [Nakao-Mikhailov 2010] and in [Asllani et al. 2014].

3.1   Turing Instability on Symmetric Networks

In Chapter 1 we have seen that, for a two species reaction-diffusion system on continuum support, Turing Instability arises when conditions (1.10) are matched. In this section we will study reaction-diffusion dynamics on undirected networks, i.e., symmetric discrete support, following mostly the pioneering work of Nakao and Mikhailov [Nakao-Mikhailov 2010].

---

[1]In general *graph* and *network* (or complex network) are synonyms, even if the first one is used more often to describe an object that has some properties of symmetry, while the latter is used more for irregular structures. It is customary to refer to *graph theory* when talking about the pure mathematics line of research, while network science is the more applied and computational branch.

Considering the discrete diffusion and the dynamics on discrete support, we can write the equations for the reaction-diffusion process of two species φ and ψ on an undirected network $\mathcal{G} = (V, E)$ with $|V| = n$ in the following way

$$\begin{cases} \dot{\varphi}_i(t) = f(\varphi_i, \psi_i) + D_\varphi \sum_{j=1}^{n} L_{ij} \varphi_j \\ \\ \dot{\psi}_i(t) = g(\varphi_i, \psi_i) + D_\psi \sum_{j=1}^{n} L_{ij} \psi_j \end{cases} \qquad \forall\, i \in \{1, ..., n\} \qquad (3.1)$$

Remark Let us observe that equations (3.1) are ODEs and not PDEs unlike the analogous on continuum support; this because the spatial dependence is inherent to the i-th node.

Let us proceed as in section 1.1, hence we start from an homogeneous fixed point (φ^*, ψ^*), we define the Jacobian matrix as before

$$J_0 = \begin{bmatrix} f_\varphi & f_\psi \\ g_\varphi & g_\psi \end{bmatrix}$$

where again we have used for the partial derivatives the following notation

$$f_\varphi = \left. \frac{\partial f}{\partial \varphi} \right|_{(\varphi, \psi)=(\varphi^*, \psi^*)}$$

so that the stability conditions are

$$\begin{cases} f_\varphi + g_\psi < 0 \\ f_\varphi g_\psi - f_\psi g_\varphi > 0 \end{cases} \qquad (3.2)$$

Now let us perturb the fixed point with a spatially inhomogeneous perturbation

$$\begin{cases} \varphi_i(t) = \varphi^* + \delta\varphi_i(t) \\ \psi_i(t) = \psi^* + \delta\psi_i(t) \end{cases}$$

hence system (3.1) becomes

$$\begin{cases} \delta\dot{\varphi}_i = f(\varphi^* + \delta\varphi_i, \psi^* + \delta\psi_i) + D_\varphi \sum_{j=1}^{n} L_{ij} \delta\varphi_j \\ \\ \delta\dot{\psi}_i = g(\varphi^* + \delta\varphi_i, \psi^* + \delta\psi_i) + D_\psi \sum_{j=1}^{n} L_{ij} \delta\psi_j \end{cases}$$

After a Taylor expansion, halting at the first order, we obtain

$$\begin{cases} \delta\dot{\varphi}_i = f_\varphi \delta\varphi_i + f_\psi \delta\psi_i + D_\varphi \sum_{j=1}^{n} L_{ij} \delta\varphi_j \\ \\ \delta\dot{\psi}_i = g_\varphi \delta\varphi_i + g_\psi \delta\psi_i + D_\psi \sum_{j=1}^{n} L_{ij} \delta\psi_j \end{cases} \qquad \forall\, i \in \{1, ..., n\} \qquad (3.3)$$

that is a $2n \times 2n$ system of equations, namely

$$\dot{\underline{\varepsilon}} = \tilde{J}\underline{\varepsilon} = (J + DL)\underline{\varepsilon} \tag{3.4}$$

where

$$\underline{\varepsilon} = \begin{bmatrix} \delta\varphi_1 \\ \vdots \\ \delta\varphi_n \\ \delta\psi_1 \\ \vdots \\ \delta\varphi_n \end{bmatrix} \quad , \quad J = \begin{bmatrix} f_\varphi I_{n\times n} & f_\psi I_{n\times n} \\ g_\varphi I_{n\times n} & g_\psi I_{n\times n} \end{bmatrix} \quad , \quad DL = \begin{bmatrix} D_\varphi L & 0_{n\times n} \\ 0_{n\times n} & D_\psi L \end{bmatrix}$$

To solve such system of equations, the Laplacian being symmetric, we can expand the perturbations on the discrete Laplacian's eigenfuntions[2] $\{\underline{\nu}^{(\alpha)}\}_{\alpha=1,\dots,n}$, which satisfy the following equations

$$\sum_{j=1}^{n} L_{ij}\nu_j^{(\alpha)} = \Lambda^{(\alpha)}\nu_i^{(\alpha)}$$

with $\Lambda^{(\alpha)}$ nonpositive eigenvalues of L.

Let us write the solutions using again the exponential growth ansatz

$$\begin{cases} \delta\varphi_i(t) = \sum_{\alpha=1}^{n} \beta_\alpha e^{\lambda_\alpha t}\nu_i^{(\alpha)} \\ \delta\psi_i(t) = \sum_{\alpha=1}^{n} \sigma_\alpha e^{\lambda_\alpha t}\nu_i^{(\alpha)} \end{cases}$$

where β_α and σ_α are constants determined by the initial conditions.

If we place the latter equations into system (3.3) we obtain n linearly independent equations, each one related to a given eigenvalue $\Lambda^{(\alpha)}$. They are characteristic equations having λ_α as solution

$$\lambda_\alpha \begin{bmatrix} \beta_\alpha \\ \sigma_\alpha \end{bmatrix} = \begin{bmatrix} f_\varphi + D_\varphi\Lambda^{(\alpha)} & g_\varphi \\ f_\psi & g_\psi + D_\psi\Lambda^{(\alpha)} \end{bmatrix} \begin{bmatrix} \beta_\alpha \\ \sigma_\alpha \end{bmatrix}$$

In analogy of how we have proceeded on continuum support, let us study the characteristic polynomial

$$det \begin{bmatrix} f_\varphi + D_\varphi\Lambda^{(\alpha)} - \lambda_\alpha & g_\varphi \\ f_\psi & g_\psi + D_\psi\Lambda^{(\alpha)} - \lambda_\alpha \end{bmatrix} = \lambda_\alpha^2 - \lambda_\alpha[\Lambda^{(\alpha)}(D_\varphi + D_\psi) + (f_\varphi + g_\psi)] + h(\Lambda^{(\alpha)})$$

where

$$h(\Lambda^{(\alpha)}) = D_\varphi D_\psi(\Lambda^{(\alpha)})^2 + (D_\varphi g_\psi + D_\psi f_\varphi)\Lambda^{(\alpha)} + (f_\varphi g_\psi - f_\psi g_\varphi)$$

---

[2]Remember that, as we have seen in the previous section, if the network is symmetric so is the Laplacian matrix; therefore for the Spectral Theorem it has a complete orthonormal set of eigenvectors.

If we solve for λ_α we obtain

$$\lambda_{\alpha_{1,2}} = \frac{1}{2}\left\{\Lambda^{(\alpha)}(D_\varphi + D_\psi) + (f_\varphi + g_\psi) \pm \sqrt{\mathcal{K}}\right\} \tag{3.5}$$

where

$$\mathcal{K} = \left[-\Lambda^{(\alpha)}(D_\varphi + D_\psi) + (f_\varphi + g_\psi)\right]^2 - 4h(\Lambda^{(\alpha)})$$

Let $\Re(\lambda_\alpha)$ the maximum of the eigenvalues' real part, that is of course a function of $\Lambda^{(\alpha)}$. Such function, i.e., $\Re(\lambda_\alpha(\Lambda^{(\alpha)}))$ defines the *dispersion relation* or *master stability function* [Pecora-Carroll 1998]; as for the theory on continuum support, we have that

- if $\forall\ \alpha\ \Re(\lambda_\alpha) < 0$ the perturbation will decay exponentially;

- if $\exists\ \alpha$ s.t. $\Lambda^{(\alpha)} \neq 0$ and $\Re(\lambda_\alpha) > 0$ the perturbation will make the system unstable and it will guide it to a new inhomogeneous equilibrium.

Let us now determine the conditions such that the perturbation makes the system unstable, i.e., the Turing conditions.
In order to have a homogeneous fixed point we need that $f_\varphi + g_\psi < 0$ and to obtain that $\Re(\lambda_\alpha) > 0$ we must impose the condition $h(\Lambda^{(\alpha)}) < 0$. Let us observe that the latter equation is analogous to the condition $h(k^2) < 0$ (see Chapter 1, Section 1.1) if we perform the following change of variable

$$\Lambda^{(\alpha)} \longrightarrow -k^2$$

Taking advantage of this last observation and repeating the same steps that we have discussed in the previous chapter, we find that the condition $h(\Lambda^{(\alpha)}) < 0$ is satisfied if and only if

$$\begin{cases} D_\varphi g_\psi + D_\psi f_\varphi > 0 \\ \\ (f_\varphi g_\psi - f_\psi g_\varphi) - \frac{1}{4}\frac{(D_\varphi g_\psi + D_\psi f_\varphi)^2}{D_\varphi D_\psi} < 0 \end{cases} \tag{3.6}$$

If we put together equations (3.6) and (3.2) we obtain the conditions for Turing instability, that are the same ones of the system on continuum support, i.e., equations (1.10). Nevertheless, let us point out that, unlike the continuous case where the eigenvalues are a countable infinite set, in this case the dispersion relation is made of n eigenvalues[3]. Hence, as we will show numerically, the Turing region of the case on symmetric network may not coincide with its analogous on continuum support due to finite size effects.

---

[3]This is because we take the maximum eigenvalue of each 2×2 system.

As an example to test numerically our theoretical results, let us consider again the Brussellator model, this time on a symmetric network $\mathcal{G} = (V, E)$ of n nodes

$$
\begin{cases}
\dot{\varphi}_i(t) = 1 - (b+1)\varphi_i(t) + c\varphi_i^2(t)\psi_i(t) + D_\varphi \sum_{j=1}^{n} L_{ij}\varphi_j(t) \\
\\
\dot{\psi}_i(t) = b\varphi_i(t) - c\varphi_i^2(t)\psi_i(t) + D_\psi \sum_{j=1}^{n} L_{ij}\psi_j(t)
\end{cases}
\quad \forall\, i \in \{1, ..., n\}
$$

where $b, c \in \mathbb{R}^+$ are the model's parameters and $D_\varphi, D_\psi \in \mathbb{R}^+$ are the species' diffusion coefficients.

Remark   When the spatial support is a network, we do not need to impose the periodic boundary conditions, because we deal with a system of ODEs instead of PDEs.

The computation to find analytically the Turing instability region is analogous to that on continuum support and lead to conditions (1.14) and (1.15), so in theory we would have the same Turing region as that displayed in figure 1.5. Practically this does not always happen, due to the fact that the system is discrete and so will be the dispersion relation. In fact we can have the situation in which the continuum dispersion relation becomes positive but the discrete one stays negative because of the value of its discrete spectrum. To observe numerically this phenomenon we have designed a code that generates networks with the same parameters and then computes the maximum of the discrete dispersion relation. We see in figures 3.1 that, when the Laplacian's eigenvalues are well distributed along the dispersion relation, the Turing region coincides with the continuous one, except for spectral fluctuations on the boundary. On the other hand, it can happen to find nonnegligible areas in which the system is supposed to be unstable but this never happen, for example because of the fact that the Laplacian's spectrum is clustered near the origin, as in figures 3.2, or because it has one or more spectral gaps, as in figures 3.3 and 3.4. The latter case is typical of networks with a high connectivity while the former one is mostly found in networks with a low connectivity and especially when the maximum degree is small.

For what concerns the patterns, since the perturbation is expanded on the Laplacian's eigenfunctions, that are finite, they depend on the network's structure. In figures 3.5 we see an example of pattern formation due to Turing instability on an Erdős-Rényi network of 100 nodes and in figure 3.6 we show the corresponding dispersion relation.

As for the case on continuum support, we cannot have Turing wave patterns for a two species reaction-diffusion system on a symmetric network, but only oscillations that drive the system back to its stable homogeneous equilibrium; this fact that can be understood looking at equation (3.5). To obtain wave patterns we need to avoid the restriction on the imaginary part of the dispersion relation, which can

Figure 3.1: Figure up: statistics over 100 Watts-Strogatz networks with $p = 0.1$ and $k = 14$ for the Brussellator model with $D_\varphi = 0.1$ and $D_\psi = 1$; the areas in red are the ones for which the system is always unstable, while the red-shaded areas are the ones that, due to spectral fluctuations, may be stable; figure down: dispersion relation with $b = 4$ and $c = 6$.

Figure 3.2: Figure up: statistics over 100 Watts-Strogatz networks with $p = 0.03$ and $k = 2$ for the Brussellator model with $D_\varphi = 0.1$ and $D_\psi = 1$; the areas in red are the ones for which the system is always unstable, while the red-shaded areas are the ones that, due to spectral fluctuations, may be stable; figure down: dispersion relation with $b = 3.8$ and $c = 8$.
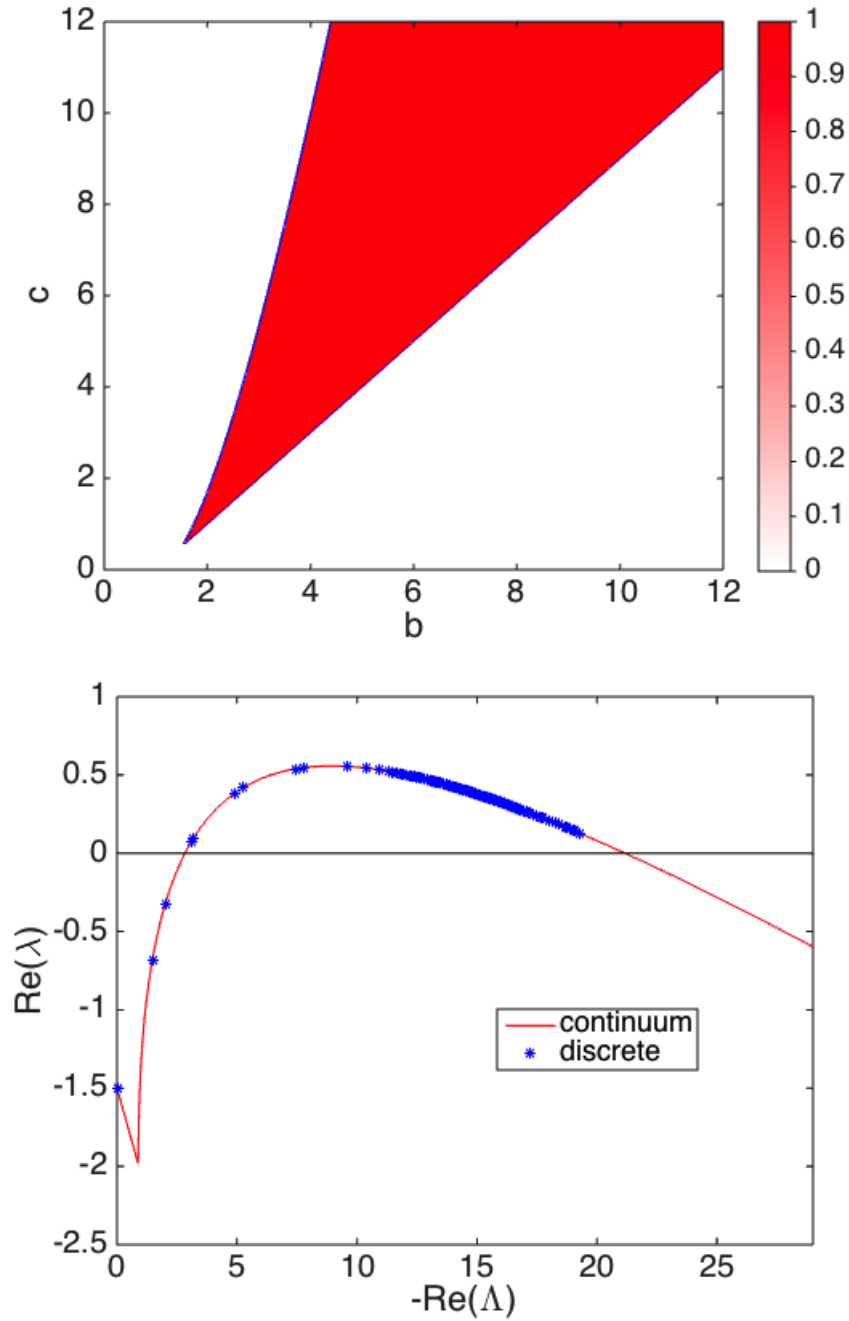
Figure 3.3: Figure up: statistics over 100 Watts-Strogatz networks with $p = 0.03$ and $k = 40$ for the Brussellator model with $D_\varphi = 0.1$ and $D_\psi = 0.25$; the areas in red are the ones for which the system is always unstable, while the red-shaded areas are the ones that, due to spectral fluctuations, may be stable; figure down: dispersion relation with $b = 9$ and $c = 9.5$.

Figure 3.4: Figure up: statistics over 100 Watts-Strogatz networks with $p = 0.03$ and $k = 40$ for the Brussellator model with $D_\varphi = 0.1$ and $D_\psi = 1$; the areas in red are the ones for which the system is always unstable, while the red-shaded areas are the ones that, due to spectral fluctuations, may be stable; figure down: dispersion relation with $b = 2.5$ and $c = 3$.
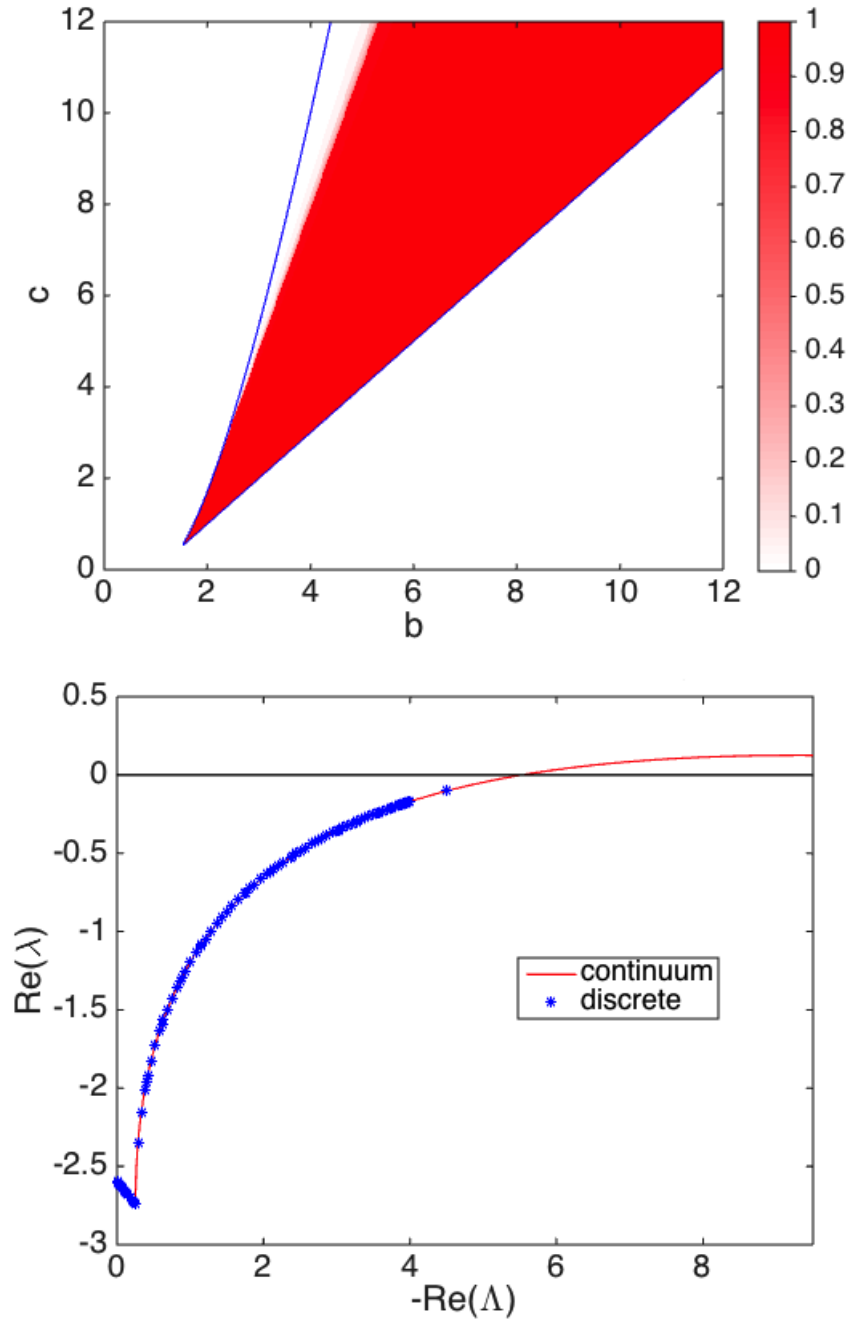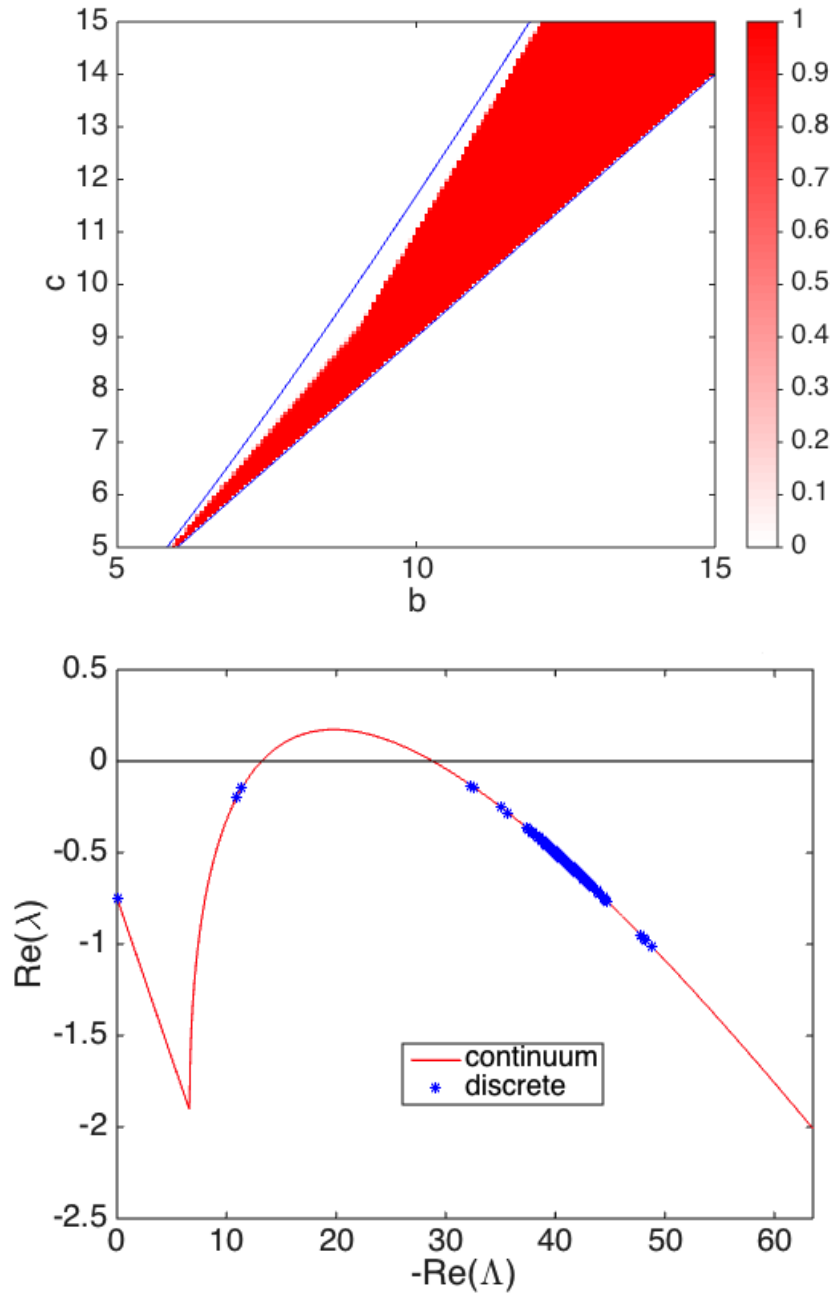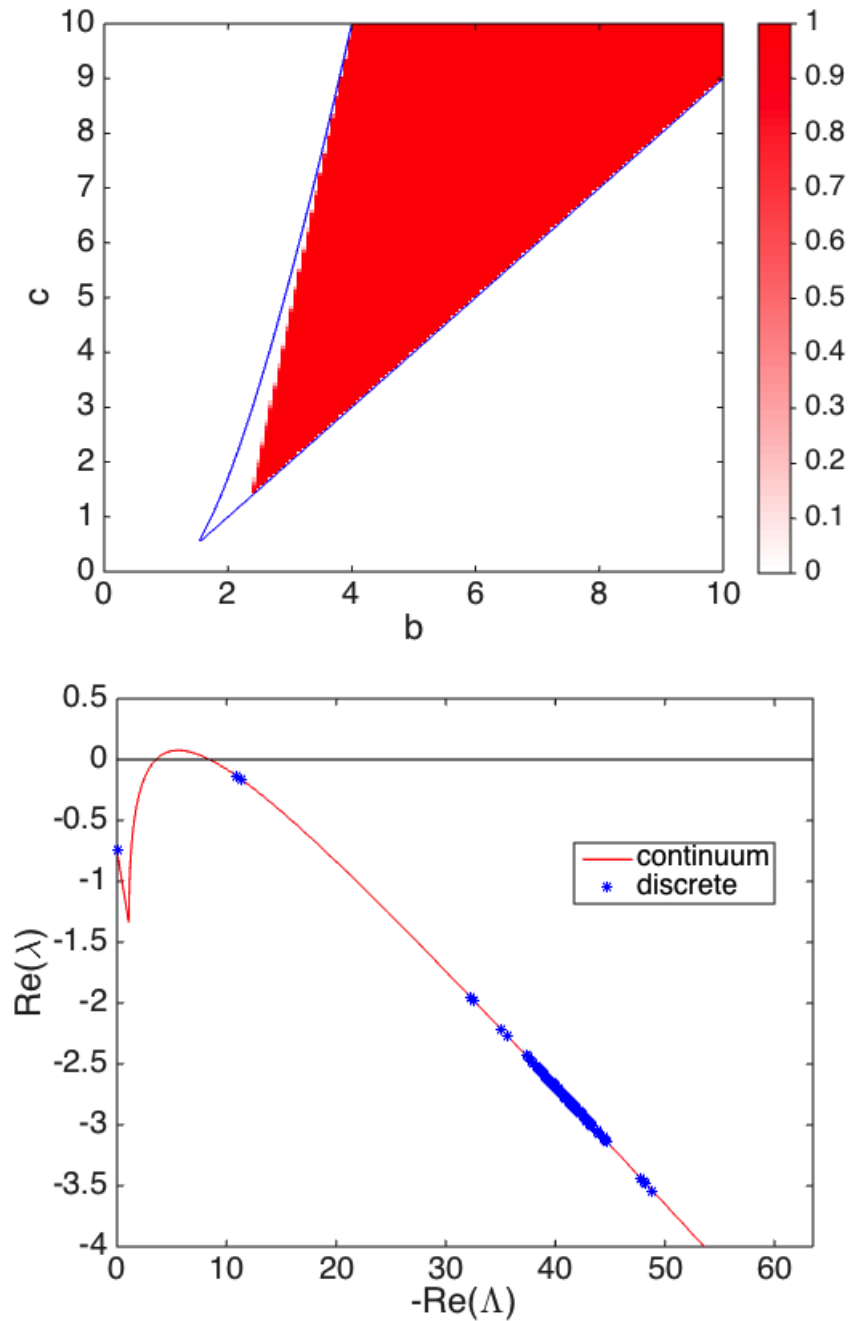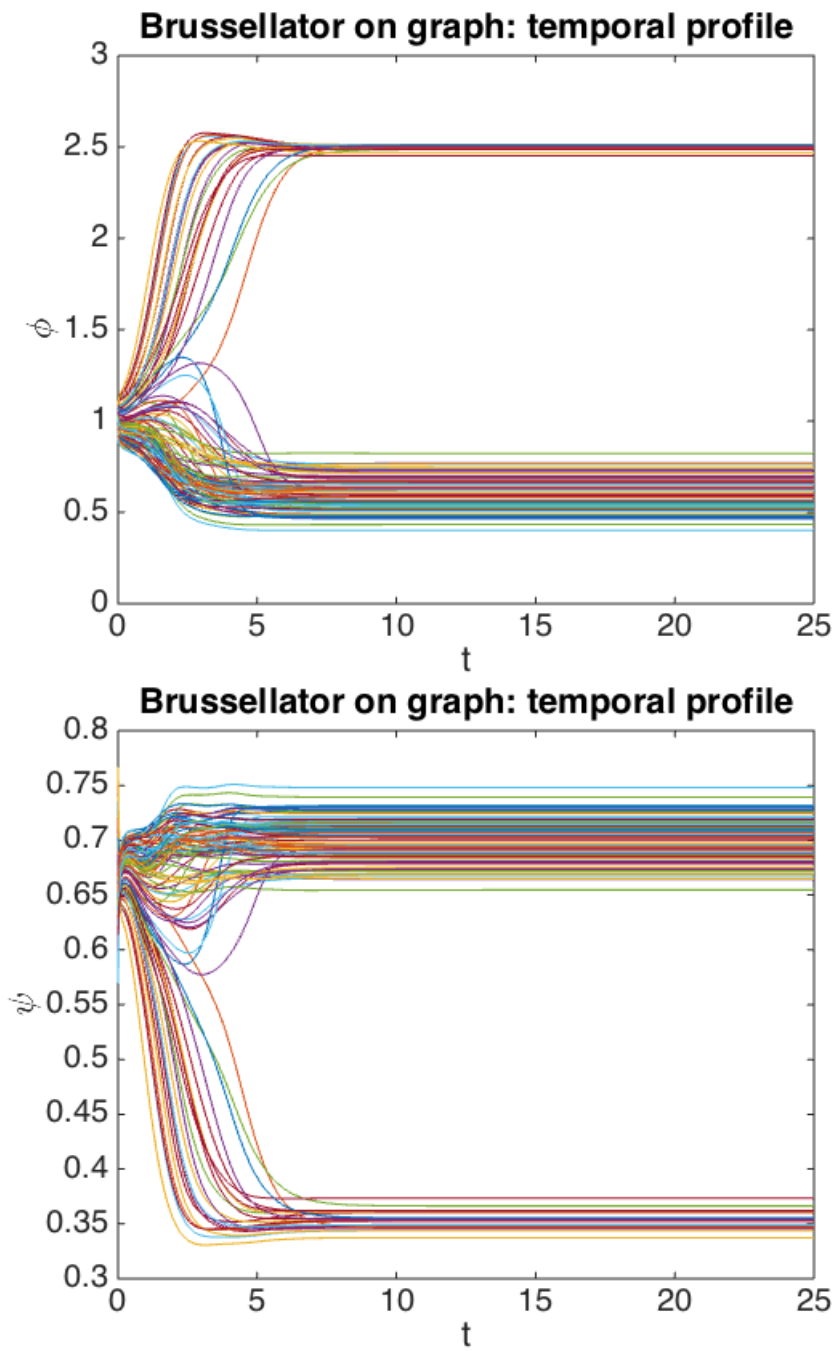
Figure 3.5: Patterns for the Brussellator model with $D_{\varphi} = 0.07$, $D_{\psi} = 0.5$, $b = 8$ and $c = 12$ on a Erdős-Rényi network of 100 nodes and $p = 0.5$.
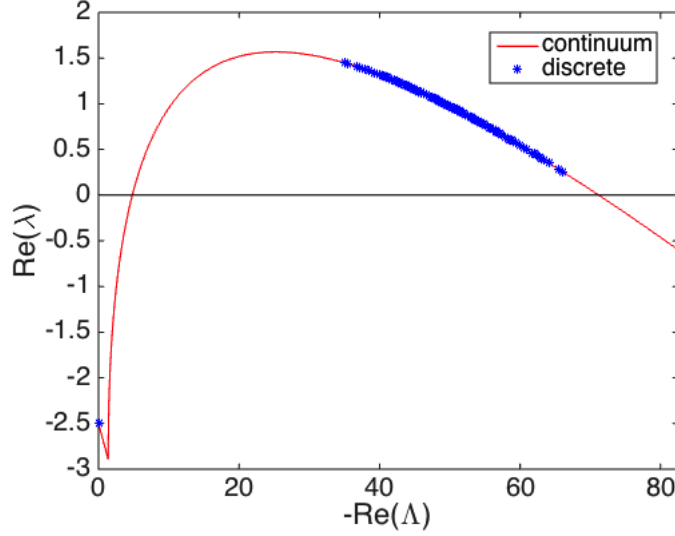
Figure 3.6: Dispersion relation for the Brussellator model with $D_\varphi = 0.07$, $D_\psi = 0.5$, $b = 8$ and $c = 12$ on a Erdős-Rényi network of 100 nodes and $p = 0.5$.

be nonzero only when the real part is negative, hence we need the Laplacian's eigenvalues to be imaginary. This condition, as we will see in the next section, may occur when the network is asymmetric.

3.2   Topology-Driven Instability

Let us study a reaction-diffusion process of two species φ and ψ on a directed network[4] $\mathcal{G}$ of n nodes

$$\begin{cases} \dot{\varphi}_i(t) = f(\varphi_i, \psi_i) + D_\varphi \sum_{j=1}^{n} L_{ij}\varphi_j \\[2em] \dot{\psi}_i(t) = g(\varphi_i, \psi_i) + D_\psi \sum_{j=1}^{n} L_{ij}\psi_j \end{cases} \qquad \forall\, i \in \{1, ..., n\}$$

The network being asymmetric, L is asymmetric.

We have again a system of $2n$ equations, but this time, the Laplacian being asymmetric, we need to be careful before proceeding with the eigendecomposition (i.e, studying each 2×2 system separately); in fact we need the matrix to be diagonalizable [Golub-Van Loan 1996]:

Theorem Let $A \in \mathbb{C}^{n \times n}$ diagonalizable, let $\underline{w}_i$, $i = 1, ...n$, be its n linearly independent eigenvectors and W the matrix whose i-th column is $\underline{w}_i$. Let λ_i, $i = 1, ...n$, A's eigenvalues and Λ the diagonal matrix s.t. $\Lambda_{ii} = \lambda_i$. Then

$$A = W \Lambda W^{-1}$$

---

[4]In this section we will follow [Asllani et al. 2014] and [Asllani 2015].

Remark   Throughout this work we will always deal with matrices that are diagonalizable, hence we will always project the $2n \times 2n$ system into n systems 2×2, without any problems. If the matrix is not diagonalizable but only Jordanizable, in principle we could do the same operation using the generalized eigenvectors. Such technical issues go beyond the aim of our work and no further details on the subject will be given.

As in Section 2.1, let us assume that the system has a homogeneous fixed point, let us impose its stability, let us perturb inhomogeneously such equilibrium and perform a Taylor expansion up to the first order. What we obtain is a $2n \times 2n$ system of equations, analogous to equation (3.4), with the only difference that now L is asymmetric and so is $\tilde{J}$. However, under the hypothesis of $\tilde{J}$ diagonalizable, we can proceed as before, expanding the perturbation on L's eigenfunctions $\{\underline{\nu}^{(\alpha)}\}_{\alpha=1,...,n}$

$$\sum_{j=1}^{n} L_{ij}\nu_j^{(\alpha)} = \Lambda^{(\alpha)}\nu_i^{(\alpha)}$$

where the Laplacian's eigenvalues are $\Lambda^{(\alpha)} = \Re(\Lambda^{(\alpha)}) + i\Im(\Lambda^{(\alpha)})$ with $\Re(\Lambda^{(\alpha)}) < 0$ due to Geršgorin Circle Theorem (Section 2.2). Hence the n matrices that we want to study are of the form

$$\tilde{J}_\alpha = \begin{bmatrix} f_\varphi + D_\varphi \Lambda^{(\alpha)} & g_\varphi \\ f_\psi & g_\psi + D_\psi \Lambda^{(\alpha)} \end{bmatrix} \quad , \quad \alpha \in \{1, ..., n\}$$

In order to study the dispersion relation, i.e., when $\tilde{J}_\alpha$'s eigenvalues λ_α are with positive real parts, we need to proceed as in Section 1.3. Therefore, let us discriminate between real and imaginary parts

$$\begin{cases} \Re(tr\tilde{J}_\alpha) = \tilde{J}_1^\alpha = f_\varphi + g_\psi + \Re(\Lambda^{(\alpha)})(D_\varphi + D_\psi) \\ \Im(tr\tilde{J}_\alpha) = \tilde{J}_2^\alpha = \Im(\Lambda^{(\alpha)})(D_\varphi + D_\psi) \\ \Re(det\tilde{J}_\alpha) = \tilde{J}_3^\alpha = [(\Re(\Lambda^{(\alpha)}))^2 - (\Im(\Lambda^{(\alpha)}))^2]D_\varphi D_\psi - \Re(\Lambda^{(\alpha)})(f_\varphi D_\psi + g_\psi D_\varphi) + f_\varphi g_\psi - f_\psi g_\varphi \\ \Im(det\tilde{J}_\alpha) = \tilde{J}_4^\alpha = \Im(\Lambda^{(\alpha)})(f_\varphi D_\psi + g_\psi D_\varphi) + 2\Re(\Lambda^{(\alpha)})\Im(\Lambda^{(\alpha)})D_\varphi D_\psi \end{cases}$$

so that

$$tr\tilde{J}_\alpha = \tilde{J}_1^\alpha + i\tilde{J}_2^\alpha \quad , \quad det\tilde{J}_\alpha = \tilde{J}_3^\alpha + i\tilde{J}_4^\alpha$$

and

$$\lambda_{\alpha_{1,2}} = \frac{1}{2}\left\{ tr\tilde{J}_\alpha \pm \left[(tr\tilde{J}_\alpha)^2 - 4det\tilde{J}_\alpha\right]^{\frac{1}{2}}\right\} = \frac{1}{2}\left\{ (\tilde{J}_1^\alpha + i\tilde{J}_2^\alpha) \pm \left[(\tilde{J}_1^\alpha + i\tilde{J}_2^\alpha)^2 - 4(\tilde{J}_3^\alpha + i\tilde{J}_4^\alpha)\right]^{\frac{1}{2}}\right\}$$

Such relation can be studied by using the property of complex numbers discussed in Section 1.3, i.e.,

$$z = x + iy \in \mathbb{C} \implies \sqrt{z} = \pm\left(\sqrt{\frac{x + |z|}{2}} + i\sqrt{\frac{-x + |z|}{2}}sgn(y)\right)$$

Hence, our equation for $\lambda_{\alpha_{1,2}}$ becomes

$$\lambda_\alpha = \frac{1}{2}\left(\tilde{J}_1^\alpha + \gamma\right) + \frac{1}{2}i\left(\tilde{J}_2^\alpha + \eta\right)$$

where

$$\gamma = \sqrt{\frac{A + \sqrt{A^2 + B^2}}{2}} \quad , \qquad \eta = \sqrt{\frac{-A + \sqrt{A^2 + B^2}}{2}}$$

and

$$A = (\tilde{J}_1^\alpha)^2 - (\tilde{J}_2^\alpha)^2 - 4\tilde{J}_3^\alpha \quad , \qquad B = 2\tilde{J}_1^\alpha \tilde{J}_2^\alpha - 4\tilde{J}_4^\alpha$$

For the system to be unstable, the following condition needs to be matched

$$\Re(\lambda_\alpha) > 0 \quad \Longleftrightarrow \quad |\tilde{J}_1^\alpha| \leq \gamma$$

A straightforward, although cumbersome, calculation allows us to rewrite the above condition in a different and compact form

$$\Theta_2(\Re(\Lambda^{(\alpha)}))[(\Im(\Lambda^{(\alpha)}))^2] \leq -\Theta_1(\Re(\Lambda^{(\alpha)})) \tag{3.7}$$

where Θ_1 and Θ_2 are polynomials of forth and second degree in $\Re(\Lambda^{(\alpha)})$, explicitly given by

$$\begin{cases} \Theta_1(\Re(\Lambda^{(\alpha)})) = \Xi_{14}(\Re(\Lambda^{(\alpha)}))^4 + \Xi_{13}(\Re(\Lambda^{(\alpha)}))^3 + \Xi_{12}(\Re(\Lambda^{(\alpha)}))^2 + \Xi_{11}(\Re(\Lambda^{(\alpha)})) + \Xi_{10} \\ \Theta_2(\Re(\Lambda^{(\alpha)})) = \Xi_{22}(\Re(\Lambda^{(\alpha)}))^2 + \Xi_{21}(\Re(\Lambda^{(\alpha)})) + \Xi_{20} \end{cases}$$

whose coefficients are

$$\begin{cases} \Xi_{14} = D_\varphi D_\psi (D_\varphi + D_\psi)^2 \\ \Xi_{13} = (D_\varphi + D_\psi)^2(f_\varphi D_\psi + g_\psi D_\varphi) + 2(f_\varphi + g_\psi)D_\varphi D_\psi(D_\varphi + D_\psi) \\ \Xi_{12} = (f_\varphi g_\psi - f_\psi g_\varphi)(D_\varphi + D_\psi)^2 + (f_\varphi + g_\psi)^2 D_\varphi D_\psi + 2(f_\varphi + g_\psi)(D_\varphi + D_\psi)(f_\varphi D_\psi + g_\psi D_\varphi) \\ \Xi_{11} = 2(f_\varphi + g_\psi)(D_\varphi + D_\psi)(f_\varphi g_\psi - f_\psi g_\varphi) + (f_\varphi + g_\psi)^2(f_\varphi D_\psi + g_\psi D_\varphi) \\ \Xi_{10} = (f_\varphi g_\psi - f_\psi g_\varphi)(f_\varphi + g_\psi)^2 \\ \Xi_{22} = D_\varphi D_\psi (D_\varphi - D_\psi)^2 \\ \Xi_{21} = (D_\varphi - D_\psi)^2(f_\varphi D_\psi + g_\psi D_\varphi) \\ \Xi_{20} = f_\varphi g_\psi (D_\varphi - D_\psi)^2 \end{cases}$$

To test numerically out theory we have integrated the Brussellator equations on a directed Small-World network generated with the Newman-Watts algorithm, that is variation to Watts-Strogatz algorithm described in Section 2.1[5]. As we show in figures 3.7, on asymmetric support we can obtain wave patterns. In fact this time, the dispersion relation can be positive when the imaginary part is nonzero, therefore we do not have anymore the restriction on wave instability that we had on symmetric support. In figure 3.8 we can see how the dispersion relation is "pushed up" as

---

[5]In the WS algorithm, we start with a 1D k-regular lattice and, with probability p, we rewire the links; in the WN algorithm, we start with a 1D k-regular lattice and, with probability p, we add long range links. More details are given in the book [Newman 2010].
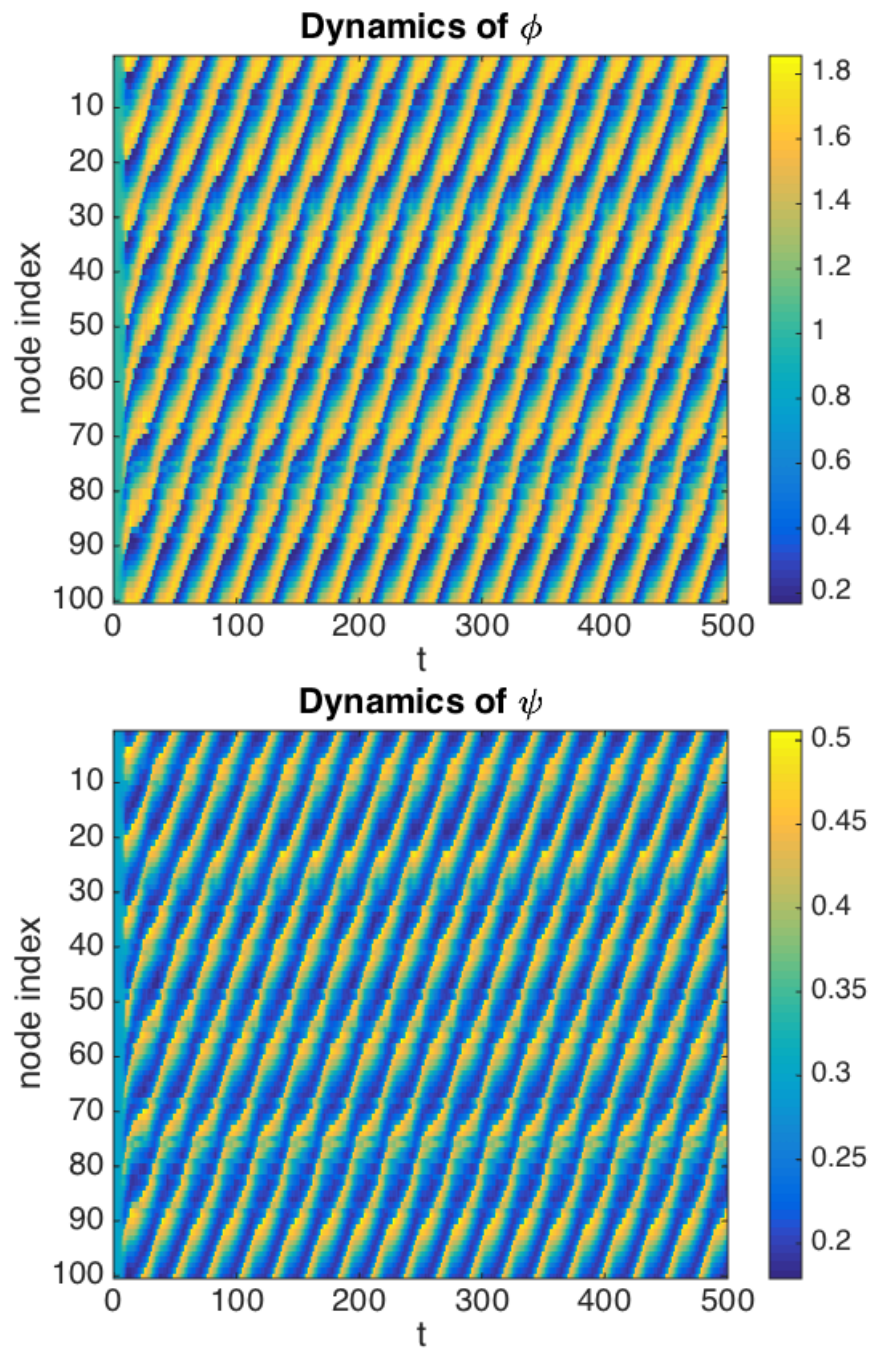
Figure 3.7: Wave patterns for the Brussellator model with $D_\varphi = 1$, $D_\psi = 7$, $b = 9$ and $c = 30$ on a Newman-Watts directed network of 100 nodes, $p = 0.1$ and $k = 3$.

Figure 3.8: Dispersion relation for the Brussellator model with $D_\varphi = 1$, $D_\psi = 7$, $b = 9$ and $c = 30$ on a Newman-Watts directed network of 100 nodes, $p = 0.1$ and $k = 3$.

compared to the continuous one, leading to a *topology-driven instability* that would not be allowed without the imaginary part.

In figures 3.9 we show, with the same code employed in last section, a statistics of the instability regions on directed networks and the enlargement of the classical Turing region, due to the asymmetric topology, with the related dispersion relation. Using condition (3.7) we can visualize the instability region in a different way with respect to the dispersion relation. In figures 3.10 and 3.11 we can see the dependence that the instability region has on the Laplacian's spectrum.

In this section we have showed how the Turing region can be expanded by the asymmetric topology, which pushes the dispersion relation up as compared to the one obtained on a symmetric and continuum support.

What we would like to do next is to enlarge even more the instability region. One way would be to obtain patterns when the systems is in principle stable, i.e., when the dispersion relation is entirely negative; in order to do so, we need to introduce a new mathematical concept: that of *nonnormality*.
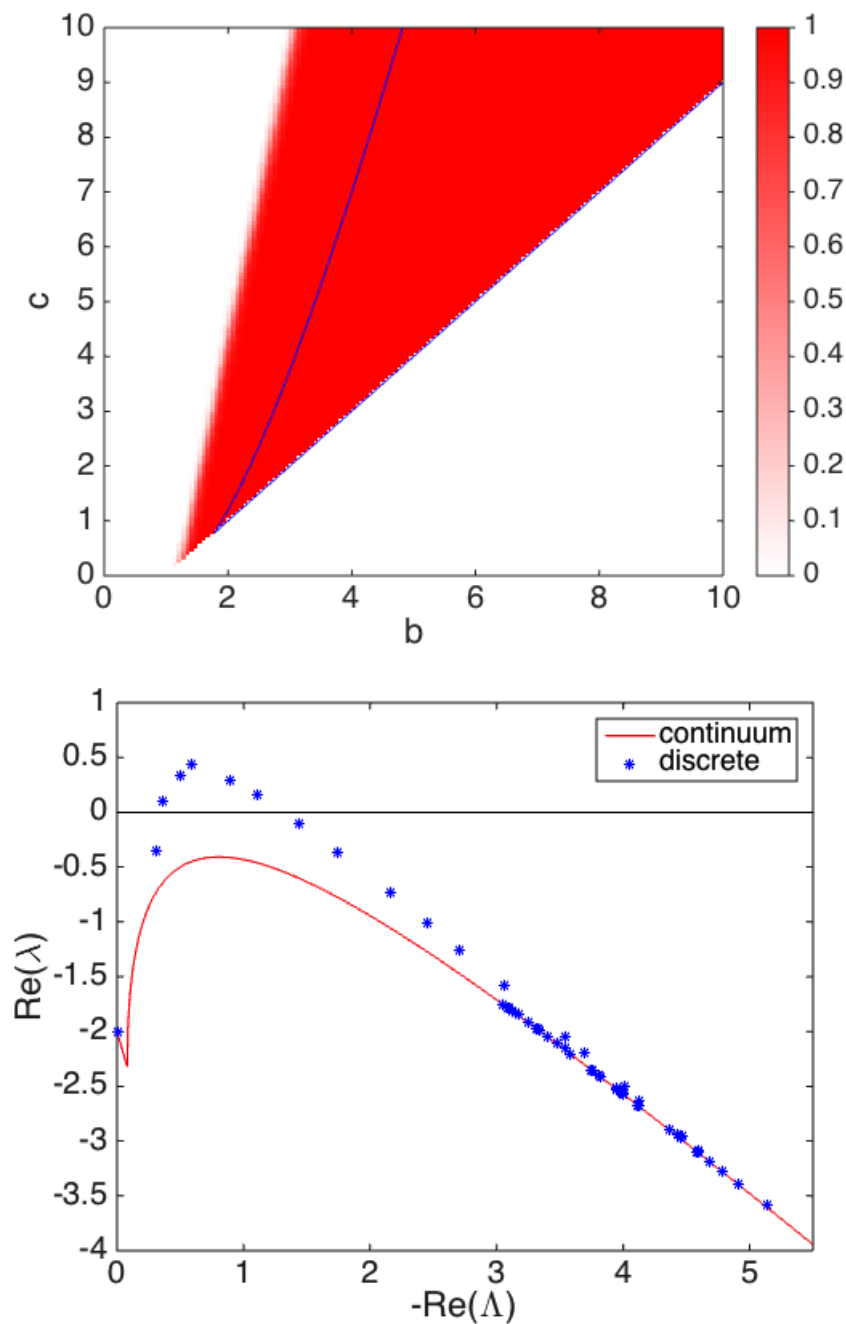
Figure 3.9: Figure up: statistics over 100 Newman-Watts directed networks with $p = 0.07$ and $k = 3$ for the Brussellator model with $D_\varphi = 1$ and $D_\psi = 7$; figure down: dispersion relation with $b = 3$ and $c = 6$.
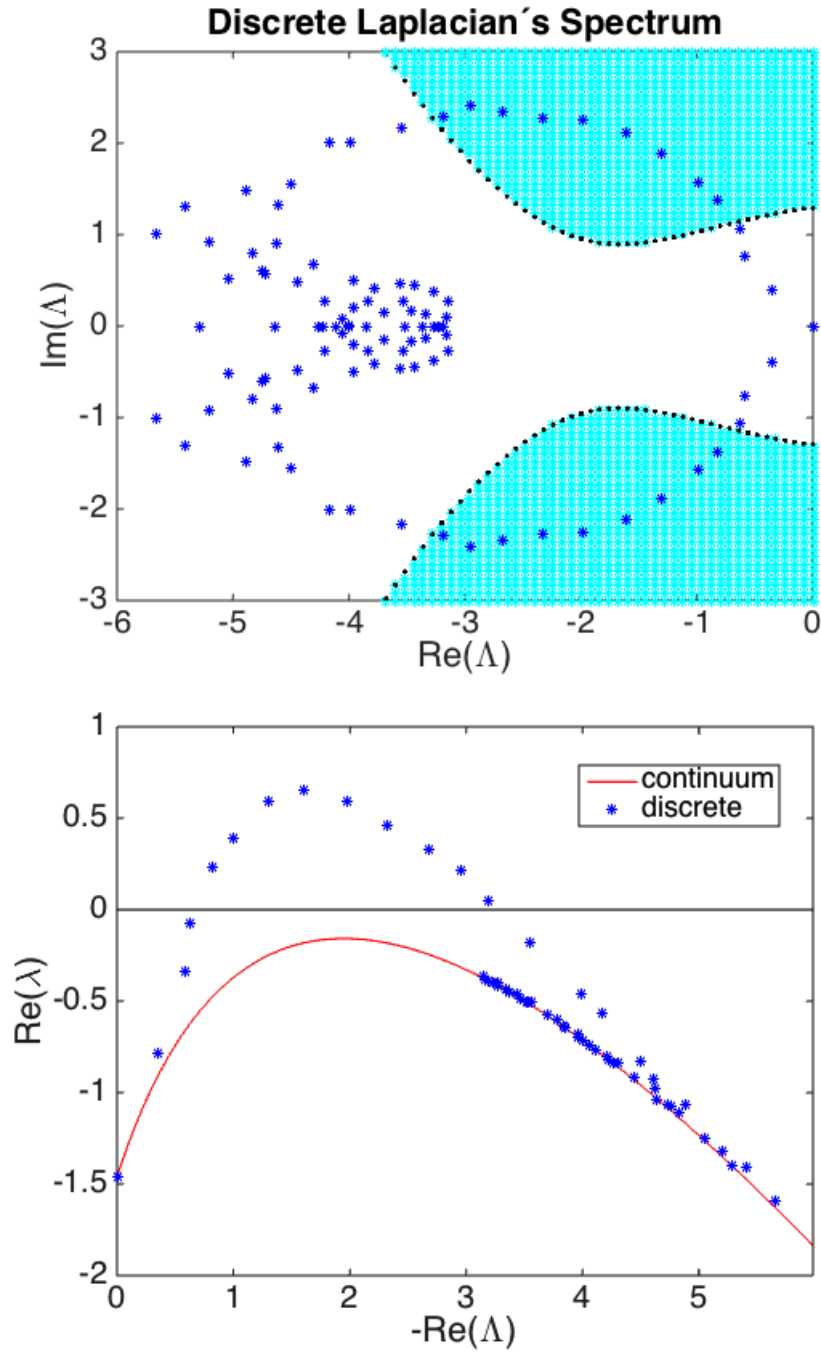
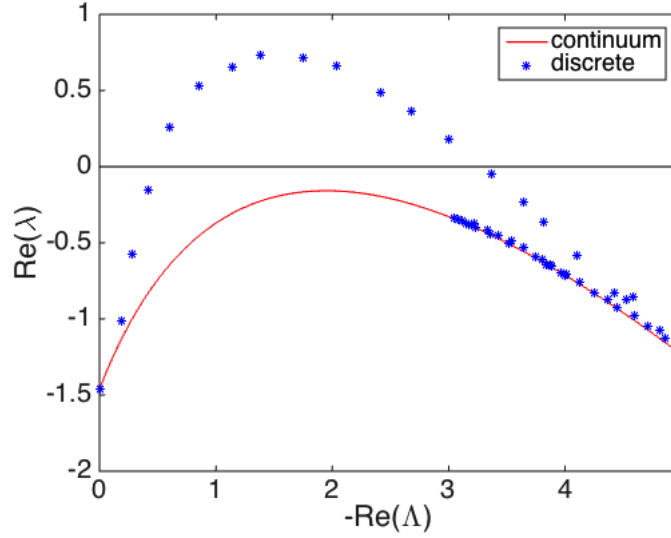**Figure 3.10:** Brussellator model with $D_\varphi = 1$, $D_\psi = 7$, $b = 9$ and $c = 30$ on a Newman-Watts directed network of 100 nodes, $p = 0.2$ and $k = 3$; on the figure up we show the Laplacian's spectrum and the instability regions (in cyan), while on the figure down we see the dispersion relation.
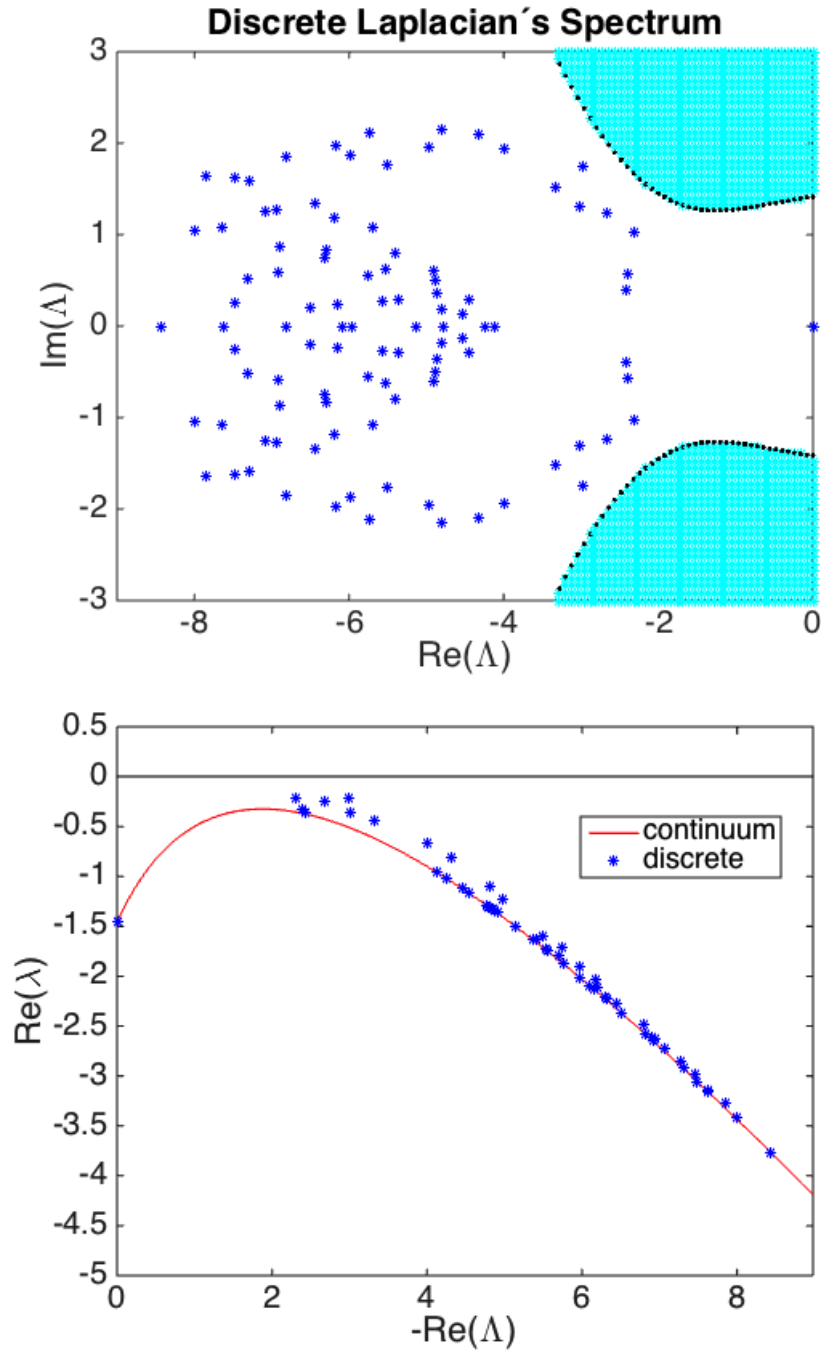
Figure 3.11: Brussellator model with $D_\varphi = 1$, $D_\psi = 6.5$, $b = 9$ and $c = 30$ on a Newman-Watts directed network of 100 nodes, $p = 0.9$ and $k = 3$; on figure up we see the Laplacian's spectrum and the instability regions (in cyan), while on the figure down we show the dispersion relation.

4   Nonnormality and Transient Dynamics

A matrix or an operator is said to be **normal** when it commutes with its transposed conjugate. Usually such matrices and operators are used in quantum mechanics [Bransden-Joachain 2000] or spectral problems [Magnus-Winkler 1966], since they admit an othornormal basis of eigenvectors, allowing to project on it an observable in a way that the sum of its components is conserved. Hence, in applications it is common to imply that the matrix or the operator describing the problem is normal. However there are some situations in which the operators are **nonnormal** and eigenvalues' analysis fails to describe the system's behavior [Trefethen et al. 1993]; such cases show interesting dynamics and give account to observations that do not match classical stability analysis. In the last years the study of nonnormal matrices and operators has become a field of interest and some notable results have been obtained, both from a pure and an applied point of view; the reference textbook for the behavior of nonnormal matrices and operators is [Trefethen-Embree 2005].

In the first part of this chapter we will introduce the concept of nonnormality giving some basic definitions and showing its effects on linear dynamics. Then we will study its effects on nonlinear dynamics, in particular on reaction-diffusion systems in which Turing patterns arise; we will see that nonnormality is necessary for Turing pattern formation and that, if we study reaction-diffusion systems on networks that are not regular lattices, a new mechanism of pattern formation emerges. A deeper and more detailed study of nonnormality will be left for the last part of this work.

4.1   Basic Definitions

Let us now give some rigorous definitions of **normal** and **nonnormal**[1] matrices.

Definition   Let $A \in \mathbb{C}^{n \times n}$ be a matrix. A is **normal** if $A^*A = AA^*$, where by A^* we denote the transposed and conjugate of A.

The next equivalent definition of *normality* can be more enlightening about the geometrical properties of such matrices:

---

[1]As for *nonlinear*, the word *nonnormal* can also be written as *non-normal*.

Definition Let $A \in \mathbb{C}^{n \times n}$ be a matrix. A is **normal** if $\exists \, U \in \mathbb{R}^{n \times n}$ *unitary* s.t. $U^T A U = D$, where $D \in \mathbb{R}^{n \times n}$ is diagonal.

In literature we can find other 89 equivalent definitions of normal matrix [Groone et al. 1987], [Elsner-Ikramov 1998]; of course such detailed study goes far beyond the aim of our work.

Definition Therefore, a **nonnormal matrix** A is a matrix s.t. $A^*A \neq AA^*$, or equivalently, a matrix that cannot be diagonalized with an orthonormal basis.

Remark From the previous definition we can assert that a nonnormal matrix is a matrix that does not have an orthonormal set of eigenvectors.

Remark A trivial observation is that every symmetric matrix is normal. However if a matrix is asymmetric, that does not automatically mean that it is nonnormal. For example *circulant matrices*[2] are asymmetric but normal [Davis 1994]; we will see an example in the next chapter.

Let us now introduce some concepts that will be fundamental throughout our work[3].

Definition Let $A \in \mathbb{C}^{n \times n}$ be a matrix; the **Hermitian part** of A is defined as

$$H(A) = \frac{A + A^*}{2}$$

The greatest real part of A's spectrum is called **spectral abscissa** $\alpha(A)$, while the greatest eigenvalue of $H(A)$ is called **numerical abscissa** $\omega(A)$; in formulas[4]

$$\alpha(A) = \sup(\Re(\sigma(A))) \tag{4.1}$$

---

[2]A *circulant matrix* is a Toeplitz matrix $C \in \mathbb{C}^{n \times n}$ s.t. every row of the matrix is a right cyclic shift of the row above, e.g.

$$C = \begin{bmatrix} a_0 & a_{n-1} & \ldots & a_2 & a_1 \\ a_1 & a_0 & a_{n-1} & \ldots & a_2 \\ \vdots & a_1 & a_0 & \ddots & \vdots \\ a_{n-2} & \ddots & \ddots & \ddots & a_{n-1} \\ a_{n-1} & a_{n-2} & \ddots & a_1 & a_0 \end{bmatrix}$$

[3]Such concepts are found in the book [Trefethen-Embree 2005] as well as in other papers that we will cite throughout the chapter ([Neubert-Caswell 1997], [Neubert et al. 2002], [Ridolfi et al. 2011] and [Asllani-Carletti 2018a]).

[4]One legitimate question would be why in the definitions of α and ω we have "*sup*" instead of "*max*", despite the fact that the spectrum of a matrix is discrete; the answer is that such definitions are more general and valid also for operators, whose spectra are discrete [Trefethen-Embree 2005].

$$\omega(A) = \sup(\sigma(H(A))) \tag{4.2}$$

When a matrix is normal, its numerical abscissa is equal to the spectral abscissa, while for a nonnormal matrix we have that $\omega > \alpha$; in principle we will use $\omega - \alpha$ as a "measure" for the *nonnormality* of a matrix.

This difference between spectral and numerical abscissa for a nonnormal matrix may have some interesting consequences on the dynamics. For instance, let us consider a linear 2×2 dynamical system of the form

$$\begin{cases} \dot{\underline{x}} = A\underline{x} \\ \underline{x}(0) = \underline{x}_0 \end{cases} \quad A \in \mathbb{R}^{2\times 2} \text{ stable and nonnormal} \tag{4.3}$$

whose solution is

$$\underline{x}(t) = e^{At}\underline{x}_0$$

The matrix being stable, $\alpha(A) < 0$, the equilibrium solution $\underline{x}^* = \underline{0}$ is stable, i.e., $e^{At} \longrightarrow 0$ as $t \longrightarrow +\infty$. A is *nonnormal*, hence $\omega(A) > \alpha(A)$. If $\omega(A) > 0$ we observe a **transient** growth of the solution before the exponential decay, as shown in figure 4.1. This transient dynamics was first studied in ecology, where ω is known as the **reactivity** of the system [Neubert-Caswell 1997].

The *numerical abscissa* gives a measure of the short time behavior of the system

$$\begin{aligned} \omega(A) := \sup_{||\underline{x}_0|| \neq \underline{0}} \left[\left(\frac{1}{||\underline{x}||} \frac{d||\underline{x}||}{dt} \right) \Big|_{t=0} \right] &= \sup_{||\underline{x}_0|| \neq \underline{0}} \left[\left(\frac{1}{||\underline{x}||} \frac{d\sqrt{\underline{x}^T \cdot \underline{x}}}{dt} \right) \Big|_{t=0} \right] \\ &= \sup_{||\underline{x}_0|| \neq \underline{0}} \left[\left(\frac{\underline{x}^T \cdot (d\underline{x}/dt) + (d\underline{x}/dt)^T \cdot \underline{x}}{2||\underline{x}||^2} \right) \Big|_{t=0} \right] \\ &= \sup_{||\underline{x}_0|| \neq \underline{0}} \left[\left(\frac{\underline{x}^T(A + A^*) \cdot \underline{x}}{2||\underline{x}||^2} \right) \Big|_{t=0} \right] \\ &= \sup_{||\underline{x}_0|| \neq \underline{0}} \left[\frac{\underline{x}^T H(A) \cdot \underline{x}}{\underline{x}_0^T \cdot \underline{x}_0} \right] \end{aligned}$$

where we have assumed $\underline{x}, \underline{x}_0$ real. From Rayleigh's principle[5] [Horn-Johnson 1985] we obtain equation (4.2). The *spectral abscissa* instead, gives us information about the long time behavior of the system

$$\alpha(A) := \sup_{||\underline{x}_0|| \neq \underline{0}} \left[\lim_{t \to +\infty} \left(\frac{1}{||\underline{x}||} \frac{d||\underline{x}||}{dt} \right) \right]$$

and, as known, the eigenvalue with the largest real part completely determines the asymptotic behavior, hence we obtain equation (4.1).

---

[5]Given a Hermitian matrix $A \in \mathbb{C}^{n \times n}$ whose smallest and largest eigenvalues are λ_{min} and λ_{max} and given $\underline{v} \in \mathbb{C}^n$ nonzero vector, we have the following relations

$$\lambda_{min} = \min_{\underline{v} \neq \underline{0}} \frac{\underline{v}^* A \cdot \underline{v}}{\underline{v}^* \cdot \underline{v}} \quad , \quad \lambda_{max} = \max_{\underline{v} \neq \underline{0}} \frac{\underline{v}^* A \cdot \underline{v}}{\underline{v}^* \cdot \underline{v}}$$
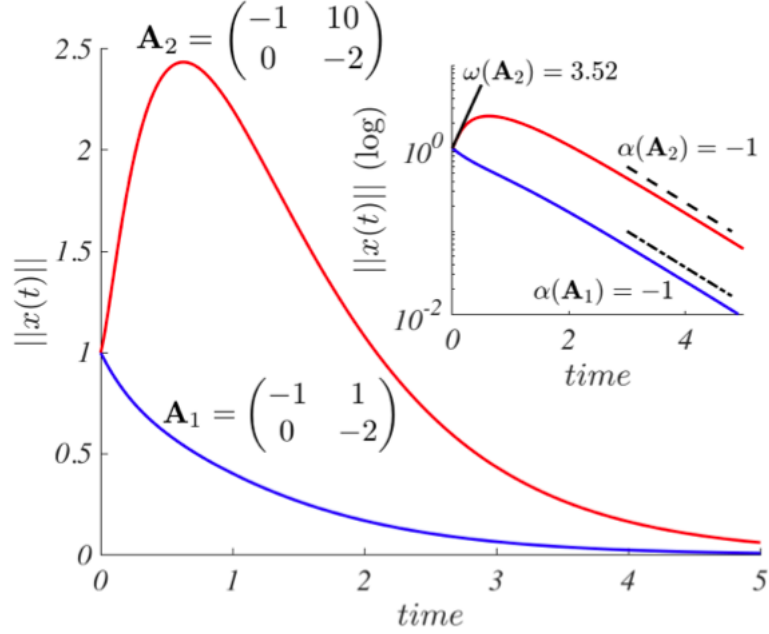
Figure 4.1: Time evolution of the norm of the solution of $\underline{\dot{x}} = A\underline{x}$ where A is nonnormal: in blue we plot the case with $A = A_1$ s.t. $0 > \omega(A_1) > \alpha(A_1)$, in red the case with $A = A_2$ s.t. $\omega(A_2) > 0 > \alpha(A_1)$; when $\omega > 0$ we observe a transient dynamics; let us notice that $\alpha(A_1) = \alpha(A_2)$; [Asllani-Carletti 2018a].

Now, with an example, let us find the general conditions for this transient dynamics. Given a matrix

$$A = \begin{bmatrix} a & b \\ c & d \end{bmatrix} \in \mathbb{R}^{2 \times 2} \tag{4.4}$$

we want its spectral abscissa to be negative and its numerical abscissa to be positive. The *Hermitian part* of A is

$$H(A) = \begin{bmatrix} a & \dfrac{b+c}{2} \\ \dfrac{b+c}{2} & d \end{bmatrix}$$

As we already said, $\alpha(A) < 0$ if $tr(A) < 0$ and $det(A) > 0$, i.e.,

$$\begin{cases} a + d < 0 \\ ad - bc > 0 \end{cases}$$

Now, to obtain $\omega(A) > 0$, we have to set $det(H(A)) < 0$, i.e.,

$$ad - \frac{(b+c)^2}{4} < 0 \iff (b+c)^2 > 4ab$$

Therefore, given a dynamical system of the form $\underline{\dot{x}} = A\underline{x}$, with A as in equation

(4.4), we observe a transient dynamics if the following conditions are matched

$$\begin{cases} a + d < 0 \\ ad - bc > 0 \\ (b + c)^2 > 4ab \end{cases} \tag{4.5}$$

Let us consider again the linear 2×2 system (4.3). This transient dynamics is easily understood intuitively thinking about the degenerate case [Mattuck et al. 2011], i.e., $\sigma(A) = \{\lambda\}$ where A is not a multiple of the identity (λ has algebraic multiplicity 2 but A has only one nonzero eigenvector)[6]. In fact, in such case the matrix has only one nonzero eigenvector $\underline{v}_1$, but, the systems being 2×2, there must be two linearly independent solutions. One is obviously

$$\underline{x}_1 = e^{\lambda t} \underline{v}_1$$

The second solution is

$$\underline{x}_2 = e^{\lambda t}(t\underline{v}_1 + \underline{v}_2)$$

where $\underline{v}_2$ is any vector satisfying

$$(A - \lambda I_{2\times 2})\underline{v}_2 = \underline{v}_1$$

Taking the Euclidean norm of the solution

$$||\underline{x}|| = ||c_1\underline{x}_1 + c_2\underline{x}_2||$$

with c_1, c_2 constants set by the initial conditions, we can see that the t multiplying the exponential in $\underline{x}_2$ is responsible for the transient growth.

However, as shown in figure 4.1, such transient growth does not occur only for the degenerate case, but for every nonnormal matrix A such that $\alpha(A) < 0$ and $\omega(A) > 0$. This fact, in the case of distinct eigenvalues, it is not as intuitive as in the degenerate case, like we are about to see.

Hence, with reference to the same system (4.3), let us consider the case of two distinct eigenvalues. We want to prove that if the norm of the solution has a maximum[7], i.e., we observe a transient growth, then the eigenvectors of the matrix are not orthogonal, i.e., the matrix is nonnormal. We will assume, without any loss of generality, the case of real eigenvalues.

Proposition Let us consider the dynamical system $\underline{\dot{x}} = A\underline{x}$, with $A \in \mathbb{R}^{2\times 2}$, $\sigma(A) = \{\lambda_1, \lambda_2\} \subseteq \mathbb{R}^-$ with $\lambda_1 \neq \lambda_2$. Let $\underline{v}_1$ and $\underline{v}_2$ be A's eigenvectors, linearly independent, and

$$\underline{x}(t) = e^{\lambda_1 t}\underline{v}_1 + e^{\lambda_2 t}\underline{v}_2$$

---

[6]If A is a multiple of the identity, the eigenvalues are repeated but there are two linearly independent eigenvectors.

[7]In principle it could be a minimum, but since we are examining the case of a stable matrix, such case is *a priori* excluded.

with c_1 and c_2 real nonzero constants set by the initial conditions. Therefore

$$\frac{d}{dt}||\underline{x}(t)|| = 0 \implies \underline{v}_1^T \cdot \underline{v}_2 \neq 0$$

or, in an equivalent formulation, if the system undergoes a transient dynamics, then the matrix has nonorthogonal eigenvectos, i.e., it is nonnormal.

Proof Let

$$\underline{v}_1 = \begin{bmatrix} w_1 \\ w_2 \end{bmatrix} \quad \text{and} \quad \underline{v}_2 = \begin{bmatrix} u_1 \\ u_2 \end{bmatrix}$$

Obviously $\underline{v}_1 \neq \underline{0}$ and $\underline{v}_2 \neq \underline{0}$.
If we compute the norm we obtain

$$||\underline{x}|| = \sqrt{c_1^2 e^{2\lambda_2 t} \underline{v}_1^T \cdot \underline{v}_1 + c_2^2 e^{2\lambda_2 t} \underline{v}_2^T \cdot \underline{v}_2 + c_1 c_2 e^{(\lambda_1+\lambda_2)t} \underline{v}_1^T \cdot \underline{v}_2} = \sqrt{f(t)}$$

Hence

$$\frac{d}{dt}||\underline{x}|| = \frac{1}{\sqrt{f(t)}} f'(t)$$

and, because $f(t) \neq 0 \ \forall \ t$, we have that

$$\frac{d}{dt}||\underline{x}|| = 0 \iff f' = 0$$

$$f'(t) = 2\lambda_1 c_1^2 e^{2\lambda_1 t} \underline{v}_1^T \cdot \underline{v}_1 + 2\lambda_2 c_2^2 e^{2\lambda_2 t} \underline{v}_2^T \cdot \underline{v}_2 + (\lambda_1 + \lambda_2)c_1 c_2 e^{(\lambda_1+\lambda_2)t} \underline{v}_1^T \cdot \underline{v}_2$$

Let us rename

$$\begin{cases} 2c_1^2 e^{2\lambda_1 t} \underline{v}_1^T \cdot \underline{v}_1 = f_1(t) > 0 \ \forall t \\ 2c_2^2 e^{2\lambda_2 t} \underline{v}_2^T \cdot \underline{v}_2 = f_2(t) > 0 \ \forall t \\ c_1 c_2 e^{(\lambda_1+\lambda_2)t} \underline{v}_1^T \cdot \underline{v}_2 = f_3(t) \neq 0 \ \forall t \iff \underline{v}_1^T \cdot \underline{v}_2 \neq 0 \end{cases}$$

Hence

$$f'(t) = \lambda_1 f_1(t) + \lambda_2 f_2(t) + (\lambda_1 + \lambda_2)f_3 \tag{4.6}$$

Remembering that $\lambda_1, \lambda_2 < 0$, looking at equation (4.6), we can conclude that $f' = 0$ only if $c_1 c_2 \underline{v}_1^T \cdot \underline{v}_2 < 0$, therefore $\underline{v}_1^T \cdot \underline{v}_2 \neq 0$, i.e., A is nonnormal.

$\square$

Here we have seen the effects of nonnormality on linear dynamics; therefore, the system being linear, we can observe only short term effects. In fact, after a transient growth, the solutions will inevitably decay with an exponential rate towards the stable equilibrium. In the next section we will study such effects on nonlinear systems, observing richer and more interesting behaviors.

4.2 Turing-Like Instability on Symmetric Support

In this section we will see the effects of nonnormality on Turing pattern formation. First we will reproduce some known results[8] for what concerns continuum support; then, for reaction-diffusion systems on symmetric networks, we will show an original result: a new mechanism of pattern formation beyond the one described by Turing. We will call this extension of Turing theory **Turing-like pattern formation**.

Let us consider a reaction-diffusion system of two species on continuum support

$$\begin{cases} \dfrac{\partial}{\partial t}\varphi(\underline{x}, t) = f(\varphi, \psi) + D_\varphi \nabla^2 \varphi(\underline{x}, t) \\[4mm] \dfrac{\partial}{\partial t}\psi(\underline{x}, t) = g(\varphi, \psi) + D_\psi \nabla^2 \psi(\underline{x}, t) \end{cases} \quad \text{with } \underline{x} \in \mathbb{R}^n,\ t \in \mathbb{R}^+$$

The extended Jacobian of the system is

$$\tilde{J} = J_0 - k^2 D = \begin{bmatrix} f_\varphi - k^2 D_\varphi & f_\psi \\ g_\varphi & g_\psi - k^2 D_\psi \end{bmatrix}$$

and its Hermitian part is

$$H(\tilde{J}) = \begin{bmatrix} f_\varphi - k^2 D_\varphi & \dfrac{f_\psi + g_\psi}{2} \\[3mm] \dfrac{f_\psi + g_\psi}{2} & g_\psi - k^2 D_\psi \end{bmatrix}$$

Remembering Section 1.1, let us recall the perturbation vector in the Fourier space

$$\underline{\mu}_k = \begin{bmatrix} \delta\varphi_k \\ \delta\psi_k \end{bmatrix} \equiv \underline{\mu}$$

and the transformed linearized reaction-diffusion system, that can be written in compact form as

$$\underline{\dot{\mu}} = \tilde{J}\underline{\mu}$$

We know that, if the eigenvalues of $\tilde{J}$ have negative real part, Turing instability does not emerge.
Let us now assume that the eigenvalues of $H(J_0)$ are negative, so without the diffusion the system does not admit transient dynamics. Let us study how the norm of the perturbation vector evolves in time

$$||\underline{\dot{\mu}}|| = \frac{d}{dt}\sqrt{\underline{\mu}^T \cdot \underline{\mu}} = \frac{\underline{\mu}^T(\tilde{J} + \tilde{J}^T) \cdot \underline{\mu}}{2||\underline{\mu}||} = \frac{\underline{\mu}^T H(\tilde{J}) \cdot \underline{\mu}}{\underline{\mu}^T \cdot \underline{\mu}}||\underline{\mu}||$$

---

[8]See for example [Neubert-Caswell 1997], [Neubert et al. 2002], [Ridolfi et al. 2011] and [Biancalani et al. 2017].

If we denote with $\tilde{\lambda}$ the largest eigenvalue of $H(\tilde{J})$, by Rayleigh's principle [Horn-Johnson 1985] we have that

$$\frac{\underline{\mu}^T H(\tilde{J}) \cdot \underline{\mu}}{\underline{\mu}^T \cdot \underline{\mu}} \leq \tilde{\lambda}$$

therefore we obtain that

$$||\underline{\dot{\mu}}|| \leq \tilde{\lambda}||\underline{\mu}||$$

and if $\tilde{\lambda} < 0$ the perturbation goes to zero. Now, a straightforward computation of the Hermitian parts gives us the following relation

$$H(\tilde{J}) = H(J_0) - \frac{k^2}{2}D \tag{4.7}$$

In order to say something about the eigenvalues of $H(\tilde{J})$, we need the following theorem [Horn-Johnson 1985]:

Weyl's Theorem Let $A, B \in \mathbb{C}^{n \times n}$ be Hermitian matrices and let the respective eigenvalues of A, B and $A + B$ be

$$\{\lambda_i(A)\}_{i=1}^n \quad , \quad \{\lambda_i(B)\}_{i=1}^n \quad , \quad \{\lambda_i(A+B)\}_{i=1}^n$$

and let us arrange the eigenvalues in nondecreasing order

$$\lambda_{min} = \lambda_1 \leq \lambda_2 \leq \cdots \leq \lambda_{n-1} \leq \lambda_n = \lambda_{max}$$

Then $\forall \, i \in \{1, ..., n\}$

$$\lambda_i(A + B) \leq \lambda_{i+j}(A) + \lambda_{n-j}(B) \quad j \in \{0, 1, ..., n-i\} \tag{4.8}$$

with equality for some pair i, j if and only if $\exists$ a nonzero verctor $\underline{v} \in \mathbb{C}^n$ s.t.

$$A\underline{v} = \lambda_{i+j}(A)\underline{v} \quad \wedge \quad B\underline{v} = \lambda_{n-j}(B)\underline{v} \quad \wedge \quad (A + B)\underline{v} = \lambda_i(A + B)\underline{v}$$

Also $\forall \, i \in \{1, ..., n\}$

$$\lambda_{i-j+1}(A) + \lambda_j(B) \leq \lambda_i(A + B) \quad j \in \{0, 1, ..., i\} \tag{4.9}$$

with equality for some pair i, j if and only if $\exists$ a nonzero verctor $\underline{v} \in \mathbb{C}^n$ s.t.

$$A\underline{v} = \lambda_{i-j+1}(A)\underline{v} \quad \wedge \quad B\underline{v} = \lambda_j(B)\underline{v} \quad \wedge \quad (A + B)\underline{v} = \lambda_i(A + B)\underline{v}$$

If A and B have no common eigenvector, then inequalities (4.8) and (4.9) are strict.

Since both matrices of the right hand-side of equation (4.7) have negative eigenvalues, from Weyl's Theorem, equation (4.8), the largest eigenvalue of $H(\tilde{J})$ is negative and so the perturbation will always go zero, i.e., the system will never admit Turing instability; hence, in order to observe Turing patterns, J_0 has to be nonnormal and s.t. $\omega(J_0) > 0$, i.e., the reaction part (the model) has to be nonnormal

[Neubert et al. 2002].

We have demonstrated that transient dynamics is necessary for Turing pattern formation. Now we would like to study into details $\omega(\tilde{J})$. We want to obtain the transient dynamics, hence $tr\tilde{J} < 0$ and $det\tilde{J} > 0$ (from which Turing conditions are obtained) and then we need to set $detH(\tilde{J}) < 0$

$$(f_\varphi - k^2 D_\varphi)(g_\psi - k^2) - \frac{(f_\psi + g_\psi)^2}{4} < 0$$

$$D_\varphi D_\psi k^4 - (g_\psi D_\varphi + f_\varphi D_\psi)k^2 + f_\varphi g_\psi - \frac{(f_\psi + g_\psi)^2}{4} < 0$$

that is a parabola in k^2 which has the minimum ($D_\varphi D_\psi > 0$) for

$$k_{min}^2 = \frac{g_\psi D_\varphi + f_\varphi D_\psi}{2D_\varphi D_\psi}$$

that is also the value of k^2 that maximizes $\omega(\tilde{J})$. Of course, to be admissible, it has to be positive and that happens if

$$g_\psi D_\varphi + f_\varphi D_\psi > 0$$

When such condition is not matched, we need to study $\omega(J_0)$, that is positive if

$$detH(J_0) < 0 \iff (g_\varphi + f_\psi)^2 > 4f_\varphi g_\psi$$

We have then obtained the following conditions for ω to be positive, the first one when it is maximized by a nonzero k, the other one by $k = 0$

$$\begin{cases} g_\psi D_\varphi + f_\varphi D_\psi > 0 \\ (g_\varphi + f_\psi)^2 > 4f_\varphi g_\psi \end{cases} \tag{4.10}$$

Let us consider the Brussellator model on continuum support and let us study $\omega(\tilde{J})$.
We can recall from Chapter 1 the extended Jacobian

$$\tilde{J} = \begin{bmatrix} b - 1 - k^2 D_\varphi & c \\ -b & c - k^2 D_\psi \end{bmatrix}$$

and the equalities defining the boundaries of the Turing domain in the parameter space

$$\begin{cases} c = b - 1 \\ \\ c = \frac{D_\psi}{D_\varphi}(b + 1)\left\{1 - \sqrt{1 - \frac{(b-1)^2}{(b+1)^2}}\right\} \end{cases}$$

Now we can substitute conditions (4.10), also considered as equalities, to obtain

$$
\begin{cases}
c = (b-1)\frac{D_\psi}{D_\varphi} \\
c = -(b-2) + \sqrt{b^2 - 4b + 3} \\
c = -(b-2) - \sqrt{b^2 - 4b + 3}
\end{cases}
\tag{4.11}
$$

The Turing's conditions give us the Turing instability region, the first equation of 4.11 together with the second Turing's condition give us the region where $\omega(\tilde{J})$ is maximized by

$$
\bar{k} = \sqrt{\frac{-cD_\varphi + (b-1)D_\psi}{2D_\varphi D_\psi}}
$$

the first equation of 4.11 together with the second and third gives us the region in which $\omega(\tilde{J})$ is maximized by $k = 0$ and finally the second and third equations of 4.11 give us the region where $\omega(\tilde{J}) < 0$. The results are displayed in figure 4.2.

Let us now compute $\omega(\tilde{J})$ above the Turing bifurcation curve, i.e., where $\alpha(\tilde{J}) < 0$, as depicted in figure 4.3. We observe that the numerical abscissa increases with the parameters. We can explain qualitatively this fact looking at the form of

$$
J_0 = \begin{bmatrix} b-1 & c \\ -b & c \end{bmatrix}
$$

In fact as b and c increase we have more and more difference between the anti-diagonal elements of J_0, which are the ones that give the nonnormality, as we have seen in the previous section. Therefore we can say that, in a reaction-diffusion system of two species, the nonnormality is due to the asymmetric inter-species interaction; this fact is perfectly in line with what we know about Turing instability: in fact, recalling Murray's qualitative example in Chapter 1, we see that only when the interactions between species are asymmetric[9], we can observe Turing patterns.

Outside the Turing region (above the Turing bifurcation curve) patterns on continuum support are transient due to $\omega(\tilde{J})$ as it has been found by [Neubert et al. 2002] and [Ridolfi et al. 2011]. In figure 4.4 we show a generic solution for the Brussellator just outside the Turing region on a symmetric regular lattice, that for our numerical methods is equivalent to the continuum support[10]. If we work on discrete support, and by that we mean a symmetric network which is not a regular lattice, things should be in principle equivalent[11], as long as the support is symmetric, i.e.,

---

[9]The fire activates the reaction and diffuses slower than the grasshoppers, which inhibit the reaction; [Murray 1989].

[10]In our numerical simulations, while for the temporal part we use the Runge-Kutta IV explicit method [Press et al. 1986], for the spatial part, i.e., the Laplacian, we use the finite difference method; so if we deal with a symmetric network that is a regular lattice, there is no difference (numerically) between the continuum case and the discrete one.

[11]Of course there are differences, since the dispersion relation is discrete. For the numerical abscissa $\omega(\tilde{J})$, things works as for the dispersion relation, as we have studied in Chapter 2: analytically the regions are the same and so is the value of ω; in practice, if we exclude extreme cases, we can assert that for a symmetric network we have always $\omega(\tilde{J}_k) = \omega(\tilde{J}_\alpha)$. We have verified such fact numerically and that is what we will assume.
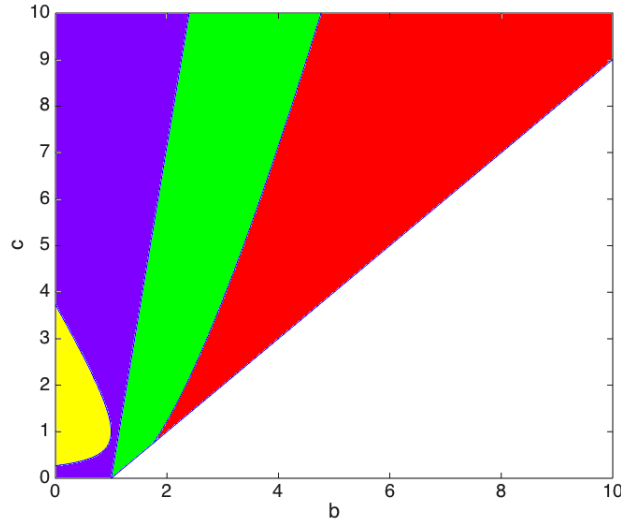
Figure 4.2: From Turing conditions and equations (4.11) we can divide the parameters's space in 4 areas: the area in yellow is where $\omega(\tilde{J}) < 0$, in purple is where $\omega(\tilde{J})$ is maximized by $k = 0$, in green is where $\omega(\tilde{J})$ is maximized by $\bar{k} = \sqrt{(-cD_\varphi + (b-1)D_\psi)/(2D_\varphi D_\psi)}$ and the area in red is the Turing region; Brussellator model with $D_\varphi = 0.07$ and $D_\psi = 0.5$.

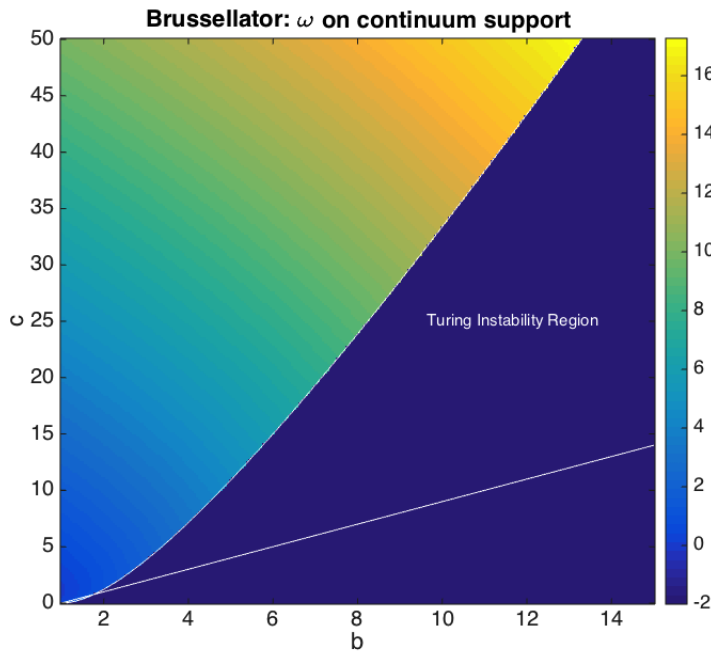
Figure 4.3: Values of $\omega(\tilde{J})$ above the Turing bifurcation curve for the Brussellator model with $D_\varphi = 0.07$ and $D_\psi = 0.5$; note that above the Turing instability region $\alpha(\tilde{J}) < 0$.
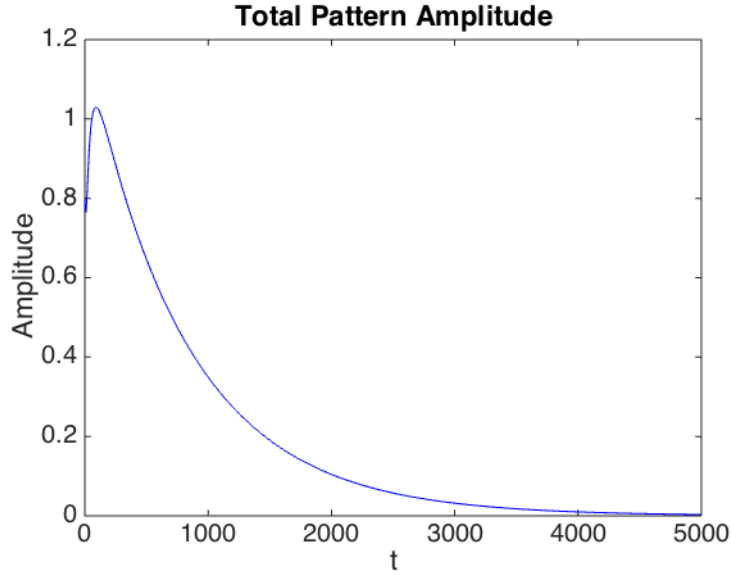
Figure 4.4: Transient patterns outside the Turing region for the Brussellator on a regular lattice of 100 nodes and 100 links (a symmetric ring); $b = 12.7$, $c = 47$, $D_\varphi = 0.07$ and $D_\psi = 0.5$; the initial perturbation is 0.1.

undirected networks.

Surprisingly, when the support is not a regular lattice, after a transient growth the solution may stabilize in an inhomogeneous equilibrium, i.e., a pattern, for high values of $\omega(\tilde{J})$ just above the Turing bifurcation curve. After the perturbation the system remains stable, so those are not Turing patterns but rather **Turing-like** patterns. In figure 4.6 we show an example of Turing-like pattern for the Brussellator on an Erdős-Rényi network. This new mechanism of pattern formation may be the result of interaction between the nonlinearities of the model and the structure of the network. However a definitive answer on the subject has not been found yet and probably it will be difficult to find, since we are dealing with a nonlinear phenomenon; we will come back to this matter in the last part of our work. The important fact is that, outside the Turing region, if ω is high enough, the solutions experience a significant transient growth and, if the network is not a regular lattice, they may stabilize in a Turing-like pattern.

To have a better understanding of this phenomenon we have written a code which maps the plane (b, c) and, in a region above the Turing bifurcation curve, it integrates the Brussellator's equations looking for the patterns. In this way we obtain, as an output, a figure with the Turing region and, if there is pattern formation outside it, a possible extension of it; we will call such procedure *mapping*. In figure 4.7 we show the results of such *mapping* for the Brussellator on an Erdős-Rényi Network for two iterations. If we look again at figure 4.3, we see that we have Turing-like patterns for high values of $\omega(\tilde{J})$.

Figure 4.5: Turing-like patterns for the Brussellator on a symmetric Erdős-Rényi Network of 100 nodes and $p = 0.5$; $b = 12.7$, $c = 47$, $D_\varphi = 0.07$ and $D_\psi = 0.5$; the initial perturbation is 0.1.

Figure 4.7: *Mapping* of Turing-like patterns: in yellow the Turing region and in shades of red the patterns outside Turing region; Brussellator model with $D_\varphi = 0.07$ and $D_\psi = 0.5$ on a Erdős-Rényi Network of 100 nodes and $p = 0.5$; 2 iterations; the initial perturbation is 0.1.
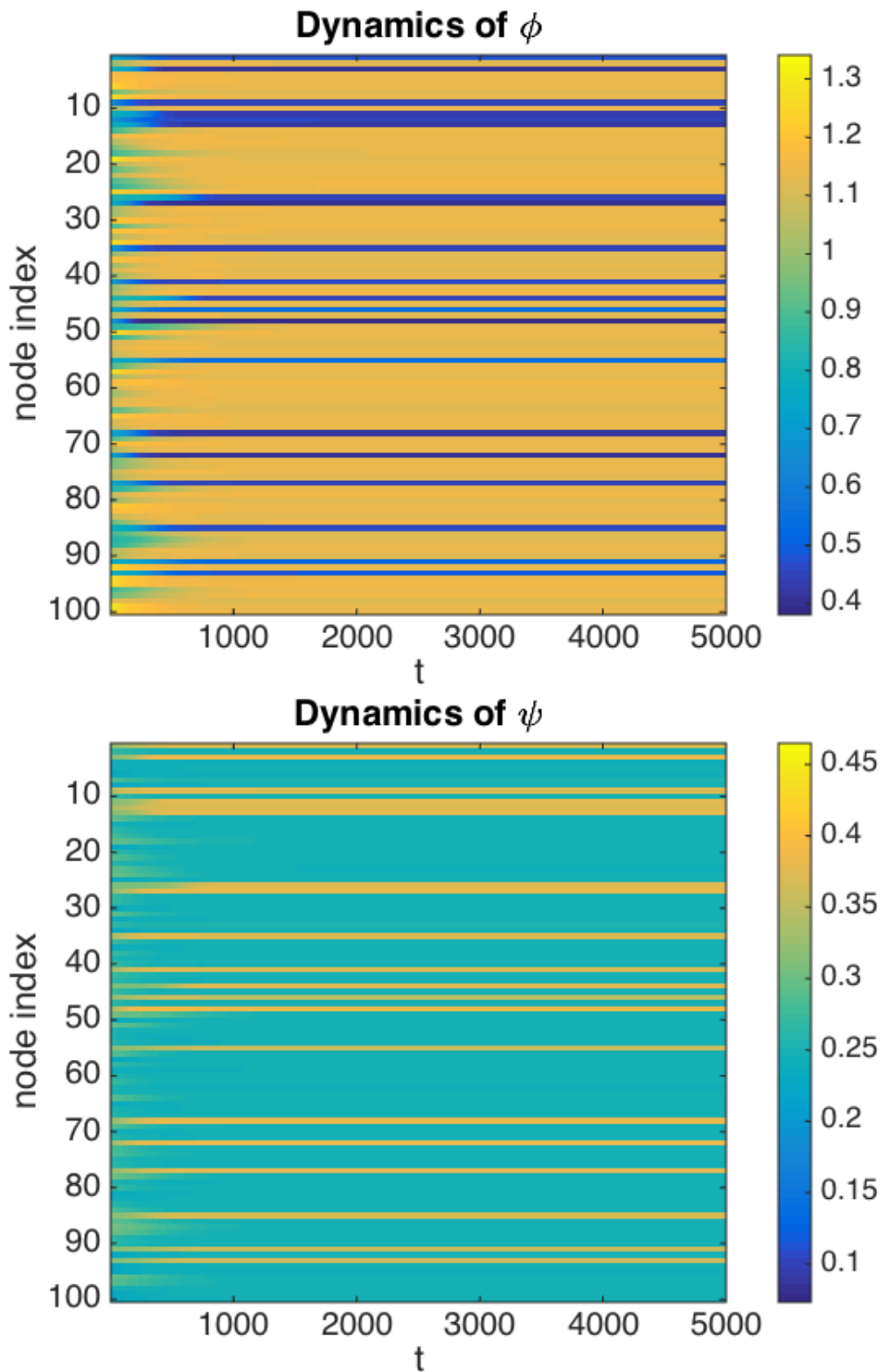

Figure 4.6: Turing-like pattern amplitude for the Brussellator on a symmetric Erdős-Rényi Network of 100 nodes and $p = 0.5$; $b = 12.7$, $c = 47$, $D_\varphi = 0.07$ and $D_\psi = 0.5$; the initial perturbation is 0.1.
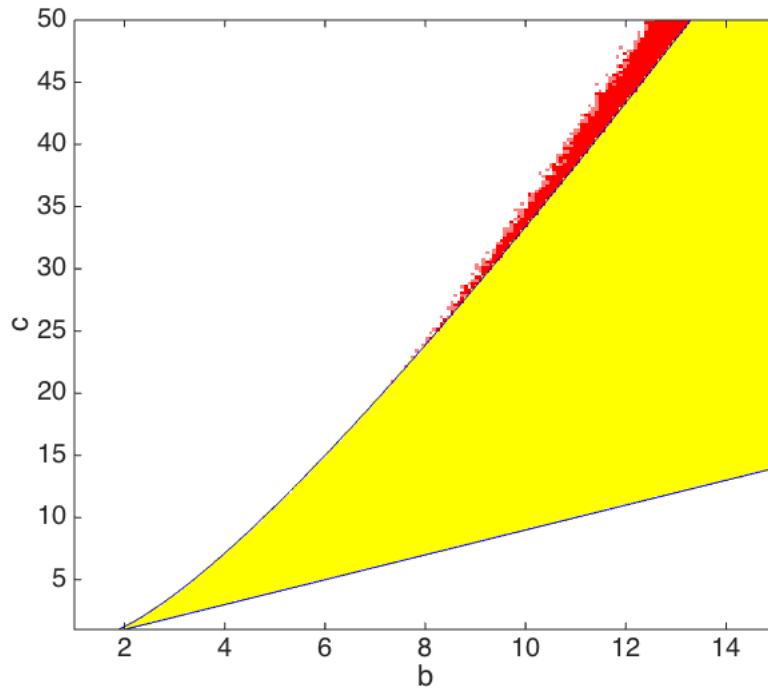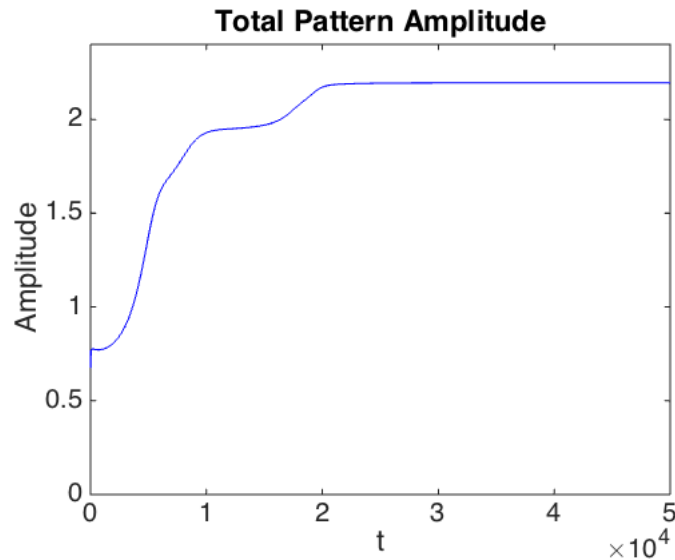
Remark   We shall stress the fact that the dynamics depends on the initial conditions, i.e., the perturbation of the fixed point[12], therefore we cannot obtain a relation between the value of $\omega(\tilde{J})$ and the transient growth.

One important question would be how, given a model with fixed parameters, we could increase the Turing region due to Turing-like pattern formation. For what we have seen above, we cannot act on the reaction part of the system, hence we need to act "from outside".

To reconnect with the case studied in Section 1.3, we could ask weather the effects of a drift can affect $\omega(\tilde{J})$. Therefore let us compute $\omega(\tilde{J})$ for the Brussellator with drift, first with $\Delta v = 0$, that we remember being the same as the case without drift, and then with $\Delta v = 9$. As we can observe in figures 4.8, with an external drift $\omega(\tilde{J})$ does not increase.
This fact can be understood analytically. Given two matrices

$$A = \begin{bmatrix} a_{11} & a_{12} \\ a_{21} & a_{22} \end{bmatrix} \quad \text{and} \quad B = \begin{bmatrix} a_{11} + ix & a_{12} \\ a_{21} & a_{22} \end{bmatrix} \quad , \quad a_{11}, a_{12}, a_{21}, a_{22}, x \in \mathbb{R}$$

let us fix $a_{11}, a_{12}, a_{21}, a_{22}$ varying only x and let us name

$$\Re(\lambda_{max}(A)) = \beta(0) \quad \text{and} \quad \Re(\lambda_{max}(B)) = \beta(x)$$

It can be shown with a Taylor expansion that

- for $x \to 0$ we have

$$\beta(x) = \beta(0) - \frac{2a_{12}a_{21}}{[(a_{11} + a_{22})^2 - 4(a_{11}a_{22} - a_{12}a_{21})]^{\frac{3}{2}}} x^2 + o(x^3)$$

- for $x \to \pm\infty$ we have

$$\beta(x) = \beta(0) + \frac{(a_{11} - a_{22})^2}{[(a_{11} + a_{22})^2 - 4(a_{11}a_{22} - a_{12}a_{21})]^{\frac{3}{2}}} + o\left(\frac{1}{x}\right)$$

Now, returning to our case of the Brussellator, we have that

$$a_{11} = b - 1 - k^2 D_\varphi \ , \quad a_{12} = a_{21} = \frac{c - b}{2} \ , \quad a_{22} = -c - k^2 D_\psi \ , \quad x = k\Delta v$$

$$A = H(\tilde{J}) \ , \quad B = H(\tilde{J}_{drift}) \ , \quad \beta(0) = \omega(\tilde{J}) = \omega(0) \ , \quad \beta(x) = \omega(\tilde{J}_{drift}) = \omega(\Delta v)$$

we have that

- for $\Delta v \to 0$

$$\omega(\Delta v) \simeq \omega(0) - C(\Delta v)^2 \quad \text{with} \ C > 0$$

---

[12]Details on how it is obtained numerically are given in Appendix C.

- for $\Delta v \to \pm\infty$

$$\omega(\Delta v) \simeq \omega(0) + D \quad \text{with} \quad D < 0$$
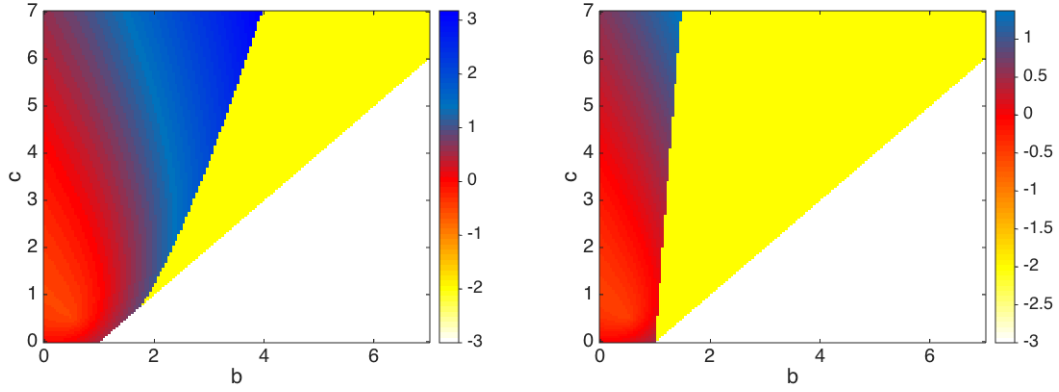
Figure 4.8: Values of $\omega(\tilde{J})$ for the Brussellator with $D_\varphi = 0.07$ and $D_\psi = 0.5$; on the left we show the case $\Delta v = 0$, while on the right we show the case with $\Delta v = 9$; we can observe from the colorbar that the value of $\omega(\tilde{J})$ does not change significantly as the drift changes.
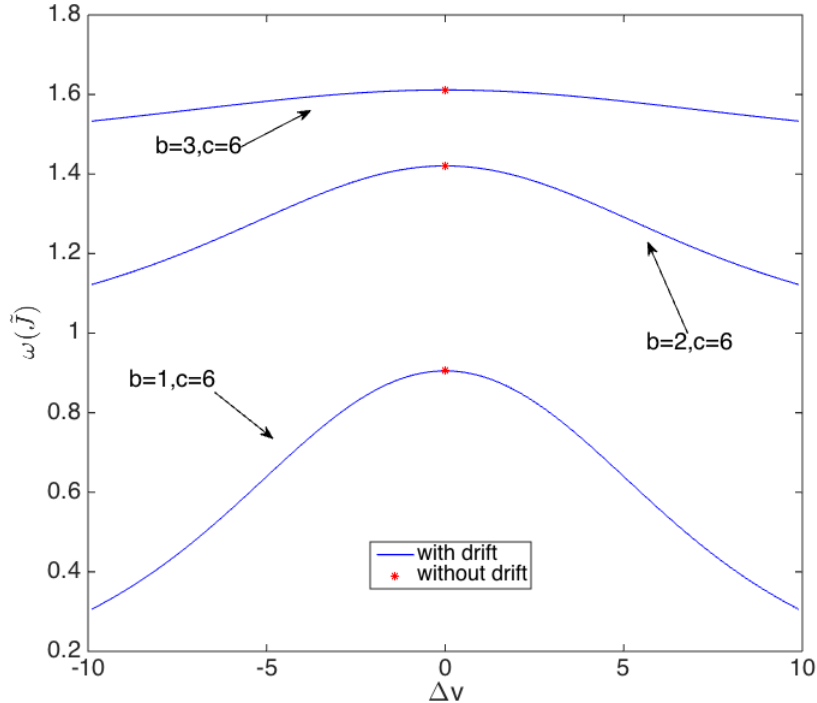
Figure 4.9: Variation of $\omega(\tilde{J})$ in function of the drift for different values of the model's parameters; as predicted analytically, $\omega(\tilde{J})$ does not increase due to the drift, but it decreases.

Therefore, when the system in subject to an external drift, $\omega(\tilde{J})$ always decreases. In figure 4.9 we show the variation of $\omega(\tilde{J})$ as a function of Δv for different values of (b, c) outside the Turing region. We can observe that in the neighborhood of $\Delta v = 0$, ω is a negative parabola, as predicted by the Taylor expansion.

In this chapter we have studied a **new** mechanism of pattern formation, that is **Turing-like** and not Turing because patterns stabilize in a region where, after a small perturbation, the system remains stable and should, in principle, asymptotically converge to the stable homogeneous state. However, we find Turing-like patterns only for high values of the model's parameters (figure 4.7), implying, for what we have studied throughout this chapter, strongly asymmetric inter-species interactions. We may remember from Chapter 1 that it is not easy to observe Turing patterns experimentally, due to the difficulty in obtaining such different diffusivities; we can assume that it would be even more difficult to recreate experimentally a setting where the inter-species interactions are so asymmetric. Moreover, if we study a system subject to a drift we have seen that its nonnormality does not increase, hence, in order to obtain Turing-like patterns for lower values of the model's parameters and enlarge the Turing region, it would be necessary to "put" the nonnormality in the diffusion part, i.e., we need a nonnormal support.

5

Pattern Formation on Nonnormal Networks

In the previous chapter, we have studied definitions and properties of nonnormal matrices and their effects on linear and nonlinear dynamics. We have seen that nonnormality is necessary for Turing pattern formation and, starting from the work of Neubert and colleagues [Neubert et al. 2002], we have identified a new mechanism of pattern formation on networks, which extends the classical Turing picture.

However, we observe Turing-like patterns only when the inter-species interactions are very asymmetric and we have explained that this setting may be difficult to be observed and reproduced experimentally. Moreover, we have shown that a drift external to the system does not affect significantly the nonnormality and consequently Turing-like pattern formation. Therefore we have argued that in principle it would be possible to observe Turing-like patterns for *realistic values*[1] of the model's parameters by studying the system on a nonnormal support (i.e., network), that is what we will do in this chapter.

In the first part of the chapter, we will introduce nonnormal networks, we will discuss their effects on linear dynamics and describe an algorithm to generate them. Then we will study reaction-diffusion systems on nonnormal networks and elaborate on their effects on nonlinear dynamics. Then, for the Brussellator model, we will observe Turing-like patterns also for low values of the reaction parameters. This is indeed the main result of this thesis. Such effect will be explained analytically in the next chapter.

5.1   Nonnormal Networks

Let us recall that a matrix A is *nonnormal* if $AA^* \neq A^*A$ and this means that its eigenvectors are not orthogonal. The definition of nonnormal network is straightforward.

---

[1]Since we are dealing with toy models with pedagogical aim, such as the Brussellator, the word *realistic* may seem out of place. However what we mean is that we are trying to get as realistic as possible, given the aim of our study.

Definition   A **nonnormal network** is a network s.t. its adjacency matrix is nonnormal.

Remark   In principle we can say that a network, whose adjacency matrix is A, is "more" nonnormal the larger $\omega(A) - \alpha(A)$ is. In the next chapter, it will be clear that other quantities can be introduced to quantify the non-normality of a given network, depending on the specific target of the analysis.

How can we generate numerically nonnormal networks such that $\omega - \alpha$ is significantly greater than zero? Let us proceed in an intuitive way.

We are looking for a network whose adjacency matrix does not possess an orthogonal set of eigenvectors, then for sure it has to be asymmetric (necessary but not sufficient condition for nonnormality)[2], that, for a network, means directionality. So let us start with the simplest possible case, a directed ring, whose adjacency matrix is

$$R = \begin{bmatrix} 0 & 1 & 0 & 0 & \dots & 0 \\ 0 & 0 & 1 & 0 & \dots & 0 \\ \vdots & \ddots & \ddots & \ddots & \ddots & \vdots \\ \vdots & \ddots & \ddots & \ddots & \ddots & \vdots \\ 0 & \dots & \dots & \dots & 0 & 1 \\ 1 & 0 & \dots & \dots & 0 & 0 \end{bmatrix}$$

Such matrix is circulant, hence it is normal ($RR^* - R^*R = 0$) [Davis 1994]. An immediate step towards the nonnormality would be to remove a link to obtain an open directed ring, whose adjacency matrix is then the canonic Jordan form

$$\tilde{R} = \begin{bmatrix} 0 & 1 & 0 & 0 & \dots & 0 \\ 0 & 0 & 1 & 0 & \dots & 0 \\ \vdots & \ddots & \ddots & \ddots & \ddots & \vdots \\ \vdots & \ddots & \ddots & \ddots & \ddots & \vdots \\ 0 & \dots & \dots & \dots & 0 & 1 \\ 0 & \dots & \dots & \dots & 0 & 0 \end{bmatrix}$$

hence $\tilde{R}\tilde{R}^* \neq \tilde{R}^*\tilde{R}$. Obviously such adjacency matrix can be achieved removing any link, not just the last one, and then renumbering the nodes.

The effects on the dynamics of R and $\tilde{R}$ can be understood with a simple and pedagogic example found in [Asllani-Carletti 2018a], paper that will serve as a guideline throughout the whole section.

Let us set 11 as the number of nodes of the inspected network and study the following dynamical system

$$\dot{x}_i = -ax_i + D \sum_{j=1}^{11} L_{ij} x_j$$

---

[2]We know that *nonnormal⇒asymmetric* but *asymmetric⇏nonnormal*.

where $a, D \in \mathbb{R}^+$, that is a diffusion equation with a sink term.

If we consider as a support the network whose adjacency matrix is R, independently of the system's parameters and the initial conditions, all the solutions will go to the equilibrium solution (the null one, in this case) following almost the same path, as shown in figure 5.1(a). If, instead, we consider the system on the network with $\tilde{R}$ as adjacency matrix, we observe that, if $D >> a$, we obtain a transient growth in the $11-th$ node, as shown in figure 5.1(b), where are plotted the solutions for each node and the solution's norm $||\underline{x}|| = \sqrt{x_1^2 + ... + x_{11}^2}$. Such phenomenon is very simple to understand physically: since the diffusion is much faster than the damping, we will have an accumulation in the last node before the solution goes to zero. And also mathematically we can appreciate this fact by looking at the explicit solution (remember that in this case $n = 11$)

$$\underline{x}(t) = c_1\underline{v}_1 + c_2 t^{n-2} e^{\lambda_2 t}\underline{v}_2 + c_3 e^{\lambda_3 t}\underline{v}_3$$

where $\lambda_1 = 0$, $\lambda_2 < 0$ and $\lambda_3 < 0$ are the nonnormal matrix' eigenvalues (λ_2 with multiplicity $n - 2$), $\underline{v}_1$, $\underline{v}_2$ and $\underline{v}_3$ are the associated eigenvectors and c_1, c_2 and c_3 are constants set by the initial conditions. As for the 2×2 linear case, the transient growth is due to the t that multiplies the solution related to the degenerate eigenvalue.

Thus it is obvious which is the way to follow if we want to generate a network that can affect the dynamics due to its nonnormality.

Let us point out that, in applications, we can deal with networks that in principle are symmetric and may become nonnormal due to the dynamics. For instance, a subway is a clear example of symmetric network[3]: in fact each line is crossed by the same number of trains both ways. However, at the rush hour, we can imagine that the majority of people will move from the suburbs to the center, giving the effect of the network whose adjacency matrix is $\tilde{R}$. Nevertheless, a directed open ring is not a suitable support for realistic[4] models; hence, to make such a network realistic, we need to consider that there still would be a few people traveling from the center to the suburbs and add some return links.

With that in mind, in the work [Asllani-Carletti 2018a] a method is described to generate nonnormal networks inspired by the Newman-Watts algorithm [Newman 2010] which somehow resembles networks found in applications. The idea is to start from a directed ring whose links are randomly weighted between 0 and a real number $\gamma > 1$; in this way we obtain the effect of a strong directionality but also the "open ring" effect, because between different links we might have a remarkable difference of weights. Then, to make such support suitable for applications, we add random return links and long range links, both with small weights compared to the directed ring. The algorithm is the following:

- we fix three parameters $\gamma > 1$, $p_1 \in [0, 1]$ and $p_2 \in [0, p_1]$;

---

[3]A subway can be thought as a network considering the stops as nodes and the railways as links.
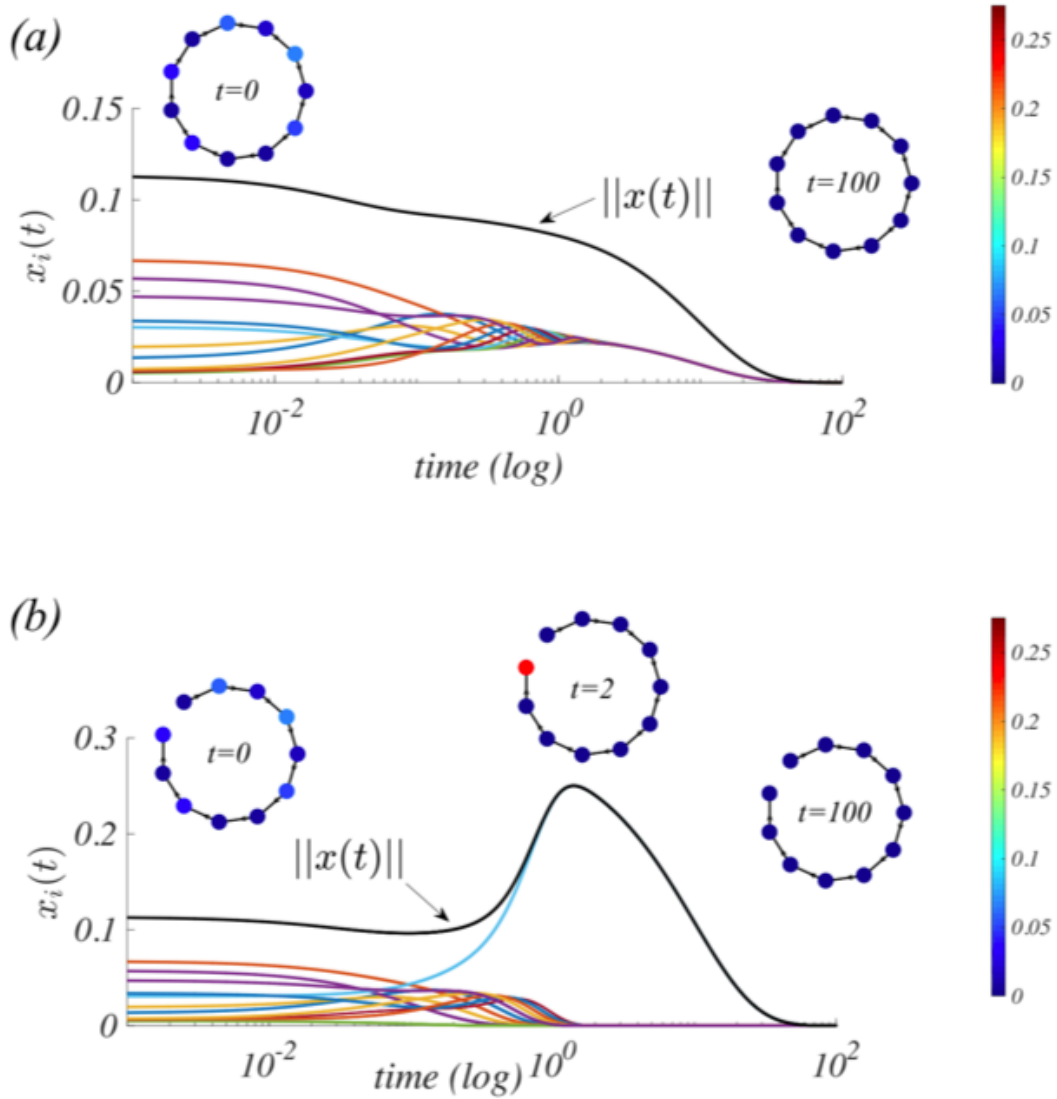
[4]See the first note of this chapter.

Figure 5.1: If we have a directed ring we do not observe any particular effect on the dynamics (a), while if we remove a link we have a transient dynamics typical of nonnormal systems, as we have seen in the previous chapter; from [Asllani-Carletti 2018a].
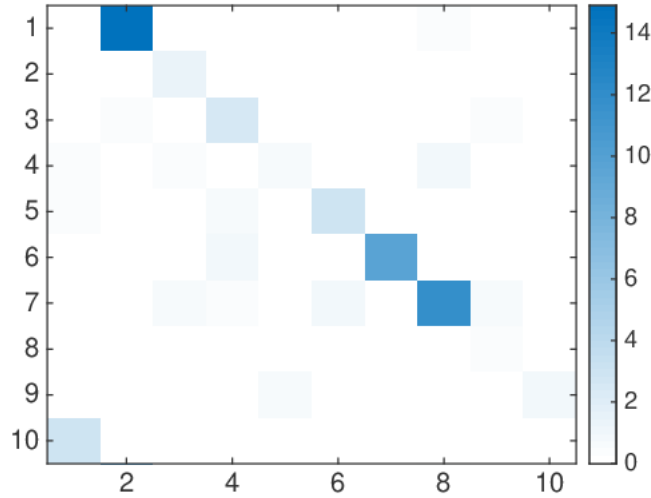
Figure 5.2: Example of a nonnormal network obtained with the algorithm described in [Asllani-Carletti 2018a].

- we generate a complete directed ring of n nodes whose links are weighted with $\gamma \cdot r_i$ where r_i, for $i = 1, ..., n$, is a uniformly distributed random number between 0 and 1;

- with probability p_1 we add return links to the ring weighted with uniformly distributed random numbers between 0 and p_1;

- with probability p_2 we add short cut links weighted with uniformly distributed random numbers between 0 and p_2.

As an outcome we obtain a network whose structure is similar to that shown in figure 5.2. Such networks have been proven to affect the reaction-diffusion dynamics of one species [Asllani-Carletti 2018a].

For example, if we set $n = 10$, $\gamma = 15$, $p_1 = 0.5$ and $p_2 = 0.2$ we obtain a network whose adjacency matrix is

$$
A = \begin{bmatrix}
0 & 14.9005 & 0 & 0 & 0 & 0 & 0 & 0.4604 & 0 & 0 \\
0 & 0 & 1.3887 & 0 & 0 & 0 & 0 & 0 & 0.0373 & 0 \\
0 & 0.2946 & 0 & 2.5029 & 0 & 0 & 0 & 0 & 0.4363 & 0 \\
0.4641 & 0.1644 & 0.4049 & 0 & 0.6844 & 0 & 0 & 0.7382 & 0 & 0 \\
0.2887 & 0 & 0 & 0.5629 & 0 & 2.8810 & 0 & 0 & 0 & 0 \\
0 & 0 & 0 & 0.7237 & 0 & 0 & 9.7321 & 0 & 0 & 0 \\
0 & 0 & 0.5841 & 0.2392 & 0 & 0.9274 & 0 & 11.8492 & 0.6418 & 0 \\
0 & 0 & 0 & 0 & 0 & 0.0528 & 0.0467 & 0 & 0.4372 & 0 \\
0 & 0 & 0 & 0 & 0.5270 & 0 & 0 & 0.1495 & 0 & 0.7505 \\
2.9927 & 0 & 0 & 0 & 0 & 0 & 0 & 0 & 0 & 0
\end{bmatrix}
$$

Figure 5.3: Adjacency matrix of a nonnormal network of *nodes* $= 10$, $\gamma = 15$, $p_1 = 0.5$ and $p_2 = 0.2$.

that can be better visualized in figure 5.3. A is such that $\omega(A) - \alpha(A) = 4.2406$, hence we are dealing with a nonnormal network. From now on, unless otherwise specified, when we talk about a *nonnormal network*, we are referring to a network generated with the above algorithm.

Remark To be fair, at the end of the algorithm we should have written "we *could* obtain", the one above being a stochastic algorithm; however what we have observed during our copious numerical simulations is that in most cases such algorithm has as an output a nonnormal network. Moreover, as we show in figure 5.4, on average, we have a nonnormal network whose *nonnormality* increases with γ.

Remark With this method we generate networks that are *unbalanced*, i.e., networks s.t. $k_i^{in} \neq k_i^{out} \ \forall \ i \in \{1, ..., n\}$.

Given a network whose adjacency matrix is A, the magnitude in which we are interested in is $(\omega(A) - \alpha(A))$ and we will us it to measure the **nonnormality of the network**[5]. A question that might arise is which are the optimal values for the number of nodes n and the parameters of the algorithm γ, p_1, and p_2 such that the nonnormality is maximized. First of all we can observe from figure 5.4 that the nonnormality is proportional to the parameter γ; then we see from figures 5.5 that, for this generating scheme, the nonnormality drops when the number of nodes increases; finally we can assert, looking at figures 5.6, that varying p_1 does not affect the nonnormality, while p_2 has a slight, though not significant, effect.
A more detailed characterization of the properties of such networks varying the parameters would be possible but it goes beyond the aim of this work; however the

---

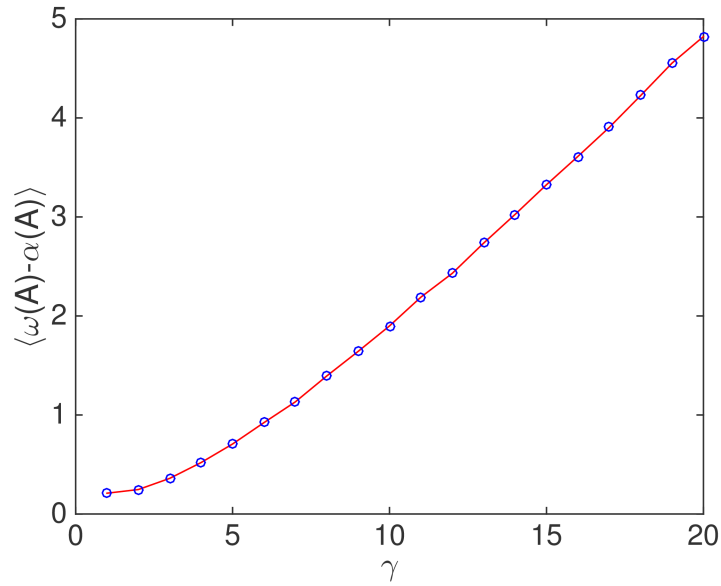[5]As already stated in the text, such measure of nonnormality is not completely accurate.

Figure 5.4: $\langle \omega(A) - \alpha(A) \rangle$ for each value of γ over 10000 nonnormal networks of 10 nodes with $p_1 = 0.5$ and $p_2 = 0.2$; we see that the *nonnormality* increases more or less linearly with γ.
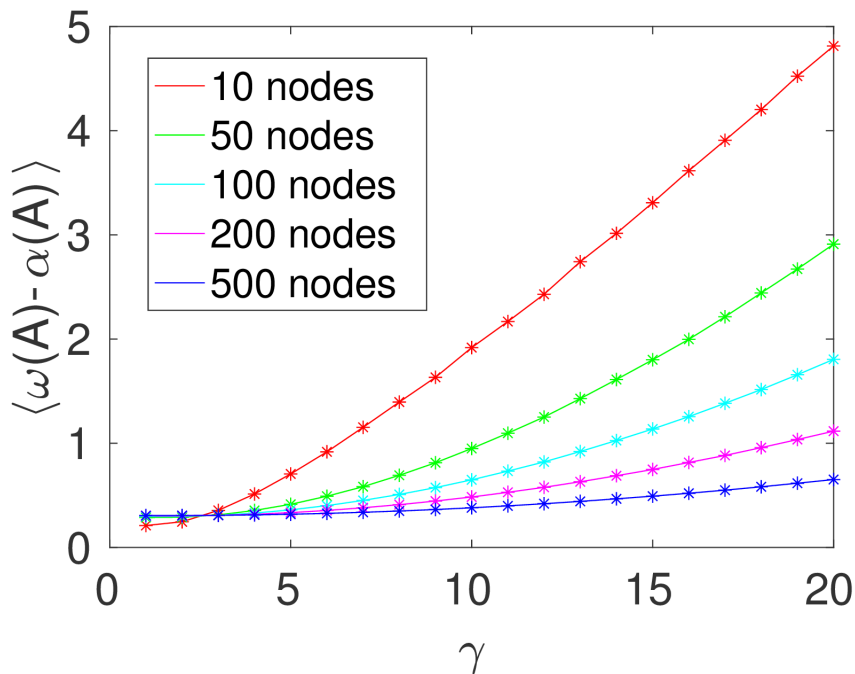

Figure 5.5: $\langle \omega(A) - \alpha(A) \rangle$ for each value of γ over 10000 nonnormal networks with $p_1 = 0.5$ and $p_2 = 0.2$; we see that the *nonnormality* decreases as the number of nodes increases.
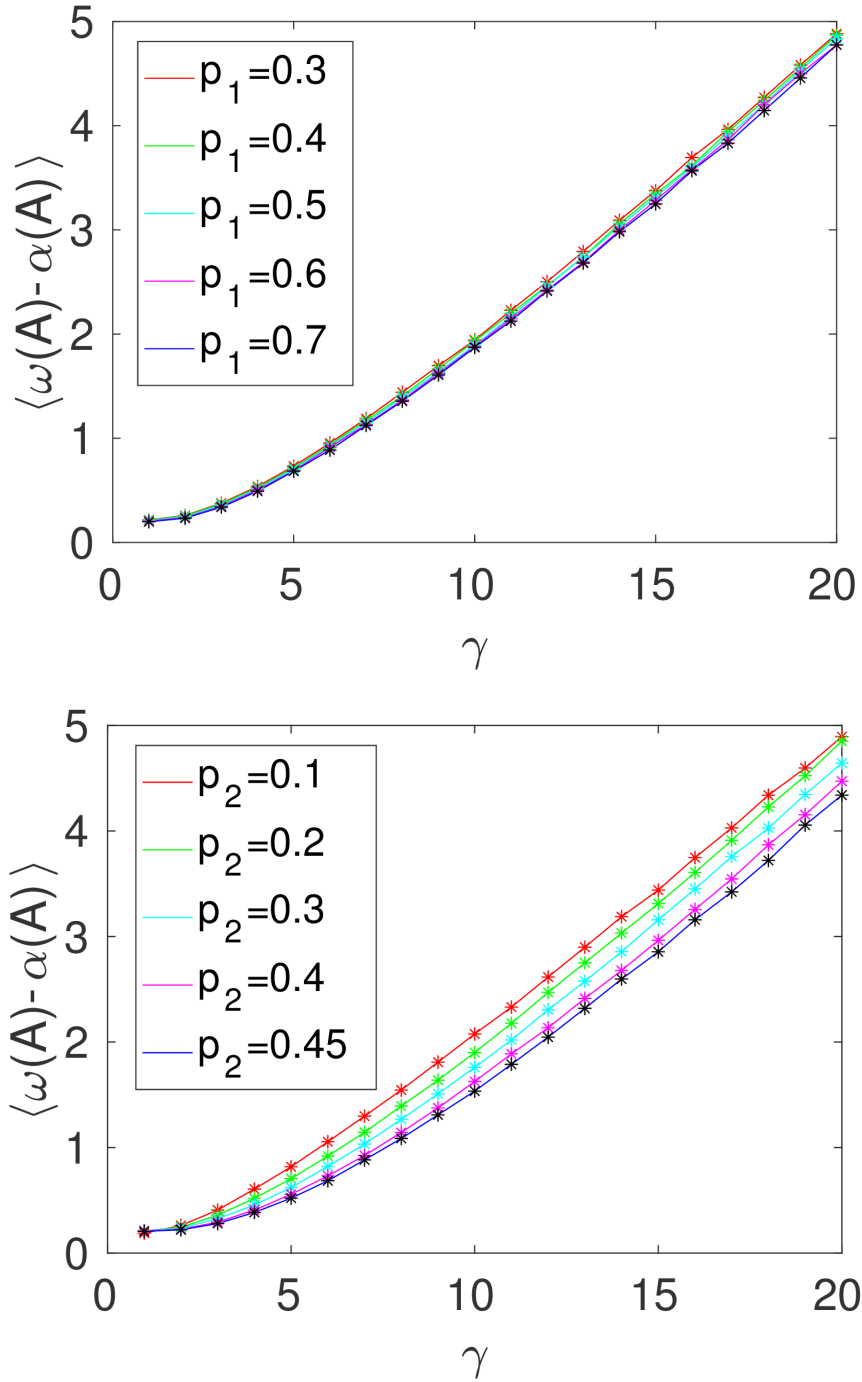
Figure 5.6: $\langle \omega(A) - \alpha(A) \rangle$ for each value of γ over 10000 nonnormal networks; left: *nodes* = 10 and $p_2 = 0.2$; right: *nodes* = 10 and $p_1 = 0.5$.

next step would be to find the **optimal nonnormal network**, i.e., the network whose adjacency matrix A has the largest possible $\langle \omega(A) - \alpha(A) \rangle$.

We can conclude this section affirming that, despite the lack of an analytic sufficient condition for the nonnormality of the network, the intuitive method illustrated formerly ensures us, at least in average, a network whose $\langle \omega(A) - \alpha(A) \rangle$ is sufficiently large if some conditions are verified, i.e., $\gamma \gtrsim 15$ and $nodes \simeq 10$. Those are the networks that will be used in the next section, where we will extend Turing theory of pattern formation to the study of reaction-diffusion systems of two species on nonnormal networks.

5.2 Turing-Like Instability on Nonnormal Networks

In this section, we are going to study Turing pattern formation for reaction-diffusion systems on nonnormal networks generated with the method described in the previous section. Considering that we want to observe Turing patterns, the system has to be intrinsically nonnormal [Neubert et al. 2002], but now the nonnormality is also external and can be increased or decreased changing the spatial support.

Before proceeding, it is necessary to state a few remarks.

Remark Before studying the model, let us point out that the networks that we will use are unbalanced, therefore, in order to develop our theory, we need the diffusion-like operator $\mathcal{L}$ instead of the Laplacian L, for the reason discussed at the end of Chapter 2.

Remark Regardless the fact that the diffusion-like operator does not conserve the mass, we will still develop our theory using the Brussellator model, that is a schematization of a chemical reaction where, indeed, the mass should be conserved. However such model is nothing but a *toy model*, i.e., a model with pedagogical aim that does not describe a real process, therefore it is suitable for an abstract and general extension of Turing's theory. Nevertheless, if one was about to study an actual model and to use $\mathcal{L}$ as a diffusion operator, she/he should either work on a balanced network (see Appendix D) or focus on settings where the number of particles is not conserved, e.g., neural networks or electric networks [Newman 2010]. In fact, due to their functioning, we expect such networks to be nonnormal [Asllani-Carletti 2018b].

We will not go through the calculations to obtain the conditions for Turing instability on discrete support again, as they can be found in Chapter 3. Let us consider the Brussellator model on a nonnormal network of n nodes and let us use,

for the reasons mentioned above, the diffusion-like operator $\mathcal{L}$

$$
\begin{cases}
\dot{\varphi}_i(t) = 1 - (b+1)\varphi_i(t) + c\varphi_i^2(t)\psi_i(t) + D_\varphi \sum_{j=1}^{n} \mathcal{L}_{ij}\varphi_j(t) \\[4ex]
\dot{\psi}_i(t) = b\varphi_i(t) - c\varphi_i^2(t)\psi_i(t) + D_\psi \sum_{j=1}^{n} \mathcal{L}_{ij}\psi_j(t)
\end{cases}
\qquad \forall\, i \in \{1, ..., n\} \quad (5.1)
$$

Integrating numerically equations (5.1), we find pattern formation outside the Turing region, i.e., Turing-like patterns, for low values of the model's parameters[6]. In figures 5.7 we show an example of Turing-like patterns where the parameters are $b = 5$ and $c = 6$ and the support is a nonnormal network of 10 nodes, generated using as parameters $\gamma = 15$, $p_1 = 0.5$ and $p_2 = 0.2$, whose nonnormality is $\omega(A) - \alpha(A) = 5.24$ (details in Appendix C). We see in figure 5.8 that the related dispersion relation is negative. The initial perturbation is $\varepsilon = 0.1$.
This result, though expected, is surprising: in fact Turing-like patterns for such low values of the model's parameters and for tiny perturbations cannot be observed on a symmetric support.

Remark Turing-like patterns depend on the initial conditions; for this reason, since our perturbation of the homogeneous equilibrium is random (details in Appendix C), we may have to repeat the numerical integration in order to find Turing-like patterns. However, for the case on nonnormal networks, as we will show in figure 5.14 (the one on the left hand side), we always observe a significant transient growth, even when the patterns do not stabilize.

Remark Turing-like patterns do not depend on the diffusion operator, as we show in Appendix D. There we study the system on a balanced network, hence using the "standard" discrete Laplacian L, and we still observe Turing-like patterns.

To better understand this new process of pattern formation, we have performed a numerical experiment: the idea is to integrate numerically the Brussellator's equation outside the Turing region for both a nonnormal network and a symmetric network and observe when and for which parameters we have Turing-like pattern formation. In order to do that, we have used the *mapping* code we have written to make figure 4.7 described in Section 4.2. We have iterated the *mapping* 10 times, to make sure to capture also the patterns that are more difficult to obtain. We used as a support a nonnormal network of 10 nodes and $\gamma = 15$ (the one used for figures 5.7 and 5.8) and a symmetric network obtained by symmetrizing the former, i.e., if A is the adjacency matrix of the nonnormal network, $\tilde{A} = (A + A^*)/2$ is the adjacency matrix of the symmetric network (details in Appendix C). The results

---

[6]At the end of last chapter we have explained into details that we are able to obtain Turing-like patterns on certain symmetric networks only for high values of the model's parameters, implying strong asymmetric inter-species interactions, and we would try to achieve Turing-like patterns for low values of the parameters.
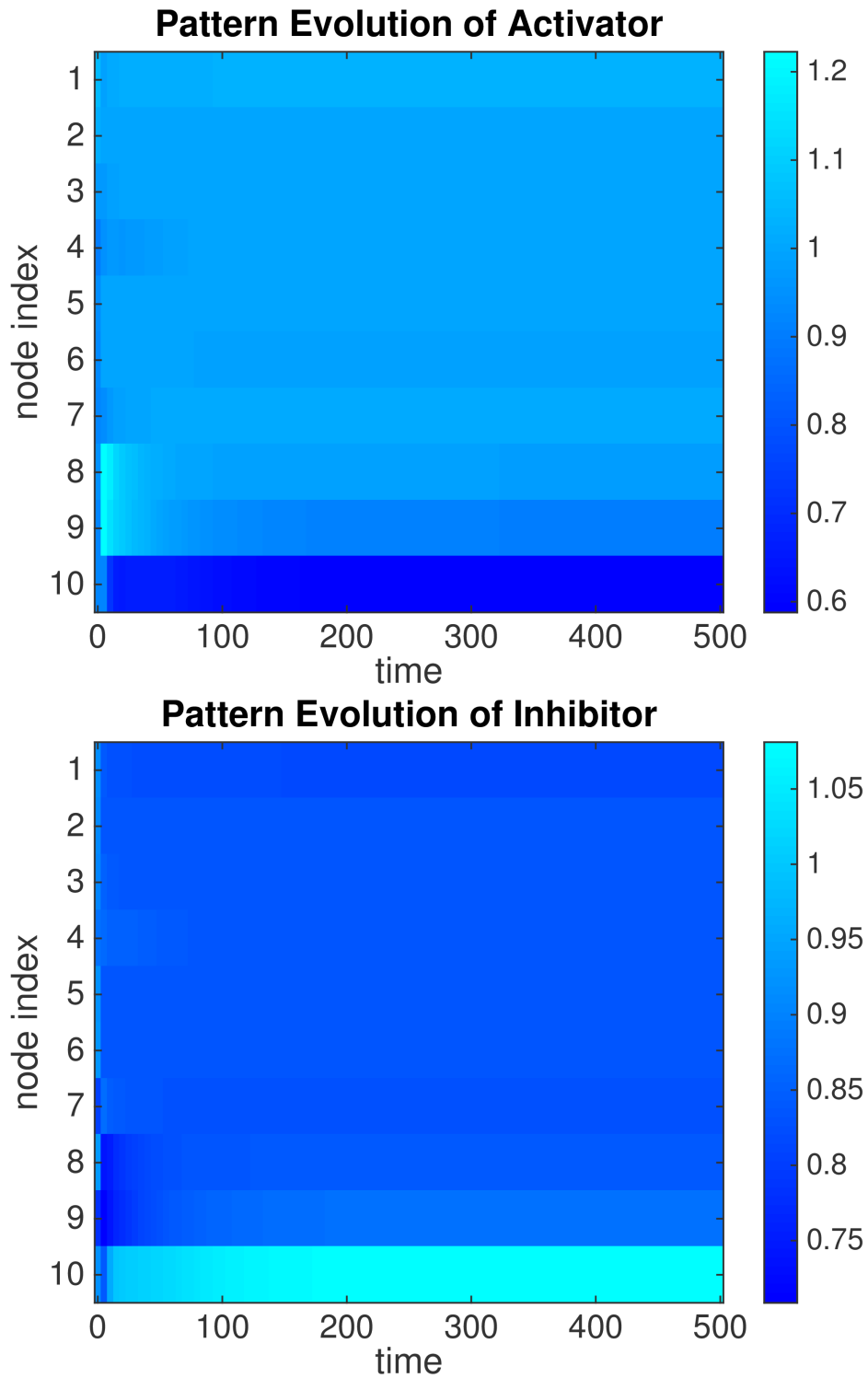
Figure 5.7: Turing-like patterns for the Brussellator on a nonnormal network; $D_\varphi = 0.1$, $D_\psi = 0.385$, $b = 5$, $c = 6$ and $\varepsilon = 0.1$.
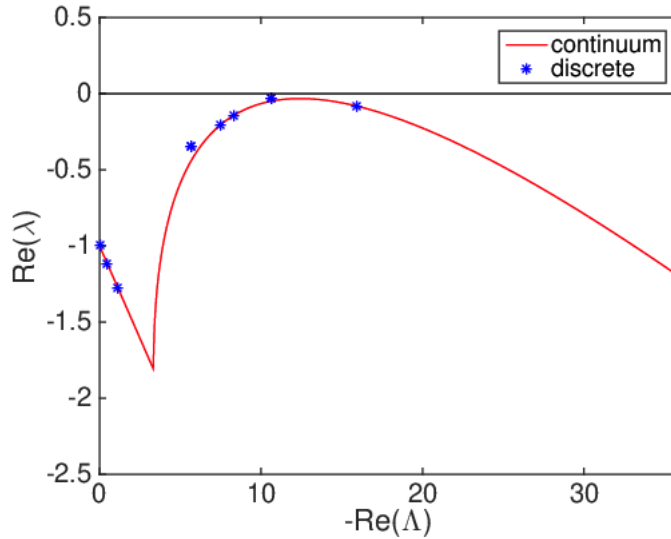
Figure 5.8: Dispersion relation for the Brussellator with $D_\varphi = 0.1$, $D_\psi = 0.385$, $b = 5$ and $c = 6$; we see 8 eigenvalues for a 10 nodes network because there are two couples of complex conjugate eigenvalues.

of these simulations are shown in figures 5.9, where we see that when the network is symmetric we do not have Turing-like patterns for low values of the parameters (as for the cases examined in Chapter 4), while, when the support is nonnormal network, such new patterns arise. Hence it is quite clear that this new phenomenon is given by the network's properties.

Remark In figures 5.9 we have cut out Turing-like patterns for $b < 4$, because, for such values of the parameters, even outside the Turing region, the system is under the influence of the Hopf bifurcation and our code may misinterpret slow oscillations towards the equilibrium with Turing-like patterns. In fact, the code used to make figures 5.9 is considerably slow, since, in the (b, c) plane, for every point in a stripe above the Turing bifurcation curve, it integrates the Brussellator's equations. In order to "capture" Turing-like patterns once they have stabilized, we need to choose a stopping time for the numerical integration that is sufficiently long. However, a stopping time necessary for oscillations close to the Hopf bifurcation to stabilize, would increase significantly the running time.

Remark From what we have studied in Section 3.2, we know that the sole fact that the network is directed may enlarge the Turing region. However, as it is obvious from figure 5.8, in the case we are considering, the discrete dispersion relation is almost coincident with the continuous one, hence the Turing-like patterns we see in figure 5.9 on the left are due to the nonnormality. On the other hand, in figures 5.10 we show the *mapping* for a case where both effects must be considered: in green we have denoted Turing pattern due to the directedness of the network and in red we have denoted Turing-like patterns, that are due to the nonnormality of the network.

Phenomenologically we can observe from figures 5.7 that the patterns due to the nonnormality are localized in a small percentage of nodes, while in the rest we have only slight variations with respect to the fixed point. Recalling figures 4.5 we can see that this fact had already emerged; indeed it is a characteristic of Turing-like patterns[7]. When the nonnormality lies only in the reaction part, this profile disappears as soon as we enter the instability zone, while when support is nonnormal, even when the system becomes unstable, we still observe such phenomenology.

In order to study transient Turing-like patterns, we have performed the *mapping*, stopping the numerical integration after a certain number of steps[8]. The results are shown in figures 5.11, where we can observe, as already anticipated, that, even when the patterns do not stabilize, the system whose support is a nonnormal network undergoes a *bigger* transient growth.

Now, the question we would like to answer is the following: why do we observe Turing-like patterns for low values of the model's parameters only when the support is a nonnormal network? For what we have studied up to this point, the answer seems obvious: of course the extended Jacobian $\tilde{J}$ has a greater numerical abscissa ω when the network is nonnormal.

To verify this assumption, we need to compute the value of $\omega(\tilde{J})$ respectively for the model on a nonnormal network and on a symmetric network and then compare the different outcomes. To do that, we have used the same code of figure 4.3, which calculates, for the Brussellator model, $\omega(\tilde{J})$ above the Turing bifurcation curve, i.e., where $\alpha(\tilde{J}) \leq 0$, first for a nonnormal network and then for a symmetric network. The networks are the same ones that we have used to obtained figures 5.9, i.e., the nonnormal one has 10 nodes, $\gamma = 15$, $p_1 = 0.5$ and $p_2 = 0.2$ and the symmetric one is the symmetrization of the latter. We would expect to obtain significant values of ω only for high values of the parameters when the network is symmetric[9]. On the contrary, we would predict much greater values of ω for the system on the nonnormal network, even when the parameters' values are low.
In figures, 5.12 we show the results of such simulations respectively for the nonnormal and symmetric case and we can observe, surprisingly, that there is only a slight difference between them, as can be noticed looking at the colorbars. Such difference can be better appreciated if we zoom on the area where $\omega < 0$, as shown in figures 5.13.
As we see in figures 5.14, where the initial perturbation is the same for both cases,

---

[7]We can observe this fact also in figures D3 in Appendix D.

[8]The number of steps is, of course arbitrary, however we chose it with observational criteria: as shown later on in the section in figures 5.14, we observe for both cases (nonnormal and symmetric) an initial transient growth, hence the number of steps we choose must not be too short; moreover it must not be too long or the transients will be long decayed also for the nonnormal case.

[9]As already discussed, the cause of the nonnormality on symmetric network is the intrinsic nonnormality within model.
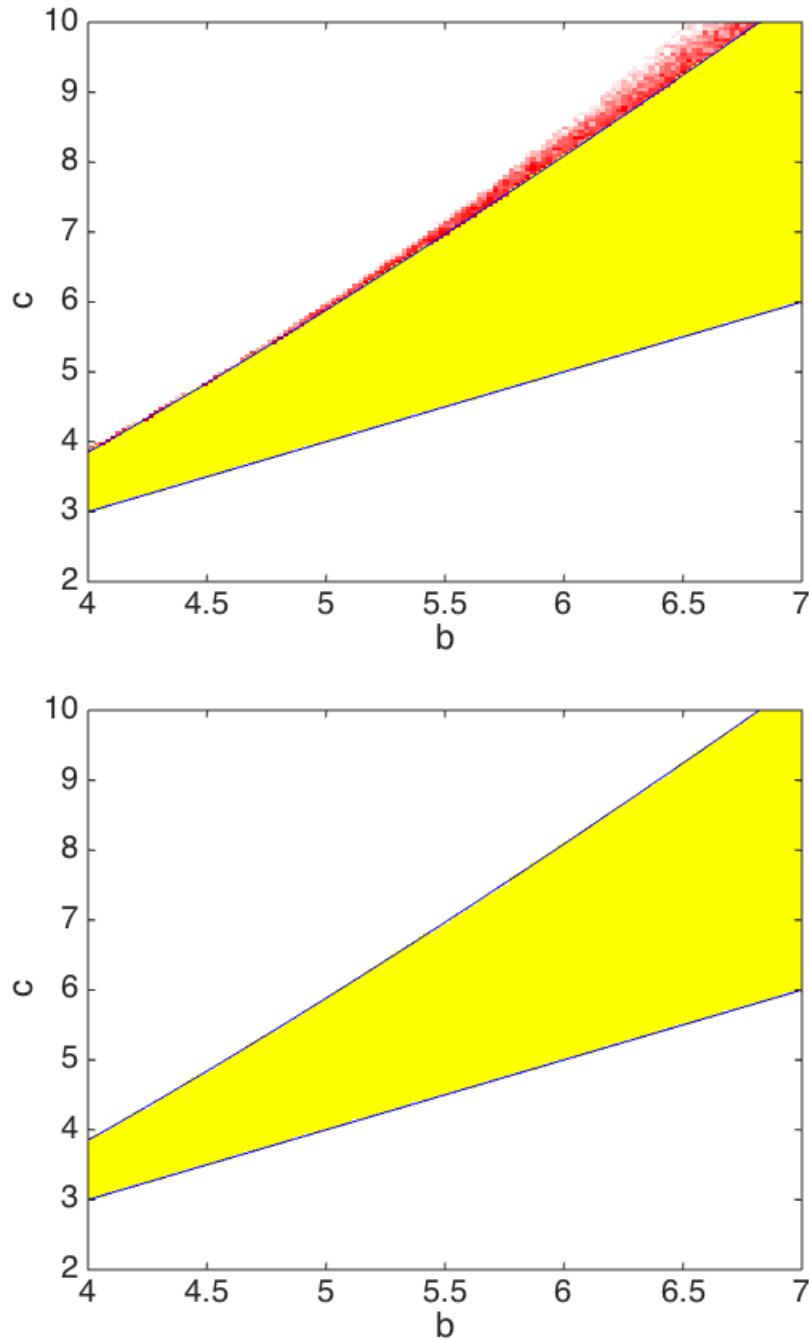
Figure 5.9: Pattern formation for the Brussellator model with $D_\varphi = 0.1$ and $D_\psi = 0.385$; the initial perturbation is $\varepsilon = 0.1$; for the figure up the support is a nonnormal network of 10 nodes with $\gamma = 15$, $p_1 = 0.5$ and $p_2 = 0.2$, while for the figure down we have a normal network that is the symmetrization of the previous, i.e., $\tilde{A} = (A + A^*)/2$; we see that we have pattern formation (red) outside the Turing region (yellow) only when the support is nonnormal; we observe different shadows of red because we have repeated the integration 10 times, so the stronger red areas are the ones where tha formation of pattern is more probable with a random perturbation.
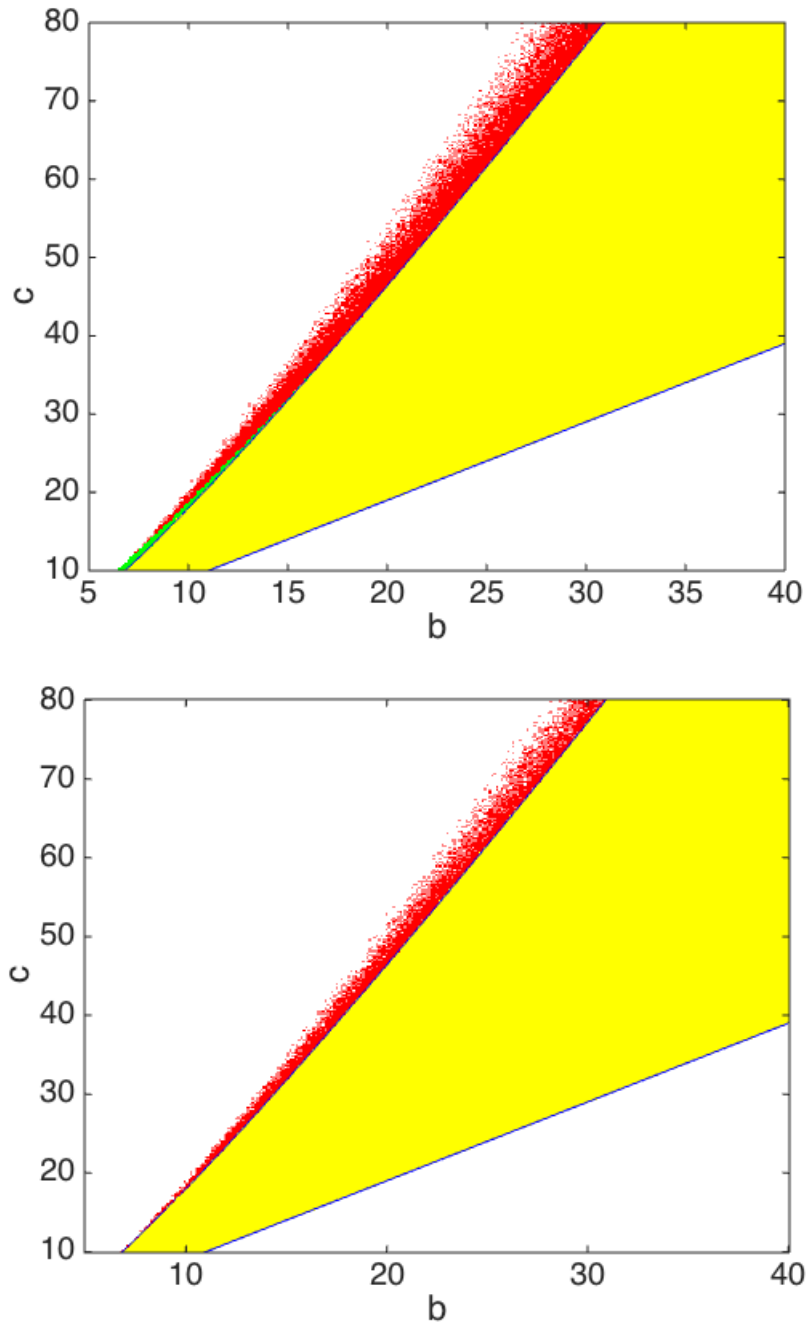
Figure 5.10: Pattern formation for the Brussellator model with $D_\varphi = 0.1$ and $D_\psi = 0.385$; the initial perturbation is $\varepsilon = 0.1$; for the figure up the support is a nonnormal network of 100 nodes with $\gamma = 20$, $p_1 = 0.4$ and $p_2 = 0.1$, while for the figure down we have a normal network that is the symmetrization of the previous, i.e., $\tilde{A} = (A + A^*)/2$; in green we have denoted the areas where the pattern formation is due to the fact that the network is directed, and that is why we observe it only on the left; in red we have signed the areas where the pattern formation is due to the nonnormality: it is clear that when the support is nonnormal (up), the red area is wider; we observe different shadows of red because we repeated the integration 2 times.
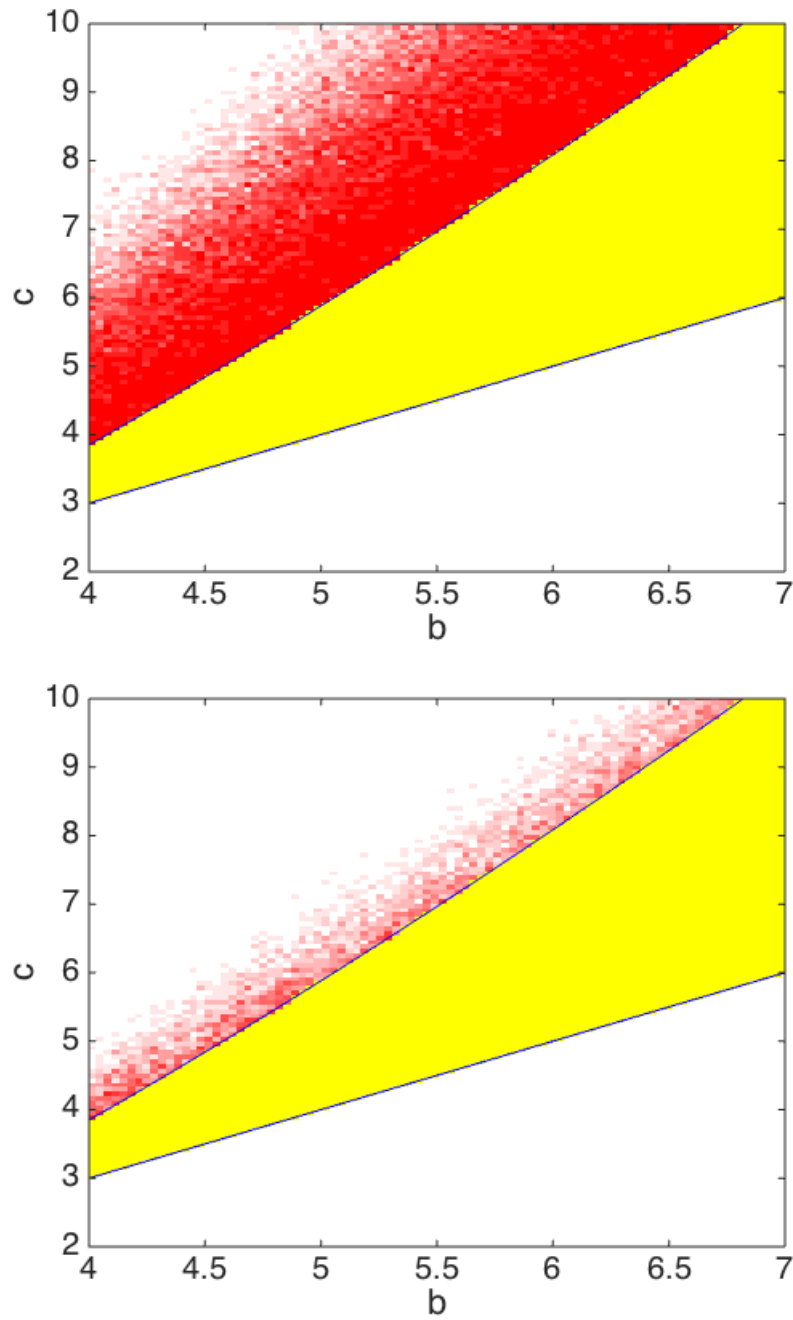
Figure 5.11: Transient Turing-like patterns for the Brussellator model with $D_\varphi = 0.1$ and $D_\psi = 0.385$; the initial perturbation is $\varepsilon = 0.1$; for the figure up the support is a nonnormal network of 10 nodes with $\gamma = 15$, $p_1 = 0.5$ and $p_2 = 0.2$, while for the figure down we have a normal network that is the previous simmetrized, i.e., $\tilde{A} = (A + A^*)/2$; we have repeated the *mapping* for 10 iterations, always stopping at 300 steps.
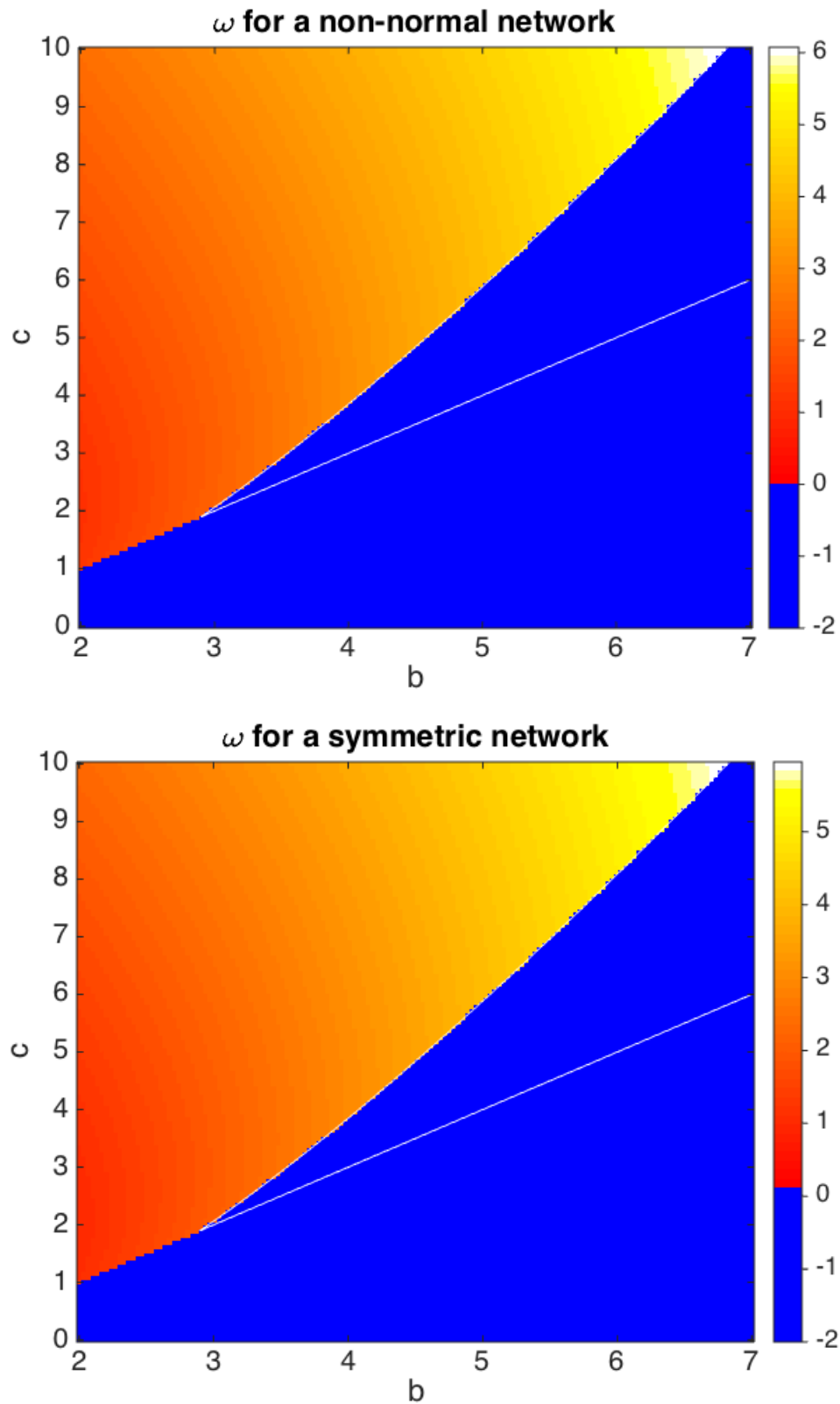
Figure 5.12: Values of $\omega(\tilde{J})$ for the Brussellator on a nonnormal network of 10 nodes (up) with $\gamma = 15$, $p_1 = 0.5$ and $p_2 = 0.2$ and on a symmetric network (down) of 10 nodes; $D_\varphi = 0.1$, $D_\psi = 0.385$; for both figures we have used the same settings as for figures 5.9; we observe that the profile of ω for the nonnormal case is slightly different if compared to the symmetric case, but not enough to justify Turing-like patterns.
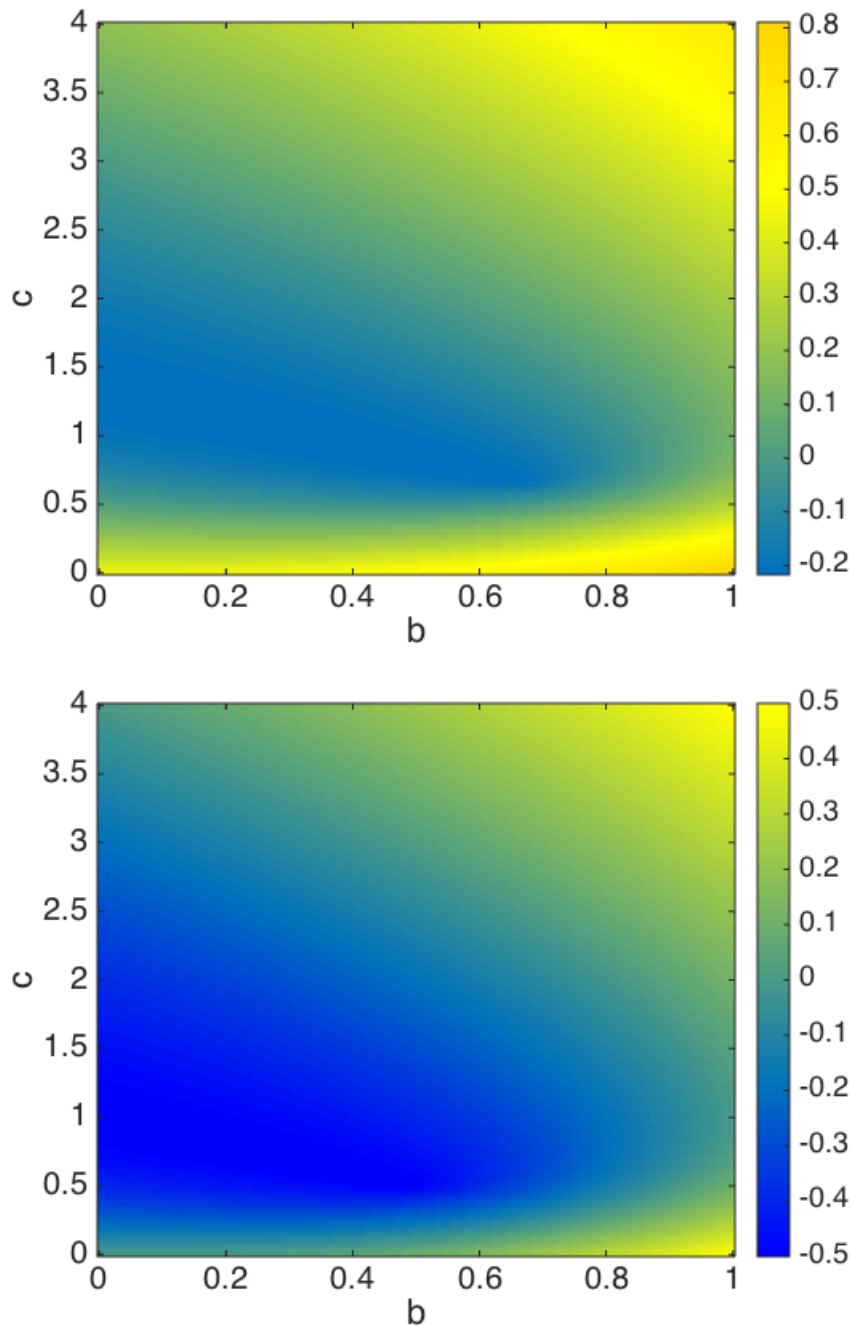
Figure 5.13: Zoom on the area where $\omega(\tilde{J}) < 0$ for the Brussellator on a nonnormal network of 10 nodes (up) with $\gamma = 15$, $p_1 = 0.5$ and $p_2 = 0.2$ and on a symmetric network (down) of 10 nodes; $D_\varphi = 0.1$, $D_\psi = 0.385$.

there is a slight difference between the peak given by $\omega(\tilde{J})$ in the nonnormal case and in the symmetric case, but such peak does not tell us if there will be Turing-like patterns or not: for example, in the nonnormal case we observe pattern formation with values of $\omega \simeq 3$ and we do not see them in the symmetric case where, as we recall from Chapter 3, we start observing the patterns from values of $\omega \simeq 10$.
Moreover, if we compare figures 5.12 and 5.9, we can understand that the value of ω is not a good measure to understand the emergence of Turing-like patterns since the region where it is positive, extends beyond the zone of parameters where patterns are observed. Of course ω must be greater than 0 in order to observe the Turing-like patterns, but as we have seen in the previous chapter, such condition is always verified for every system that allows Turing pattern formation, thus including the Brussellator.

Remark   Looking at figures 5.14, one may think that the oscillations, which give us transient Turing-like patterns, are due to the asymmetry of the network, rather than to its nonnormality. But this is not true: in fact the results that we obtain if we work on asymmetric networks "almost normal"[10] are similar to those obtained for the symmetric case.

In conclusion, we have observed a new phenomenon but, with the approach used until now to measure the nonnormality, we are not able to explain it completely; certainly ω is not very adequate as a measure to explain the emergence of Turing-like pattern formation. In order to give a reasonable explanation of such fact, we need a more sophisticated mathematical tool, that we are going to introduce in the next chapter, the last of this thesis.

---

[10]For example a Small-World network with low p is, numerically, "almost normal", since it is a regular lattice, that is circulant, with a few links that are rewired.
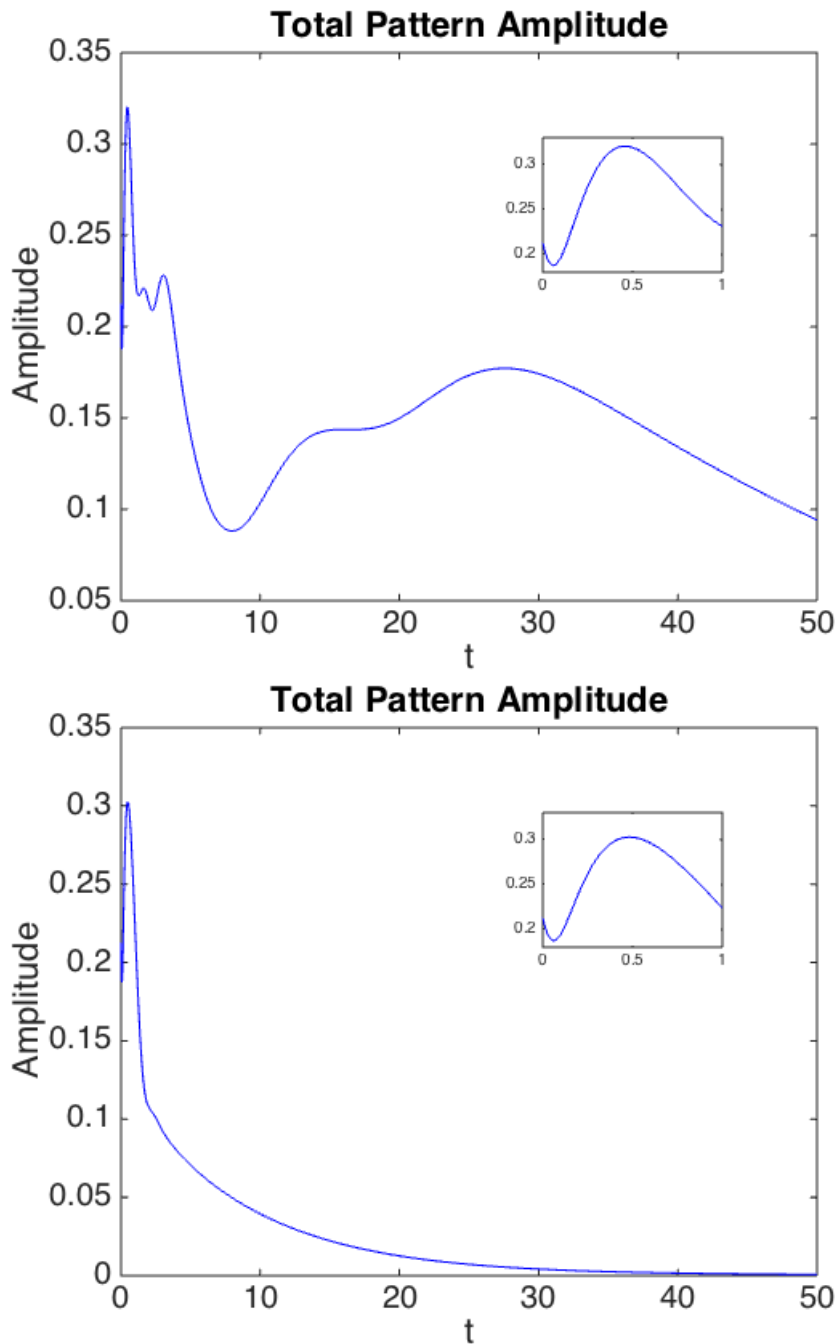
Figure 5.14: Transient Turing-like patterns for Brussellator on a nonnormal network of 10 nodes (up) with $\gamma = 15$, $p_1 = 0.5$ and $p_2 = 0.2$ and on a symmetric network (down) of 10 nodes; the initial perturbation is the same for both figures; we clearly observe how the difference between the two peaks (zoom) is minimal and not enough to give account of such different behavior; $b = 5$, $c = 6$, $D_{\varphi} = 0.1$, $D_{\psi} = 0.385$ and $\varepsilon = 0.1$.

6

Perturbed Spectra of Nonnormal Matrices

In the last chapter, we have shown that, on nonnormal networks, the region where patterns ca be found is enlarged due to Turing-like pattern formation; however, we still need to investigate such new mechanism. In order to explain Turing-like patterns, we need to understand more deeply what it means for a matrix to be nonnormal from a spectral point of view, thus we need to extend our notion of the spectrum, calling into question a more general version: *the pseudospectrum.*

In the first part of this chapter, we will introduce mathematically, without any claim of completeness, the concept of pseudospectrum following the book [Trefethen-Embree 2005] and then test our results in the light of this mathematical tool. In the last part, we will see why we need to introduce a restriction to this new concept in order to give an explanation of our results.

6.1   Pseudospectra

In the following part, with $|| \; ||$ we will refer to the Euclidean norm $|| \; ||_2$, i.e., given $A \in \mathbb{C}^{n \times n}$

$$||A||_2 = \max_{||\underline{x}||=1} ||A\underline{x}|| = \sqrt{\tilde{\lambda}}$$

where $\tilde{\lambda}$ is the largest λ s.t. $A^*A - \lambda I$ is *singular* [Golub-Van Loan 1996].

Definition   Let $A \in \mathbb{C}^{n \times n}$ and $\varepsilon > 0$ arbitrary. The ε-**pseudospectrum** $\sigma_\varepsilon(A)$ of A is the set of $z \in \mathbb{C}$ s.t. $||(z - A)^{-1}|| > \varepsilon^{-1}$.

This first definition does not give a good intuitive idea of what a pseudospectrum is; a more useful and equivalent way to see it is the following.

Definition   Let $A \in \mathbb{C}^{n \times n}$ and $\varepsilon > 0$ arbitrary. The ε-**pseudospectrum** $\sigma_\varepsilon(A)$ of A is the set of $z \in \mathbb{C}$ s.t. $z \in \sigma(A + E)$ for some $E \in \mathbb{C}^{n \times n}$ with $||E|| < \varepsilon$.

Definition Let $A \in \mathbb{C}^{n \times n}$ and $\varepsilon > 0$ arbitrary. The ε-**pseudoabscissa** $\alpha_\varepsilon(A)$ is the largest real value of A's pseudospectrum, i.e.,

$$\alpha_\varepsilon(A) = \sup(\Re(\sigma_\varepsilon(A)))$$

From the theory of pseudospectra [Trefethen-Embree 2005], we know that nonnormal matrices (and operators) are more sensible to perturbations, i.e., they have bigger pseudospectra compared with their normal analogous. It is possible to observe such fact in figures 6.1, made using the MATLAB® toolbox *Eigtool* [Wright 2002], where we show the pseudospectra of the open directed ring (figure up) and directed ring (figure down); such networks of 11 nodes are the ones that we have introduced in Section 5.1 to study the effects of the support's nonnormality on linear dynamics.

Remark In Chapters 4 and 5 we have taken as a measure of nonnormality, given a network with adjacency matrix A, the quantity $\omega(A) - \alpha(A)$. However, a more proper measure of the nonnormality is given by the ε-pseudoabscissa $\alpha_\varepsilon(A)$, as explained in the paper [Asllani-Carletti 2018b].

Using Eigtool, let us compute the **pseudo-dispersion relation**, i.e., the pseudospectrum of the extended Jacobian matrix $\tilde{J}$, for the Brussellator model on a nonnormal network and on its symmetrization. The results are shown in figure 6.2 where we see how, when the network is nonnormal, the system reaches the instability for a perturbation of $\varepsilon = 10^{-1}$, while the system on the symmetric network, despite the same set of parameters and the same perturbation, remains stable. Hence we can assert that when the operator (matrix) governing the dynamics is nonnormal, the system reaches more easily the instability; this fact, that fits perfectly with our results of last chapter, has been observed for the first time in a study on hydrodynamic instability [Trefethen et al. 1993].

Now, to corroborate our *numerical experiment*, whose result is displayed in figures 5.9 of last chapter, we can compute the ε-pseudoabscissa of the Brussellator on a nonnormal and on a symmetric network and show where it is positive. We can do that using *Eigtool* inside our previous *mapping* code; this time, instead of integrating the Brussellator's equation, we compute the ε-pseudoabscissa. If our predictions are correct, we should see a larger region when the network is nonnormal; indeed, looking at the results of such *mapping*, depicted in figures 6.3, that is what we observe.

We could be satisfied with this last result. However, for the case on nonnormal network, if we compare the *mapping* of Turing-like patterns and the *mapping* of $\alpha_\varepsilon(\tilde{J}) > 0$, we see that, while the ε-pseudoabscissa is positive in a stripe-like region of almost constant width, the area where we have Turing-like patterns increases as the parameters do so. An immediate guess would be to think about $\omega(\tilde{J})$, but we have ruled out its adequacy in Turing-like pattern formation and it is unlikely to be helpful in this matter. One possible solution would be to have a perturbation that depends on the parameters, but to obtain so, our linear analysis does not work

anymore; we need to perform a nonlinear analysis, i.e., we need to reach at least the second order in our Taylor expansion of the initial perturbation.
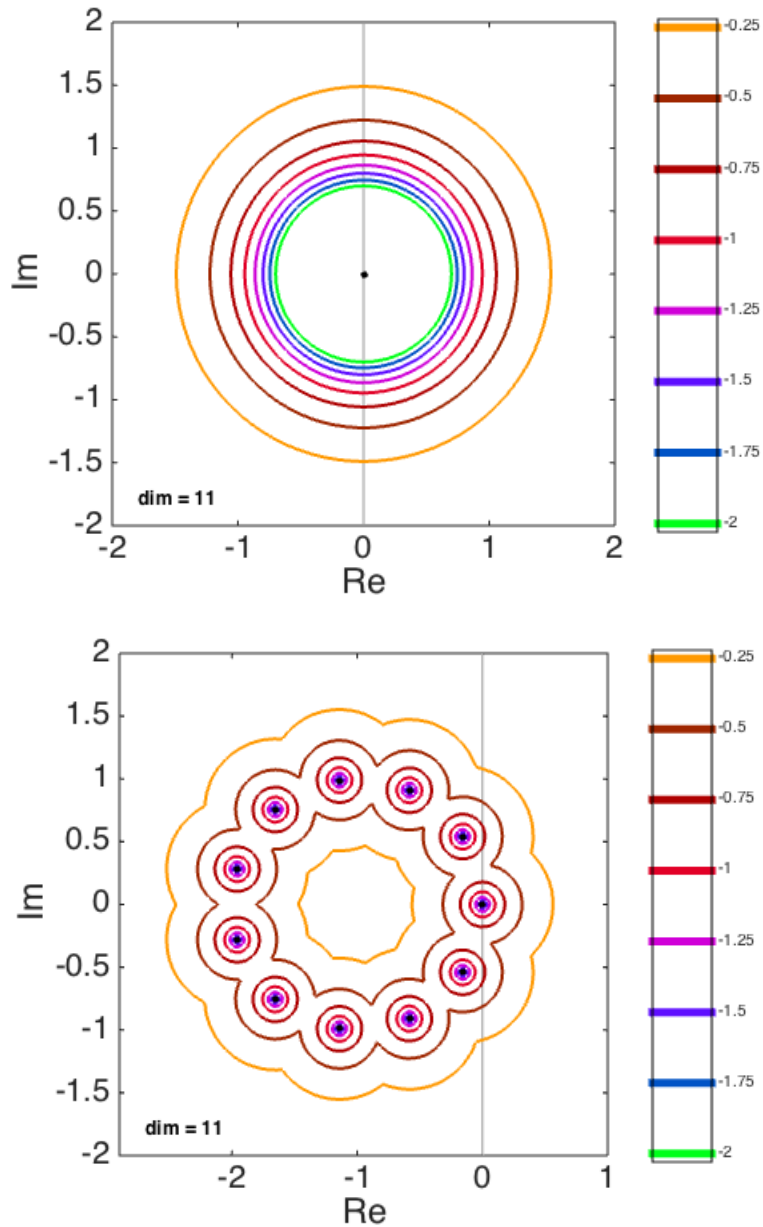

Figure 6.1: Pseudospectra of the open directed ring (up) and of the directed ring (down); we see that the nonnormal one is more sensible to perturbations, since $\alpha = 0$ for both spectra, but α_ε is greater in the nonnormal case; the lateral bar gives the magnitude of the perturbations in logarithmic scale.
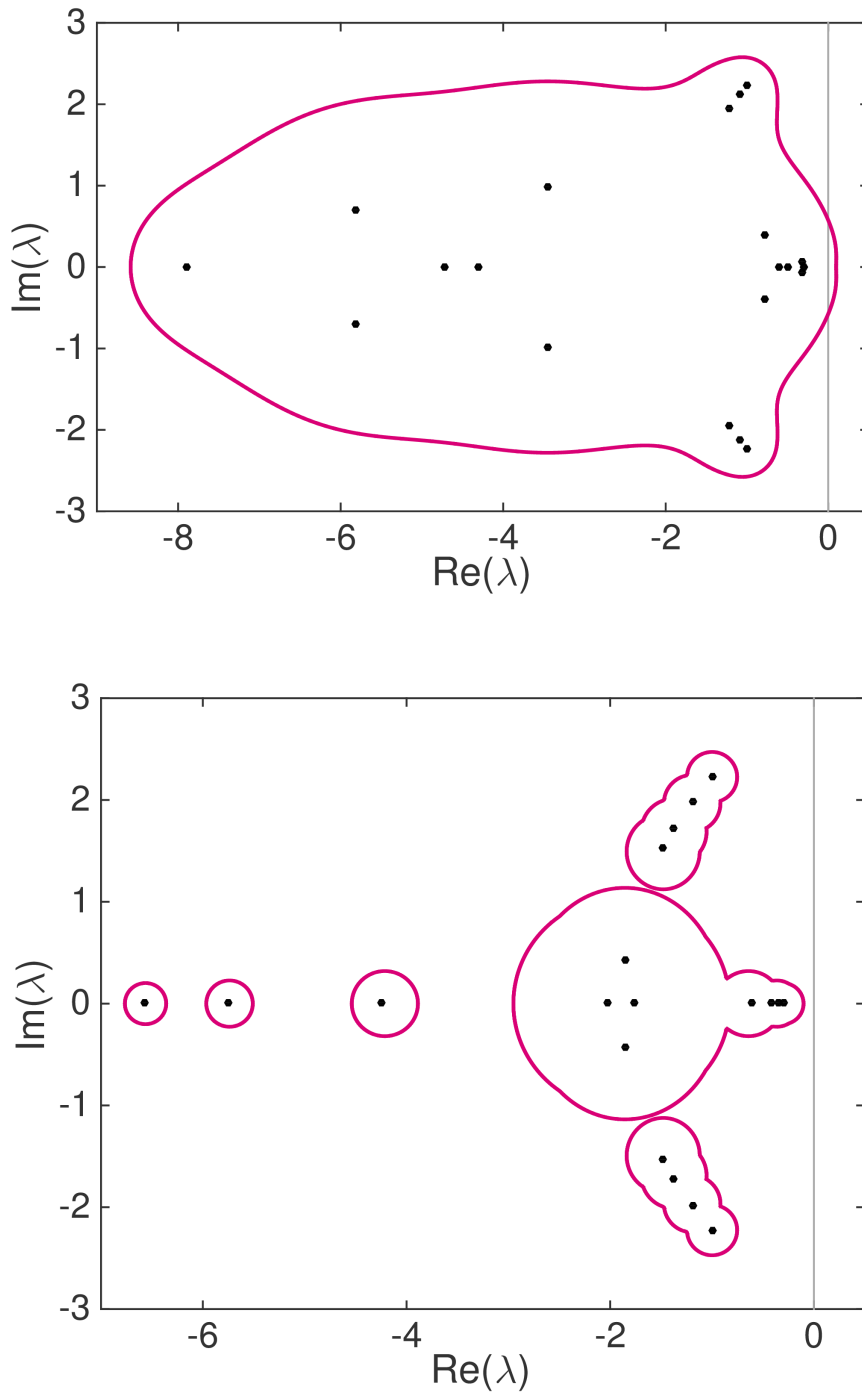
Figure 6.2: Pseudo-dispersion relation for the Brussellator on a nonnormal network (up) of 10 nodes, $\gamma = 15$, $p_1 = 0.5$ and $p_2 = 0.2$ and on a symmetric, hence normal, network (down), symmetrization of the previous one; we see that the spectrum is *stable* and so is the pseudospectrum in the symmetric case, while in the nonnormal case, the pseudospetrum becomes unstable; $b = 5$, $c = 6$, $D_\varphi = 0.09$, $D_\psi = 0.3$ and $\varepsilon = 0.1$.

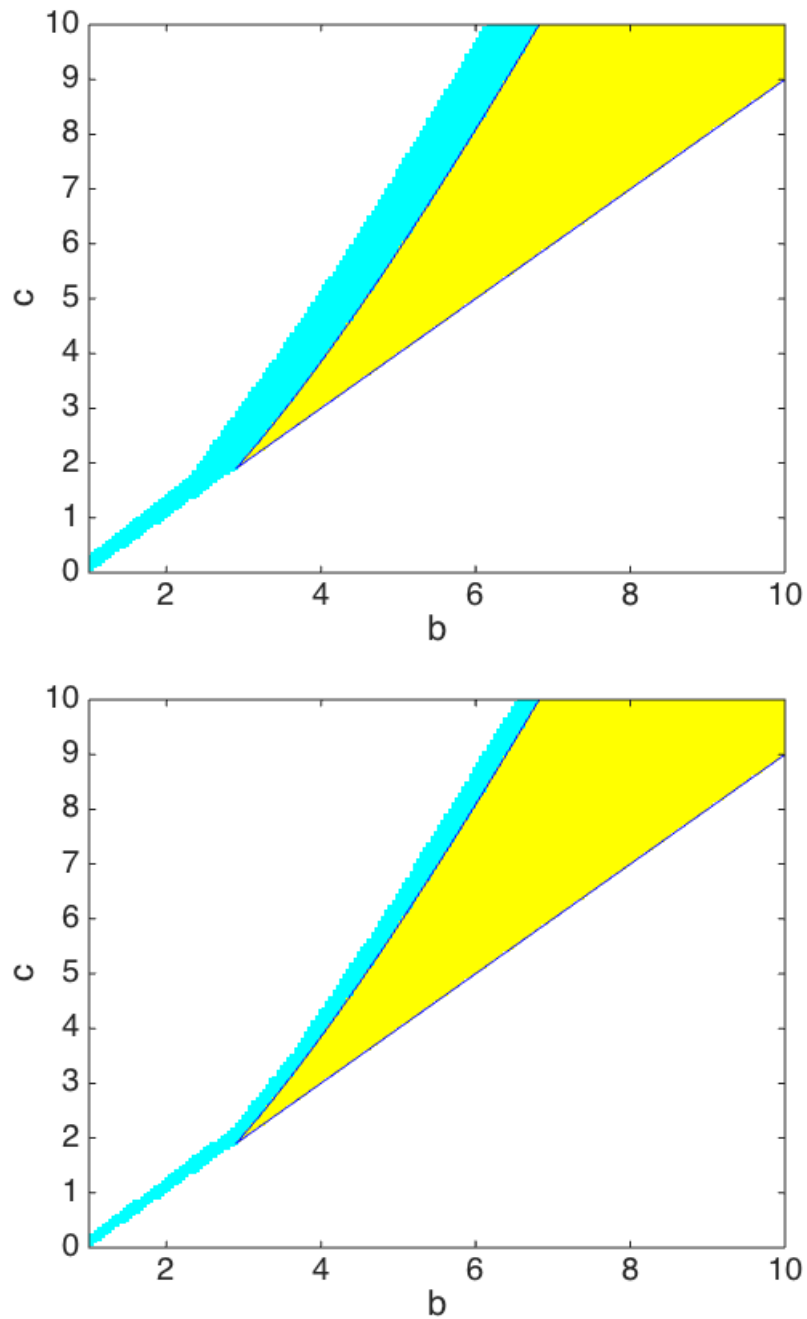**Figure 6.3:** The cyan areas are the ones where the ε-pseudoabscissa is positive, $\varepsilon = 0.1$; we see that when the network is nonnormal (up) such area are wider with respect to the case on symmetric network (down).

6.2   Second Order Analysis and Constrained Pseudospectra

Let

$$\underline{F} : \mathbb{R}^n \longrightarrow \mathbb{R}^m \quad , \quad \underline{F} = \begin{bmatrix} f_1 \\ \vdots \\ f_m \end{bmatrix}$$

be a vector valued function of several variables that is at least $C^2(\mathbb{R}^n)$, let $\underline{x}^* \in \mathbb{R}^n$ be a fixed point for $\underline{F}$, i.e., $\underline{F}(\underline{x}^*) = \underline{0}$, and let $\underline{\epsilon} = \underline{x} - \underline{x}^* \in \mathbb{R}^n$ be a perturbation of the fixed point. The Taylor expansion of $\underline{F}$ in $\underline{x}^* + \underline{\epsilon}$ at the second order [Conn et al. 2000] is

$$\underline{F}(\underline{x}^* + \underline{\epsilon}) \simeq \underline{F}(\underline{x}^*) + J_{\underline{F}}\underline{\epsilon} + \frac{1}{2}((\underline{1}^T \otimes \mathbb{E})\mathbb{H}_{\underline{F}})\underline{\epsilon}$$

where

$$J_{\underline{F}} = \begin{bmatrix} \left.\dfrac{\partial f_1}{\partial x_1}\right|_{\underline{x}=\underline{x}^*} & \cdots & \cdots & \left.\dfrac{\partial f_1}{\partial x_n}\right|_{\underline{x}=\underline{x}^*} \\ \vdots & \ddots & & \vdots \\ \vdots & & \ddots & \vdots \\ \left.\dfrac{\partial f_m}{\partial x_1}\right|_{\underline{x}=\underline{x}^*} & \cdots & \cdots & \left.\dfrac{\partial f_m}{\partial x_n}\right|_{\underline{x}=\underline{x}^*} \end{bmatrix} \in \mathbb{R}^{m \times n}$$

is the Jacobian matrix, $\otimes$ is the Kronecker product between

$$\underline{1} = \begin{bmatrix} 1 \\ \vdots \\ 1 \end{bmatrix} \in \mathbb{R}^m \quad \text{and} \quad \mathbb{E} = \begin{bmatrix} \underline{\epsilon}^T \\ \vdots \\ \underline{\epsilon}^T \end{bmatrix} \in \mathbb{R}^{m \times n} \quad \text{so that} \quad \underline{1}^T \otimes \mathbb{E} \in \mathbb{R}^{m \times nm}$$

and

$$\mathbb{H}_{\underline{F}} = \begin{bmatrix} \mathcal{H}_{f_1} \\ \vdots \\ \mathcal{H}_{f_m} \end{bmatrix} \in \mathbb{R}^{nm \times n}$$

is the matrix made by the components of the $n \times n \times m$ Hessian tensor, that are

$$H_{f_i} = \begin{bmatrix} \left.\dfrac{\partial^2 f_i}{\partial x_1^2}\right|_{\underline{x}=\underline{x}^*} & \left.\dfrac{\partial^2 f_i}{\partial x_1 \partial x_2}\right|_{\underline{x}=\underline{x}^*} & \cdots & \cdots & \left.\dfrac{\partial^2 f_i}{\partial x_1 \partial x_n}\right|_{\underline{x}=\underline{x}^*} \\ \left.\dfrac{\partial^2 f_i}{\partial x_2 \partial x_1}\right|_{\underline{x}=\underline{x}^*} & \left.\dfrac{\partial^2 f_i}{\partial x_2^2}\right|_{\underline{x}=\underline{x}^*} & \cdots & \cdots & \left.\dfrac{\partial^2 f_i}{\partial x_2 \partial x_n}\right|_{\underline{x}=\underline{x}^*} \\ \vdots & \vdots & \ddots & & \vdots \\ \vdots & \vdots & & \ddots & \vdots \\ \left.\dfrac{\partial^2 f_i}{\partial x_n \partial x_1}\right|_{\underline{x}=\underline{x}^*} & \left.\dfrac{\partial^2 f_i}{\partial x_n \partial x_2}\right|_{\underline{x}=\underline{x}^*} & \cdots & \cdots & \left.\dfrac{\partial^2 f_i}{\partial x_n^2}\right|_{\underline{x}=\underline{x}^*} \end{bmatrix} \in \mathbb{R}^{n \times n}$$

Since

$$\underline{F} \in C^2(\mathbb{R}^n) \quad \Longleftrightarrow \quad f_i \in C^2(\mathbb{R}^n) \; \forall \; i \in \{1, ..., m\}$$

from **Schwarz Theorem** [Fusco et al. 1996] we have for every f_i that

$$\left.\frac{\partial^2 f_i}{\partial x_k \partial x_l}\right|_{\underline{x}=\underline{x}^*} = \left.\frac{\partial^2 f_i}{\partial x_l \partial x_k}\right|_{\underline{x}=\underline{x}^*} \quad \forall \; k, l \in \{1, ..., n\}, \; k \neq l$$

meaning that $\mathcal{H}_{f_1}, \ldots, \mathcal{H}_{f_m}$ are symmetric.

Now, coming back to our Brussellator model on a nonnormal network of n nodes, our first order expansion gives us an equation analogous to that of Section 3.2, i.e., equation (3.4), namely

$$\underline{\dot{\epsilon}} = \tilde{J}\underline{\epsilon} = (J + D\mathcal{L})\underline{\epsilon}$$

where

$$\epsilon = \begin{bmatrix} \delta\varphi_1 \\ \vdots \\ \delta\varphi_n \\ \delta\psi_1 \\ \vdots \\ \delta\varphi_n \end{bmatrix} \quad , \quad J = \begin{bmatrix} (b-1)I_{n\times n} & cI_{n\times n} \\ -bI_{n\times n} & -cI_{n\times n} \end{bmatrix} \quad , \quad D\mathcal{L} = \begin{bmatrix} D_\varphi\mathcal{L} & 0_{n\times n} \\ 0_{n\times n} & D_\psi\mathcal{L} \end{bmatrix}$$

where $\delta\varphi_i, \delta\psi_i \in [-\varepsilon, \varepsilon] \; \forall i \in \{1, ..., n\}$ and $\varepsilon \in \mathbb{R}^+$ is a positive scalar that in general is $\varepsilon = 0.1$, in our numerical simulations.

Therefore we need to compute the second order term, something we can do, since we have assumed in Chapter 2 that the functions are at least C^2. Let us find first the Hessian tensor for our vector valued function $\underline{F} : \mathbb{R}^{2n} \longrightarrow \mathbb{R}^{2n}$

$$\underline{F} = \begin{bmatrix} f_1 \\ \vdots \\ f_n \\ g_1 \\ \vdots \\ g_n \end{bmatrix} \quad , \quad \text{where} \quad \begin{cases} f_i = f(\varphi_i, \psi_i) = 1 - (b+1)\varphi_i + c\varphi_i^2\psi_i \\ g_i = g(\varphi_i, \psi_i) = b\varphi_i(t) - c\varphi_i^2\psi_i \end{cases}$$

In order to find the components of the tensor $\mathcal{H}_{f_i}$ and $\mathcal{H}_{g_i}$ $i \in \{1, ..., n\}$, let us compute the second order derivatives

$$\begin{cases} \left.\dfrac{\partial^2 f_i}{\partial\varphi_j^2}\right|_{\underline{x}=\underline{x}^*} = 2b\delta_{ij} \\[2em] \left.\dfrac{\partial^2 f_i}{\partial\varphi_j\partial\psi_k}\right|_{\underline{x}=\underline{x}^*} = \left.\dfrac{\partial^2 f_i}{\partial\psi_j\partial\varphi_k}\right|_{\underline{x}=\underline{x}^*} = 2c\delta_{ij}\delta_{jk} \\[2em] \left.\dfrac{\partial^2 f_i}{\partial\psi_j^2}\right|_{\underline{x}=\underline{x}^*} = 0 \end{cases}$$

$$
\begin{cases}
\left. \dfrac{\partial^2 g_i}{\partial \varphi_j^2} \right|_{\underline{x}=\underline{x}^*} = -2b\delta_{ij} \\[2.5em]
\left. \dfrac{\partial^2 g_i}{\partial \varphi_j \partial \psi_k} \right|_{\underline{x}=\underline{x}^*} = \left. \dfrac{\partial^2 g_i}{\partial \psi_j \partial \varphi_k} \right|_{\underline{x}=\underline{x}^*} = -2c\delta_{ij}\delta_{jk} \\[2.5em]
\left. \dfrac{\partial^2 g_i}{\partial \psi_j^2} \right|_{\underline{x}=\underline{x}^*} = 0
\end{cases}
$$

Hence, $\mathcal{H}_{f_i}$ and $\mathcal{H}_{g_i}$ $i \in \{1,...,n\}$ are *sparse*[1] $2n \times 2n$ matrices, whose nonzero elements are

$$
\begin{cases}
(\mathcal{H}_{f_i})_{i,i} = 2b \\
(\mathcal{H}_{f_i})_{i,i+n} = (\mathcal{H}_{f_i})_{i+n,i} = 2c
\end{cases}
$$

and

$$
\begin{cases}
(\mathcal{H}_{g_i})_{i,i} = -2b \\
(\mathcal{H}_{g_i})_{i,i+n} = (\mathcal{H}_{g_i})_{i+n,i} = -2c
\end{cases}
$$

Now that we have each component of the Hessian tensor, we can compute $\underline{\epsilon}^T \mathbb{H} = \tilde{\mathcal{H}}$:

$$
\tilde{\mathcal{H}} = \begin{bmatrix} \underline{\epsilon}^T \mathcal{H}_{f_1} \\ \vdots \\ \underline{\epsilon}^T \mathcal{H}_{f_n} \\ \underline{\epsilon}^T \mathcal{H}_{g_1} \\ \vdots \\ \underline{\epsilon}^T \mathcal{H}_{g_n} \end{bmatrix} \in \mathbb{R}^{2n \times 2n}
$$

that explicitly is

$$
\tilde{\mathcal{H}} = 2 \begin{bmatrix}
(\delta\varphi_1 b + \delta\psi_1 c) & 0 & \ldots & & 0 & \delta\varphi_1 c & 0 & \ldots & & 0 \\
0 & \ddots & & & \vdots & 0 & \ddots & & & \vdots \\
\vdots & & \ddots & & \vdots & \vdots & & \ddots & & \vdots \\
0 & & \ldots & 0 & (\delta\varphi_n b + \delta\psi_n c) & 0 & & \ldots & 0 & \delta\varphi_n c \\
-(\delta\varphi_1 b + \delta\psi_1 c) & 0 & \ldots & & 0 & -\delta\varphi_1 c & 0 & \ldots & & 0 \\
0 & \ddots & & & \vdots & 0 & \ddots & & & \vdots \\
\vdots & & \ddots & & \vdots & \vdots & & \ddots & & \vdots \\
0 & & \ldots & 0 & -(\delta\varphi_n b + \delta\psi_n c) & 0 & & \ldots & 0 & -\delta\varphi_n c
\end{bmatrix}
$$

$$\tag{6.1}$$

For the sake of notation, let us set

$$
\hat{\mathcal{H}} = \frac{1}{2}\tilde{\mathcal{H}}
$$

---

[1] A matrix is said to be sparse when, called $n_{\neq 0}$ the number of nonzero elements and $n_{=0}$ the number of null elements, it is s.t. $n_{\neq 0} << n_{=0}$.
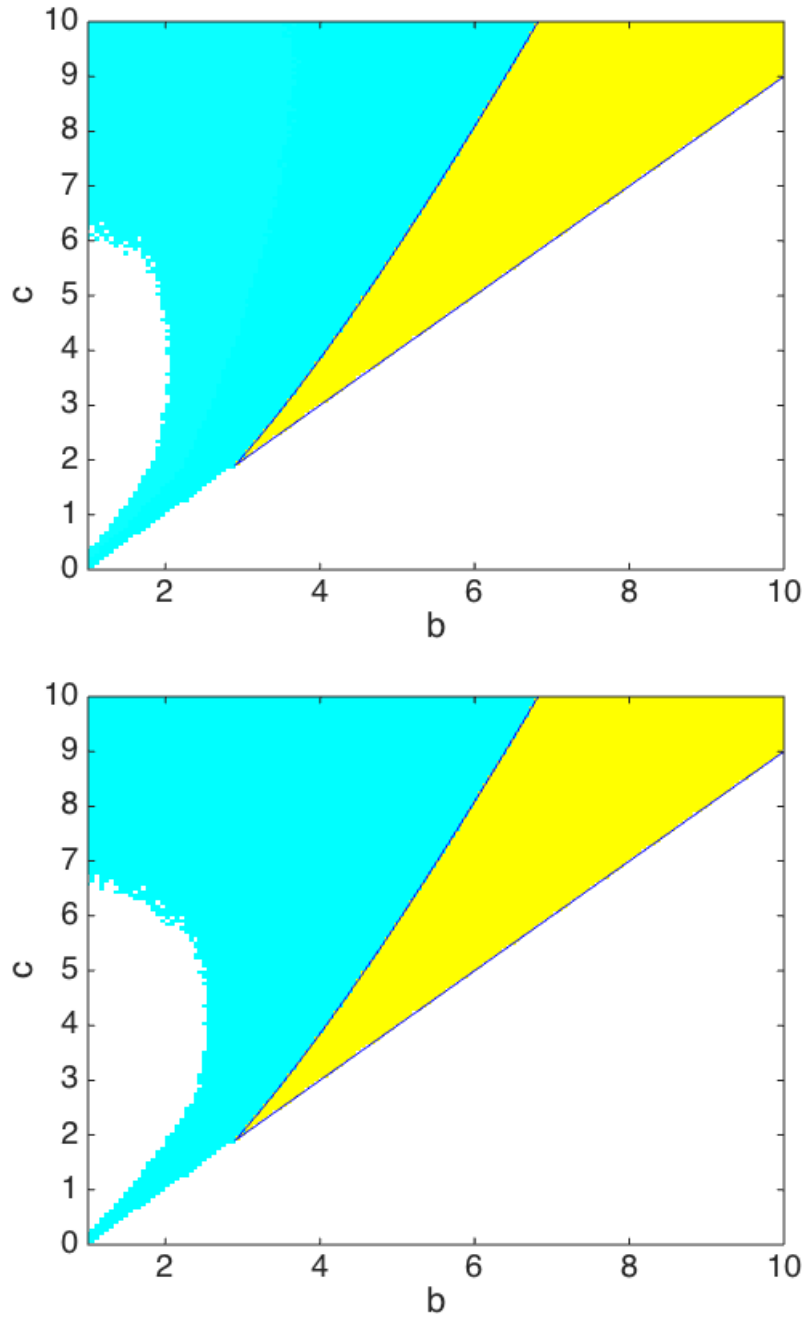
Figure 6.4: The cyan areas are the ones where the ε_{max}-pseudoabscissa is positive, for a nonnormal network of 10 nodes (up) with $\gamma = 15$, $p_1 = 0.5$ and $p_2 = 0.2$ and for a symmetric network (down) of 10 nodes; $D_\varphi = 0.1$, $D_\psi = 0.385$; $\varepsilon_{N,max}$ is defined in equation (6.3); $\varepsilon = 0.1$, $N = 100$; we see that the area where the $\varepsilon_{N,max}$-pseudoabscissa is positive is larger for the case on nonnormal network.

Finally, we have obtained our second order equation, that is

$$\dot{\underline{\epsilon}} = (\tilde{J} + \hat{\mathcal{H}})\underline{\epsilon} = (J + D\mathcal{L} + \hat{\mathcal{H}})\underline{\epsilon}$$

Let us rename our new perturbation $\hat{\varepsilon}(b, c)$, whose dependence on the model's parameters will be from now on implicit, that is

$$\hat{\varepsilon} = ||\hat{\mathcal{H}}|| \tag{6.2}$$

From equation (6.1) we can observe that $\hat{\varepsilon}$ depends also on the random inhomogeneous perturbation of the fixed point. Hence, instead of performing the *mapping* of $\alpha_{\hat{\varepsilon}}(\tilde{J})$ for every point (b, c), we need to take the maximum for a certain number of iterations. Given N the number of iterations, $N >> 1$, let us define

$$\varepsilon_{N,max} = \max_{i \in \{1,...,N\}} \hat{\varepsilon}_i \tag{6.3}$$

Notation   Before proceeding with the next part, in order to avoid confusion, let us clarify the differences between the perturbations that we have defined

- $\varepsilon \in \mathbb{R}^+$ is maximum magnitude of the initial perturbation, i.e., the input in our codes (details in Appendix C);

- $\underline{\epsilon} \in \mathbb{R}^{2n}$ is the inhomogenous perturbation of the fixed point, whose components are $\delta\varphi_i, \delta\psi_i \in [-\varepsilon, \varepsilon]$;

- $\hat{\varepsilon} \in \mathbb{R}^+$ is the second order perturbation in every point of the (b, c) plane, as defined in equation (6.2);

- $\varepsilon_{N,\max} \in \mathbb{R}^+$ is, given N iterations, the maximum of the second order perturbations in the (b, c) plane, as defined in equation (6.3).

Let us now perform numerically the *mapping* of $\alpha_{\varepsilon_{N,max}}(\tilde{J})$. The results, shown in figures 6.4, are completely overestimated and not helpful at all. In fact, it would mean that we should always observe pattern formation outside the Turing region with an initial perturbation $\varepsilon = 0.1$, also in the symmetric case, fact that is in contrast with years of studies and numerical simulations.
It is straightforward to think that maybe the pseudospectrum gives an overestimation of the perturbed spectrum, given our setting. In fact, if we compare the pseudospectrum computed by Eigtool with the "effective" perturbed spectrum of our problem, we see that the difference is remarkable, as shown in figure 6.5, where we can observe that the perturbed spectrum goes unstable, but its maximal eigenvalues in much smaller than $\alpha_{\hat{\varepsilon}}$.
This fact can be easily understood: given $A \in \mathbb{C}^{n \times n}$, the pseudospectrum is the maximum possible "area" covered by the perturbed eigenvalues; however, in our case the perturbation matrix $\hat{\mathcal{H}}$ is given[2]. Therefore, we have a constraint in the perturbed spectrum; we need a new definition of pseudospectrum that could serve
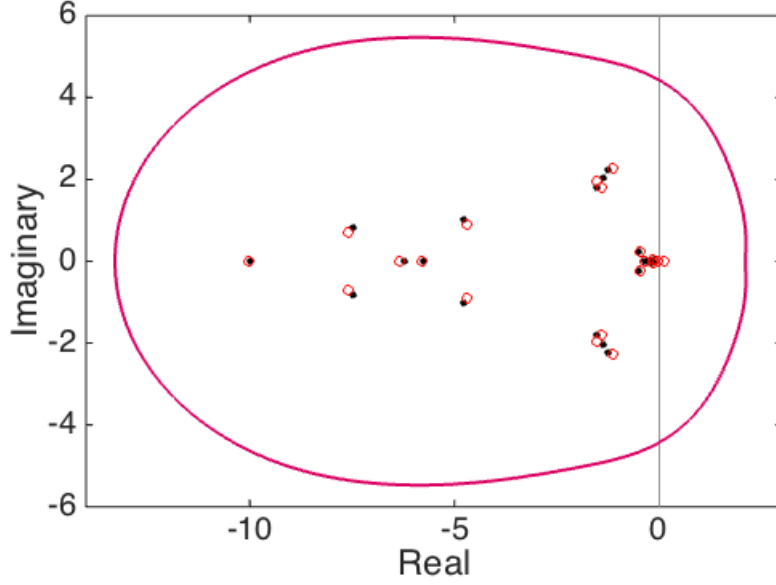
Figure 6.5: Brussellator with $b = 5$, $c = 6.5$, $D_\varphi = 0.1$ and $D_\psi = 0.385$ on a nonnormal network of 10 nodes; the black dots are the spetrum of the extended Jacobian $\tilde{J}$, that is stable; the red circles are the spectrum of the second order perturbed extended Jacobian $\tilde{J} + \hat{\mathcal{H}}$, we see that it goes unstable; the red curve is the $\hat{\varepsilon}$-pseudospectrum computed with *Eigtool*, where $\hat{\varepsilon} = 1.2303 = 10^{0.09}$.

for our case.

Given $\tilde{J}$ the extended Jacobian for the Brussellator model and $\sigma_\varepsilon(\tilde{J})$, $\varepsilon \in \mathbb{R}^+$, its pseudospectrum, the **constrained ε-pseudospectrum** of $\tilde{J}$ with respect to $\hat{\mathcal{H}} = 2\underline{\epsilon}^T \mathbb{H}$ is defined as

$$\bar{\sigma}_{\varepsilon,\hat{\mathcal{H}}}(\tilde{J}) = \sigma(\tilde{J} + \hat{\mathcal{H}}) \subset \sigma_\varepsilon(\tilde{J})$$

and its **constrained ε-pseudoabscissa** of $\tilde{J}$ with respect to $\hat{\mathcal{H}}$ is

$$\bar{\alpha}_{\varepsilon,\hat{\mathcal{H}}}(\tilde{J}) = \sup(\Re(\bar{\sigma}_{\varepsilon,\hat{\mathcal{H}}}(\tilde{J})))$$

Now we would like to perform the *mapping* of the constrained pseudospectrum outside the Turing region and detect if there is a match with the *mapping* of Turing-like patterns (figures 5.9). For the pseudospectrum we could rely on the toolbox EigTool, but we do not possess such an appliance for the constrained pseudospectrum. Owing to this fact, we can compute the constrained $\varepsilon_{N,max}$-pseudoabscissa, which means to compute the constrained $\hat{\varepsilon}$-pseudoabscissa in each point of the (b, c) plane for N random perturbations of the initial conditions and then take the maximum. With this procedure, are are able to obtain a fair estimation of the constrained pseudospectrum. In figure 6.6 we show the results for $N = 100$. We see clearly that

---

[2]By "given" we mean that the nonzero elements are fixed, though their values change.

for the case on nonormal network the area where $\bar{\alpha}_{\varepsilon_{N,max},\hat{\mathcal{H}}}(\tilde{J}) > 0$ is wider if compared to the case on symmetric network. Moreover, if we call

$$\bar{\alpha}_{\varepsilon_{N,max},\hat{\mathcal{H}}}(\tilde{J})|_{sym} \quad \text{and} \quad \bar{\alpha}_{\varepsilon_{N,max},\hat{\mathcal{H}}}(\tilde{J})|_{nn}$$

the constrained $\varepsilon_{N,max}$-pseudoabscissa with respect to $\hat{\mathcal{H}}$ respectively for the symmetric and for the nonnormal cases, we have that

$$\bar{\alpha}_{\varepsilon_{N,max},\hat{\mathcal{H}}}(\tilde{J})|_{nn} > \bar{\alpha}_{\varepsilon_{N,max},\hat{\mathcal{H}}}(\tilde{J})|_{sym}$$

Therefore, these results are a fair match to our previous results of figures 5.9 and we can say that we have found a satisfying explanation to the new phenomenon of Turing-like pattern formation.

However we cannot explain why the we have a modest difference of $\bar{\alpha}_{\varepsilon_{N,max},\hat{\mathcal{H}}}(\tilde{J})$ between case on nonnormal network and that on symmetric network (figures 6.6), if compared to the difference regarding Turing-like patterns (figures 5.9). In fact, in the symmetric case we observe that $\bar{\alpha}_{\varepsilon_{N,max},\hat{\mathcal{H}}}(\tilde{J}) > 0$ significantly above the Turing bifurcation curve, but we never observe Turing-like patterns for low values of the parameters, unlike the case on nonnormal network. Considering that the initial perturbation is expanded on the Laplacian's eigenvectors, different interactions between the nonlinearities of the model and the Laplacian's eigenvectors could explain such different behaviors between the symmetric and the nonnormal case. However, the method exposed in this section, despite a slight overestimation of the perturbed spectrum for what concerns the symmetric case, gives a reasonable mathematical explanation of nonnormality-driven Turing-like patterns.
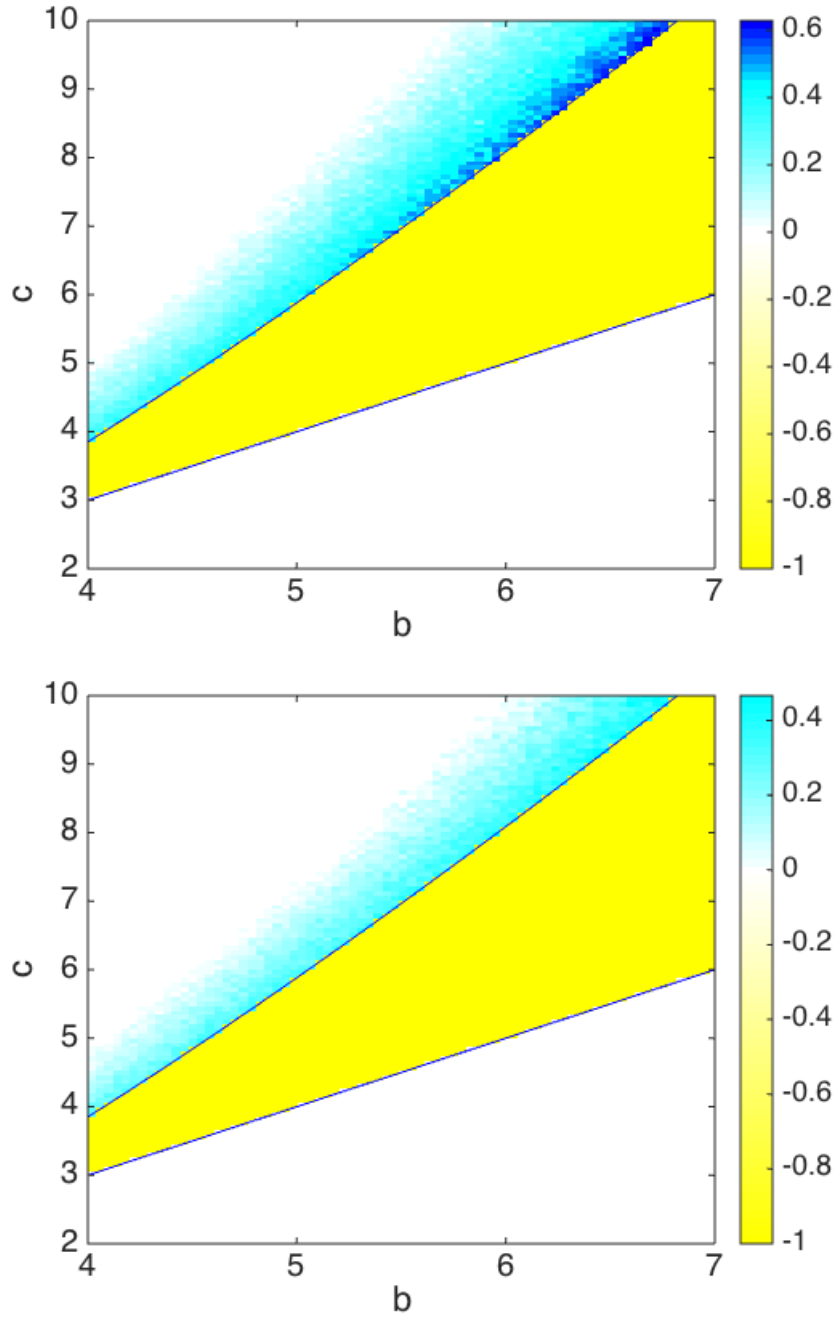
Figure 6.6: Constrained $\varepsilon_{N,max}$-pseudoabscissa for the Brussellator on a nonnormal network of 10 nodes (up) with $\gamma = 15$, $p_1 = 0.5$ and $p_2 = 0.2$ and for a symmetric network (down) of 10 nodes; the cyan-shaded areas are those where the constrained ε-pseudoascissa is positive; the part in blu (figure up) is what we gain thanks to the nonnormal network; $D_\varphi = 0.1$, $D_\psi = 0.385$; $\varepsilon = 0.1$; we display, for every point, the maximum value of $\bar{\alpha}_{\varepsilon_{N,max},\hat{\mathcal{H}}}(\tilde{J})$ over $N = 100$ iterations; $\max_{(b,c)}\{\bar{\alpha}_{\varepsilon_{N,max},\hat{\mathcal{H}}}(\tilde{J})|_{nn}\} = 0.6028$ and $\max_{(b,c)}\{\bar{\alpha}_{\varepsilon_{N,max},\hat{\mathcal{H}}}(\tilde{J})|_{sym}\} = 0.4434$.

Conclusions and Future Perspectives

In this thesis, we have introduced a new mechanism for pattern formation going beyond Turing's ingenious idea of 1952: a reaction-diffusion system of two species in an homogeneous steady state, under certain conditions can become unstable so that patterns arise; such mechanism has been known as Turing instability or Turing pattern formation and patterns obtained in such way are commonly called Turing patterns. We have been able to extend the conditions such that Turing instability emerges. Our conclusions build on three different pillars: classical Turing theory of pattern formation, Turing theory of pattern formation on networks and the theory of nonnormal matrices and operators. Building on these premises, we have studied reaction-diffusion systems on nonnormal networks, that are networks whose adjacency matrix is nonnormal, observing numerically Turing-like patterns.

In the first chapter, we have gone through the basics of Turing instability [Turing 1952], revised in a more "modern" version [Murray 1989] and we have shown some numerical results for the Brussellator model [Nicolis-Prigogine 1977] in the case of an isolated system and assuming an external drift. In the second part, we have explored the theory of pattern formation on discrete support; we have started, in Chapter 2, with the basics of network theory [Newman 2010] to then study Turing pattern formation on symmetric [Nakao-Mikhailov 2010] and asymmetric networks [Asllani et al. 2014] in the third chapter. Then, in Chapter 4, we have introduced the concept of nonnormality [Trefethen-Embree 2005] and its effects on dynamics and Turing pattern formation [Neubert et al. 2002]. In this last part, we have observed Turing-like patterns, but in a way that was already predicted by Neubert and colleagues, though indirectly, and that may be too unrealistic for applications, since the inter-species interactions would have to be strongly asymmetric. Finally, in Chapter 5, by having as a support a nonnormal network, we have been able to find Turing-like patterns for a range of parameters that is possibly more realistic. These findings are explained theoretically by resorting to the concept of pseudospectra, i.e., perturbed spectra, that for nonnormal matrices and operators are more sensible to spectral perturbations, if compared to their normal analogous, as we have discussed in Chapter 6. Since it has been discovered that networks in Nature tend to be nonnormal [Asllani-Carletti 2018b], this last fact may line up with the observations; as we have stated in the Introduction, there are way more patterns in Nature as compared to what theoretical predictions would allow, therefore, we need new mechanisms of pattern formation and less restrictive conditions for systems to yield patterns. That was the aim of our work and the results point straight in that

direction.

Our results are solid: we have detected a new mechanism of pattern formation whose cause lies in the nonnormality of the network. Due to our detailed numerical investigation, we can exclude numerical errors; in fact, the simulations performed in the symmetric case have been our *control test*. We have discussed, in Chapter 6, that, despite the fact that the analysis relying on the constrained pseudospectrum proved adequate, it may still be arduous to predict in advance weather we will have or not Turing-like patterns, since we are dealing with nonlinear phenomena. Furthermore, at present, we do not comprehend why on a symmetric support we do not observe Turing-like patterns, even for significant values of the constrained pseudoabscissa, until the numerical abscissa takes a certain value. Such issues will be object of a further analysis; in fact, a natural continuation of our work would be to extend the statistical study of the Turing region enlargement due to Turing-like patterns on various nonnormal networks and for different ranges of the model's parameters, to compute the respective constrained pseudoabscissae and to compare the results with their symmetric analogous. We prospect that such detailed research would bring deeper insights on Turing-like pattern formation.

Moreover it would be interesting to study this new mechanism of pattern formation related to other models known to exhibit Turing instability, like the Lotka-Volterra model, which might have applications in ecology such as the solution to the plankton paradox, or the Fitzhug-Nagumo model, which may have interests in neuroscience [Murray 1989]. Another interesting study that could be done, would be to investigate the dynamics on "real" networks, such as food webs or metabolic networks: in fact, by observing the patterns, one could understand *a posteriori* the role of nonnormality.

The field is new and the subject fresh; there are many open questions and lines of research that could be taken. The theory we have developed could have multiple applications, for example in neuroscience and ecology, as already discussed, but also in epidemics, cybersecurity, transport management, electric grids and the spreading of fake news. We believe that this study has brought a new light on Turing's work and that nonnormality-driven dynamics will be an intriguing domain of research in the next few years.

Turing's seminal work on morphogenesis, after more than 60 years, is still a milestone for every study on pattern formation that goes from applied mathematics to developmental biology. Alan Turing, the man and the scientist, has been an inspiration for many generations of scientists and will be for many yet to come.

Appendix A: Reaction-Diffusion Equations

Reaction-diffusion processes describe the dynamics of transport and interaction of populations, i.e., ensembles of elementary homologous constituents, represented by concentration, a function of time and space. The aim of this short appendix is to obtain the equations that describe such processes starting from a microscopic framework. In the first section we will reach the form of a reaction-diffusion equation, while in the second we will study a diffusion process where the probability of diffusing depends on the direction; such process will lead to a diffusion equation with drift. The references are [Biancalani 2009] for the first paragraph and [Di Patti et al. 2016] for the second paragraph.

Reaction-Diffusion Equation

Let us start retrieving the famous **law of mass action**, enunciated for the first time by Waage and Guldberg in 1864. Such chemical law refers to nonspatial systems, e.g. a homogeneous chemical solution.

Law of Mass Action   *The rate of a chemical reaction is directly proportional to the molecular concentrations of the reacting substances.*

In formulas, given the concentration of a species (chemical, ecological, etc) in time, i.e., the number of individuals in a volume, we have

$$\frac{d}{dt}\varphi(t) = f(\varphi(t))$$

where $f(\varphi(t))$ is the function describing the reaction dynamics.

The law of mass action assumes that each individual can interact with all the others of the same species, but in realistic situations this could never happen, being that the interactions only local. So let us introduce explicitly the space, i.e., $\varphi = \varphi(\underline{x}, t)$, where $\underline{x} \in \Omega \subseteq \mathbb{R}^n$ and $\Omega \neq \emptyset$ is an open subset of $\mathbb{R}^n$.

Let us work in $\mathbb{R}^3$ and consider a volume $V \subseteq \mathbb{R}^3$ bounded by an orientable closed surface Σ whose external normal is $\hat{n}$; from the **continuity equation** with obtain

$$\frac{\partial}{\partial t} \int_V \varphi(\underline{x}, t) dV = - \int_\Sigma \hat{n} \cdot \underline{J} d\sigma + \int_V f(\varphi(\underline{x}, t)) dV$$

where

$$\frac{\partial}{\partial t} \int_V \varphi(\underline{x}, t) dV$$

stands for the variation of the concentration inside the volume V;

$$- \int_\Sigma \hat{n} \cdot \underline{J} d\sigma$$

is the transport term, i.e., tells what comes in or out the volume V passing through the surface Σ;

$$\int_V f(\varphi(\underline{x}, t)) dV$$

is the *source* term, i.e., gives the rate at which particles are produced or extinct due to the reaction.

Let us observe that the vector representing the current $\underline{J}$ is what gives us the effects of transport, i.e., spatial diffusion.

Let us assume that all the functions involved are as regular as necessary to apply the exchange between integral and differential operators; using the *Divergence Theorem*, the above equation becomes

$$\int_V \left[\frac{\partial}{\partial t} \varphi(\underline{x}, t) + \underline{\nabla} \cdot \underline{J} - f(\varphi(\underline{x}, t)) \right] dV = 0$$

Now, the volume being arbitrary, such equation is valid also locally, i.e.,

$$\frac{\partial}{\partial t} \varphi(\underline{x}, t) = -\underline{\nabla} \cdot \underline{J} + f(\varphi(\underline{x}, t)) \tag{a1}$$

To complete the model we need an explicit expression for the current $\underline{J}$. We serve this purpose applying **Fick's Law of Diffusion**

$$\underline{J} = -D_\varphi \underline{\nabla} \varphi(\underline{x}, t) \tag{a2}$$

where D_φ is a nonnegative magnitude giving the diffusing ability of species φ, i.e., the *diffusion coefficient* ($[D] = [m^2/s]$).

Substituting (a2) into (a1) we obtain

$$\frac{\partial}{\partial t} \varphi(\underline{x}, t) = f(\varphi(\underline{x}, t)) + D_\varphi \nabla^2 \varphi(\underline{x}, t) \tag{a3}$$

which is the equation describing a reaction-diffusion process, like those studied throughout this work.

Diffusion Equation with Drift

Let us start by considering a diffusion process in a one dimensional lattice with periodic boundary conditions. To be able to describe what happens at a microscopic scale, let us "discretize" the lattice so as to have an undirected ring-network of

$n >> 1$ nodes.

The diffusion process is then described by the following equation

$$\dot{\varphi}_i = \sum_{j=1}^{n} L_{ij}\varphi_j \quad , \quad \forall i \in \{1, ..., n\} \tag{a4}$$

where $L_{ij} = A_{ij} - \delta_{ij}k_i$ is the discrete Laplacian operator defined in Chapter 2 and $\varphi(x,t)$ the concentration of the diffusing particles.

Giving the probabilities for a particle to diffuse "left" or "right", i.e.,

- a is the probability of jumping from i-th node to $(i+1)$-th node,

- b is the probability of jumping from i-th node to $(i-1)$-th node,

with the constraint that $a + b = 1$, the discrete Laplacian L results in a tridiagonal Toeplitz matrix whose entrances are

$$\begin{cases} L_{i,i} = -(a+b) \\ L_{i,i+1} = b \\ L_{i,i-1} = a \end{cases}$$

In the hypothesis of isotropic space, i.e., $a = b = \frac{1}{2}$, equation (a4) becomes

$$\dot{\varphi}_i = \frac{1}{2}\{\varphi_{i+1} + \varphi_{i-1} - 2\varphi_i\} = \frac{\Delta x^2}{2}\left\{\frac{\varphi_{i+1} + \varphi_{i-1} - 2\varphi_i}{\Delta x^2}\right\}$$

where Δx is the length of the discretization.

Performing the continuum limit $\Delta x \to 0$, we obtain

$$\frac{\partial}{\partial t}\varphi(x,t) = D\frac{\partial^2}{\partial x^2}\varphi(x,t) \tag{a5}$$

that is the one dimensional continuous diffusion equation[3].

Now let us consider the case of anisotropic space, i.e., $a \neq b$. Physically this situation can arise when there is something external to the the system that affects the diffusion, e.g. an external uniform electric field. In such case, equation (a4) becomes

$$\begin{aligned} \dot{\varphi}_i &= a\varphi_{i-1} + b\varphi_{i+1} - (a+b)\varphi_i = a\varphi_{i-1} + b\varphi_{i+1} - \varphi_i + \frac{b}{2}\varphi_{i-1} - \frac{b}{2}\varphi_{i-1} + \frac{a}{2}\varphi_{i+1} - \frac{a}{2}\varphi_{i+1} = \\ &= \frac{1}{2}(a+b)\varphi_{i-1} - \varphi_i + \frac{1}{2}(a+b)\varphi_{i+1} + \frac{1}{2}(a-b)\varphi_{i-1} + \frac{1}{2}(b-a)\varphi_{i+1} = \\ &= \frac{1}{2}(\varphi_{i-1} - 2\varphi_i + \varphi_{i+1}) + \frac{1}{2}(a-b)(\varphi_{i-1} - \varphi_{i+1}) = \\ &= \frac{\Delta x^2}{2}\left\{\frac{\varphi_{i-1} - 2\varphi_i + \varphi_{i+1}}{\Delta x^2}\right\} + \frac{\Delta x}{2}(b-a)\left\{\frac{\varphi_{i+1} - \varphi_{i-1}}{\Delta x}\right\} \end{aligned}$$

---

[3]Formally, to obtain D we should make explicit the probability over time of jumping to the adjacent node, namely $\delta = D\Delta x^2$; however a formal derivation of such equation, goes beyond the aim of this work and can be found in [Baracca 1980].

where again Δx is the discretization.

Let us point out that $|b - a|$ is the difference of boost between the left and the right side; let us observe that, in the setting of one dimensional lattice with periodic boundary conditions, it does not matter the sign of the boost but only its magnitude, as demonstrated in the first chapter.

Again, if we perform the continuum limit on the above equation, it becomes

$$\frac{\partial}{\partial t}\varphi(x,t) = D\frac{\partial^2}{\partial x^2}\varphi(x,t) + v\frac{\partial}{\partial x}\varphi(x,t) \tag{a6}$$

that is a diffusion equation with drift. If we add to qquation (a6) a reaction term, i.e., a linear function f describing the reaction, we obtain a reaction-diffusion equation like those studied in Chapter 1

$$\frac{\partial}{\partial t}\varphi(x,t) = f(\varphi(x,t)) + D_\varphi\frac{\partial^2}{\partial x^2}\varphi(x,t) + v_\varphi\frac{\partial}{\partial x}\varphi(x,t) \tag{a7}$$

Appendix B: Linear Stability Analysis

The stability of linear systems is very important, because, as we will see at the end of this appendix, nonlinear systems, which are the ones interesting for applications, are "locally" linear. We will follow the approach of [Strogatz 1994].

Linear Systems

Let $A \in \mathbb{R}^{2 \times 2}$ be a matrix with constant coefficients and $\underline{x} = \begin{bmatrix} x \\ y \end{bmatrix} \in \mathbb{R}^2$ be a vector and let us consider the following system of equations

$$\begin{cases} \underline{\dot{x}}(t) = A\underline{x}(t) \\ \underline{x}(0) = \underline{x}_0 \end{cases} \tag{b1}$$

The general solution is of the form

$$\underline{x}(t) = c_1 e^{\lambda_1 t} \underline{v}_1 + c_2 e^{\lambda_2 t} \underline{v}_2$$

where c_1, $c_2 \in \mathbb{R}$ are constants set by the initial conditions, λ_1, $\lambda_2 \in \mathbb{C}$ are A's eigenvalues and $\underline{v}_1$, $\underline{v}_2 \in \mathbb{R}^2$ are A's eigenvectors.

Definition A point $\underline{x}^* = (x^*, y^*) \in \mathbb{R}^2$ is a **fixed point** (or *critical point*) for the system (b1), where A is a nonsingular matrix, if $A\underline{x}^* = \underline{0}$.

Remark Since $\underline{\dot{x}} = \underline{0}$ when $\underline{x} = \underline{0}$, $\underline{x}^* = \underline{0}$ is always a fixed point for the system (b1).

The system being linear, we can predict its behavior, i.e., the stability of its fixed points, just by its eigenvalues. Before going into details, let us define what we mean by *stability*.

Definition Let $\underline{x}(t)$ be a solution of the system (b1) and $\underline{\hat{x}}$ a fixed point. Such fixed point will be

- **stable** (or *Lyapunov stable*) if $\forall \; \varepsilon > 0 \; \exists \; \delta(\epsilon, t)$ s.t. if $||\underline{x}(0) - \underline{\hat{x}}|| < \delta$ then $||\underline{x}(t) - \underline{\hat{x}}|| < \varepsilon \; \forall \; t > 0$;

- **asymptotically stable** if $\lim_{t \to +\infty} ||\underline{x}(t) - \underline{\hat{x}}|| = 0$;
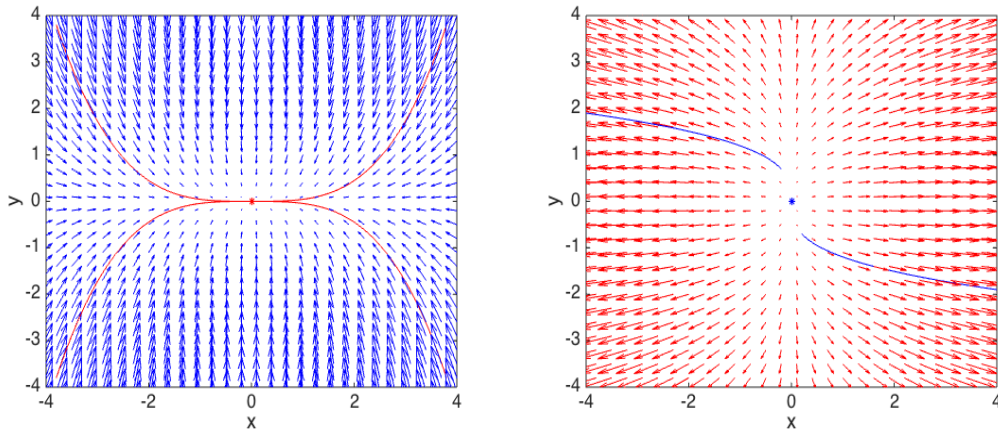
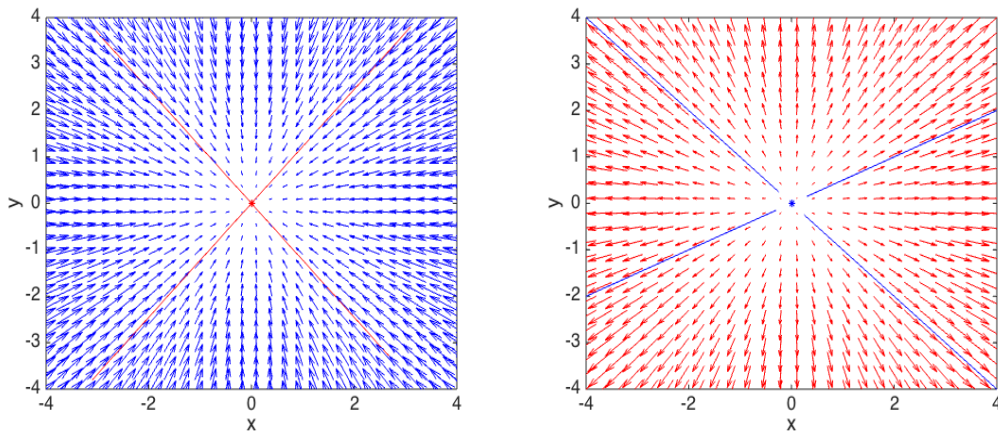**Figure B1:** Stable (blue) and unstable (red) nodes.

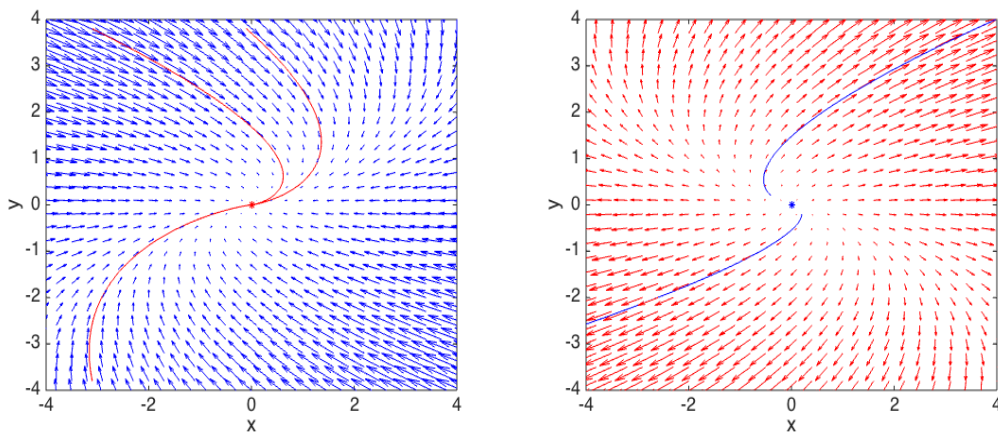**Figure B2:** Stable (blue) and unstable (red) star nodes.

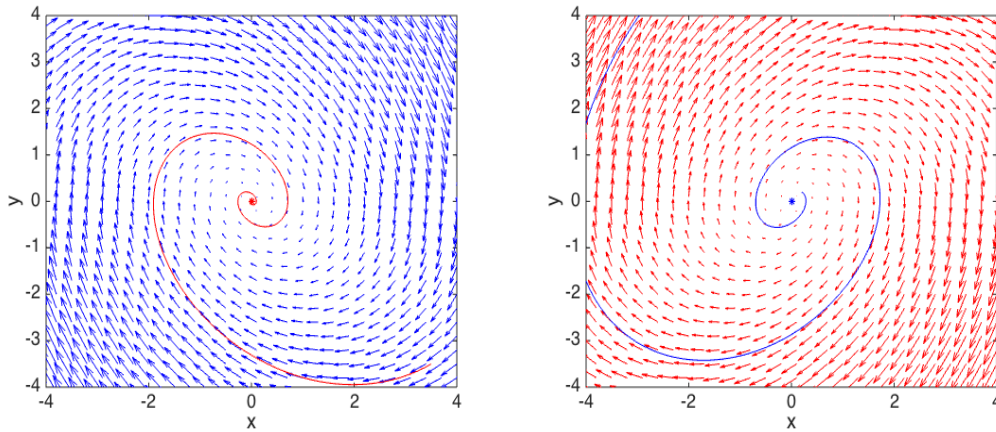

Figure B3: Stable (blue) and unstable (red) degenerate nodes.

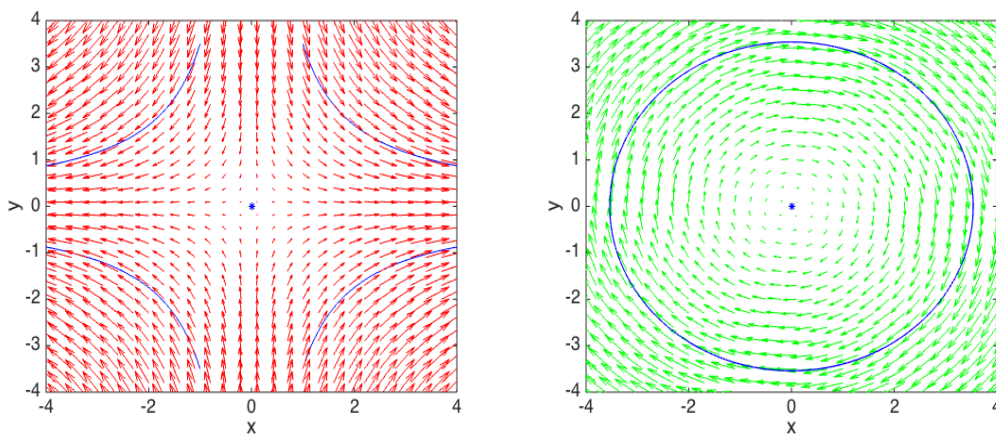**Figure B4:** Stable (blue) and unstable (red) spirals.
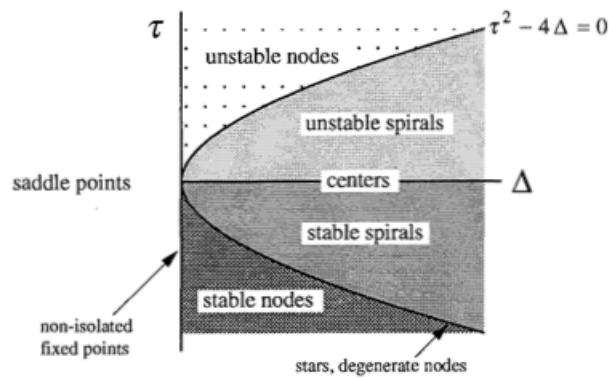

Figure B5: Saddle (red) and center (green).

Figure B6: Stability analysis using the sign of the trace and the determinant, $\tau = trA$ and $\Delta = detA$, from [Strogatz 1994].

- **unstable** otherwise.

Now we can proceed with the stability analysis based on the eigenvalues:

- $\lambda_1, \lambda_2 \in \mathbb{R} \;\wedge\; \lambda_1 \neq \lambda_2 \;\wedge\; \lambda_1\lambda_2 > 0$: If both eigenvalues are negative we have a **stable node**, while if they are positive we have an **unstable node** (figures B1);

- $\lambda_1, \lambda_2 \in \mathbb{R} \;\wedge\; \lambda_1 \neq \lambda_2 \;\wedge\; \lambda_1\lambda_2 < 0$: In this case we have a **saddle point** (figure B5 on the left);

- $\lambda_1, \lambda_2 \in \mathbb{R} \;\wedge\; \lambda_1 = \lambda_2$: If A is diagonalizable we have a **star node**, stable or unstable depending on the eigenvalues' sign, while if A is only Jordanizable we have a **degenerate node**, stable or unstable depending on the eigenvalues' sign (figures B2 and B3);

- $\lambda_1, \lambda_2 \in \mathbb{C} \;\wedge\; \lambda_1 = \bar{\lambda}_2$: In this case we have a **spiral**, stable if the real part of the eigenvalues is negative, unstable if it is negative (figures B4);

- $\lambda_1, \lambda_2 \in \mathbb{C} \;\wedge\; \Re(\lambda_1) = \Re(\lambda_2) = 0$: In this case we have a **center** and it is the only case which is stable but not asymptotically stable (figure B5 on the right).

For a 2×2 matrix the eigenvalues are computed using the trace and determinant solving the following equation

$$\lambda^2 - trA\lambda + detA = 0$$

so the behavior of the system can be studied also using the signs of such magnitudes, as summarized in figure B6, where $\tau = trA$ and $\Delta = detA$.

Nonlinear Systems

The previous discussion can fit also for nonlinear systems. Such systems are extremely difficult to study and characterize, but, fortunately, they exhibit a linear behavior sufficiently close to a fixed point.

Thus let us take a system

$$\begin{cases} \dot{x}(t) = \zeta(x,y) \\ \dot{y}(t) = \xi(x,y) \end{cases} \tag{b2}$$

where $\zeta(x,y)$ e $\xi(x,y)$ are nonlinear functions of x and y and let us assume that such system has at least one fixed point (x^*, y^*), i.e.,

$$(x^*, y^*) \text{ t.c. } \zeta(x^*, y^*) = \xi(x^*, y^*) \equiv 0$$

Then let us perturb the system close to its fixed point with two *small* scalars $\varrho(x,t)$ and $\sigma(x,t)$ that are spatially inhomogeneous. If $\varrho, \sigma << 1$ we can perform a Taylor expansion halting at first order

$$
\begin{cases} x = x^* + \varrho \\ y = y^* + \sigma \end{cases} \Rightarrow \begin{cases} \dfrac{\partial}{\partial t}\varrho \simeq \zeta(x^*, y^*) + \dfrac{\partial \zeta}{\partial x}\big|_{(x^*,y^*)}\varrho + \dfrac{\partial \zeta}{\partial y}\big|_{(x^*,y^*)}\sigma \\ \\ \dfrac{\partial}{\partial t}\sigma \simeq \xi(x^*, y^*) + \dfrac{\partial \xi}{\partial x}\big|_{(x^*,y^*)}\varrho + \dfrac{\partial \xi}{\partial y}\big|_{(x^*,y^*)}\sigma \end{cases}
$$

Notation From now on we will indicate ζ and ξ in the fixed point with the following notation:

$$
\begin{cases} \zeta_x = \dfrac{\partial \zeta}{\partial x}\bigg|_{(x,y)=(x^*,y^*)} \\ \\ \zeta_y = \dfrac{\partial \zeta}{\partial y}\bigg|_{(x,y)=(x^*,y^*)} \\ \\ \xi_x = \dfrac{\partial \xi}{\partial x}\bigg|_{(x,y)=(x^*,y^*)} \\ \\ \xi_y = \dfrac{\partial \xi}{\partial y}\bigg|_{(x,y)=(x^*,y^*)} \end{cases}
$$

Hence, the system (b2) becomes

$$
\begin{cases} \dfrac{\partial}{\partial t}\varrho = \zeta_x \varrho + \zeta_y \sigma \\ \\ \dfrac{\partial}{\partial t}\sigma = \xi_x \varrho + \xi_y \sigma \end{cases}
$$

In a compact form, that can be written as:

$$
\underline{\dot{\mu}} = J\underline{\mu} \quad \text{where} \quad \underline{\mu} = \begin{bmatrix} \varrho \\ \sigma \end{bmatrix} \quad \text{and} \quad J = \begin{bmatrix} \zeta_x & \zeta_y \\ \xi_x & \xi_y \end{bmatrix}
$$

where J is the Jacobian matrix. Such system is obviously linear.

Therefore, our nonlinear system (b2) is *locally linear* sufficiently close to its fixed point and it is possible to study and characterize its local behavior by looking at the eigenvalues of J, as in the previous section. This process of *linearization* is valid as long as the fixed point is **hyperbolic**[4], as stated by the *Hartman-Grobman Theorem*, which gives the conditions s.t. systems (b1) and (b2) are *topologically equivalent*, i.e., they have the same qualitative structure near the origin [Perko 2001].

---

[4]This excludes the center among the possible phase portraits, but this is not a problem, the center being stable but not asymptotically stable, hence not interesting for the dynamical processes studied throughout our work.

Appendix C: Some Details on the Numerical Simulations

In this brief appendix we give some details on the numerical simulations on the software MATLAB® that we have performed during this work: we explicit the nonnormal network used in Chapter 5 and give the details of the inhomogeneous perturbation of the fixed point.

Nonnormal Networks Used

In Section 5.1 we have described an algorithm to generate nonnormal networks [Asllani-Carletti 2018a]. Then in Sections 5.2 we have performed some numerical simulations using often a nonnormal network of 10 nodes and its symmetrizations. To obtain such network we have used the algorithm with $\gamma = 15$, $p_1 = 0.5$ and $p_2 = 0.2$; its adjacency is the following

$$
A = \begin{bmatrix}
0 & 0.2415 & 0.4156 & 0.8358 & 0 & 0.8733 & 0 & 0 & 0.9855 & 0 \\
0.5785 & 0 & 6.6650 & 0.2479 & 0 & 0 & 0 & 0 & 0 & 0 \\
0 & 0.8535 & 0 & 5.1432 & 0 & 0 & 0.4903 & 0 & 0 & 0.9120 \\
0 & 0 & 0 & 0 & 0.4582 & 0 & 0 & 0 & 0 & 0.3795 \\
0 & 0 & 0 & 0 & 0 & 4.8264 & 0 & 0 & 0 & 0 \\
0 & 0 & 0 & 0 & 0.4485 & 0 & 6.5822 & 0 & 0 & 0.8792 \\
0 & 0 & 0 & 0.6203 & 0 & 0.5235 & 0 & 10.463 & 0 & 0 \\
0 & 0 & 0 & 0 & 0 & 0 & 0 & 0 & 14.914 & 0 \\
0 & 0 & 0 & 0.7953 & 0 & 0 & 0.0438 & 0 & 0 & 6.2093 \\
0.4606 & 0 & 0 & 0 & 0 & 0 & 0 & 0 & 0.0429 & 0
\end{bmatrix}
$$

and its *nonnormality* is $\omega(A) - \alpha(A) = 5.24$. Its symmetrization

$$
\tilde{A} = \frac{A + A^*}{2}
$$

is

$$
\tilde{A} =
\begin{bmatrix}
0 & 16.892 & 0.2254 & 0 & 0 & 0.4317 & 0 & 0 & 0 & 8.7342 \\
16.892 & 0 & 0.8159 & 0 & 0 & 0.1386 & 0.0118 & 0 & 0 & 0.0739 \\
0.2254 & 0.8159 & 0 & 15.357 & 0 & 0.2486 & 0.0064 & 0 & 0 & 0 \\
0 & 0 & 15.357 & 0 & 16.4394 & 0 & 0 & 0 & 0 & 0 \\
0 & 0 & 0 & 16.4394 & 0 & 19.774 & 0 & 0.4833 & 0 & 0 \\
0.4317 & 0.1386 & 0.2486 & 0 & 19.774 & 0 & 19.498 & 0 & 0 & 0 \\
0 & 0.0118 & 0.0064 & 0 & 0 & 19.498 & 0 & 0.2051 & 0.3940 & 0 \\
0 & 0 & 0 & 0 & 0.4833 & 0 & 0.2051 & 0 & 4.7607 & 0 \\
0 & 0 & 0 & 0 & 0 & 0 & 0.3940 & 4.7607 & 0 & 17.497 \\
8.7342 & 0.0739 & 0 & 0 & 0 & 0 & 0 & 0 & 17.497 & 0
\end{bmatrix}
$$

Perturbation of the Homogeneous Fixed Point

As we have discussed throughout this work, a system in a stable homogeneous equilibrium undergoes Turing instability under certain conditions if the homogeneous fixed point is perturbed inhomogeneously. In listings $C1$ we show how we perturbed such fixed point for the simulations of Chapters 1 and 4 (continuum support), while listings $C2$ and $C3$ are for the simulations of Chapters 3, 4 and 5 (networks).

Listing C1: Inhomogeneous perturbation of the fixed point on continuum support

```
rng('shuffle')
for i = 1:(nx+1)
phi(i,1) = phiStar+pert*2*(rand(1)-0.5);
psi(i,1) = psiStar+pert*2*(rand(1)-0.5);
end
```

Listing C2: Inhomogeneous perturbation of the fixed point on network

```
rng('shuffle')
for i=1:nodes
phi(i,1)=phiStar+pert*2*(rand(1)-0.5);
psi(i,1)=psiStar+pert*2*(rand(1)-0.5);
end
```

Listing C3: Inhomogeneous perturbation of the fixed point on network (compact form)

```
rng('shuffle')
phi0=phiStar*ones(1,nodes)+pert*2*(rand(1,nodes)-0.5*ones(1,
    nodes));
psi0=psiStar*ones(1,nodes)+pert*2*(rand(1,nodes)-0.5*ones(1,
    nodes));
```

- *phiStar* and *psiStar* are the fixed points of the Brussellator model $\varphi^* = 1$ and $\psi^* = b/c$;

- *nx* is the spatial grid and *nodes* is the number of nodes of the network;

- *pert* is the magnitude of the perturbation, that in general we have set to 0.1;

- *rand(1)* is a function that generates random numbers between 0 and 1 uniformly distributed;

- *rng('shuffle')* controls the generation of random numbers, so that the series of random number is different every time.

Appendix D: Nonnormal and Balanced Networks

In Chapters 4 and 5 we have shown a new mechanism of pattern formation, through which we obtain patterns outside the Turing region as an effect of the nonnormality within the extended Jacobian $\tilde{J}$. If the support is symmetric, e.g., a network that is not a regular lattice, we obtain Turing-like patterns only for significant values of $\omega(\tilde{J})$ ($\simeq 10$), i.e., for high values of the model's parameter, meaning that we have very asymmetric inter-species interactions; on the other hand if the support is a nonnormal network we find Turing-like patterns also for low values of the parameters and this is the main result of this thesis. However nonnormal networks suitable for applications are unbalanced, i.e., $k_i^{in} \neq k_i^{out} \; \forall \; i$ node, meaning that to develop our theory we must use, instead of the discrete Laplacian $L_{ij} = A_{ij} - k_i^{out}\delta_{ij}$, a *diffusion-like* operator $\mathcal{L} = A_{ji} - k_i^{out}\delta_{ij}$ [Asllani et al. 2014], as we have discussed in details at the end of Chapter 2.

The aim of this appendix is to show that the Turing-like patterns obtained in Chapter 5 do not depend on the diffusion operator. In order to do so, we have designed an algorithm to generate networks that are nonnormal but balanced. The networks that come from such algorithm have no use in applications, since they are unrealistic; however they allow us to develop out theory using the Laplacian L instead of $\mathcal{L}$ and see that we obtain Turing-like patterns.

Let us now describe the algorithm to generate a nonnormal and balanced network:

- we fix the number of nodes n;

- we connect node 1 to node 2 with a directed link of weight $n-1$, then we connect node 2 to node 3 with a directed link of weight $n-2$ and so on, until we connect node $n-1$ to node n with a directed link of weight 1 and do the same for node n to node 1; we have obtained a directed close ring with decreasing weights, except for the last two links whose weights are 1;

- finally we connect from node 2 to $n-1$, each to node 1 with directed links of weight 1.

In figure D1 we show an example with $n = 10$ and in figure D2 we show that the nonnormality grows with the number of nodes.
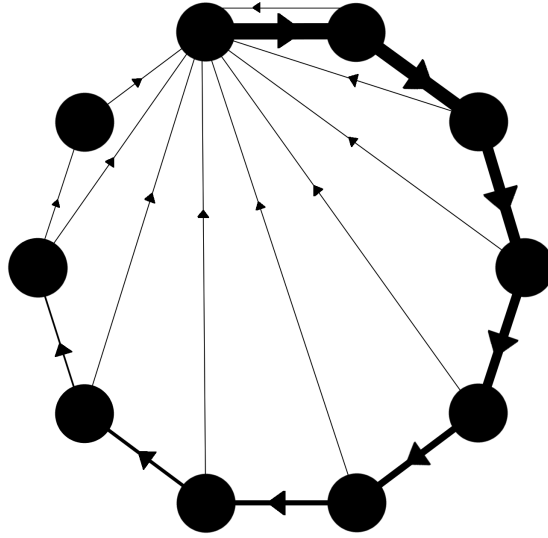
116

Figure D1: Network that is nonnormal but balanced, obtained with the algorithm described in the text; 10 nodes, $\omega - \alpha = 0.501$.

In figures D3 and D4 we show the Turing-like patterns and the dispersion relation for the Brussellator model; we can observe that the dispersion relation is all negative, hence, as for the case studied in Chapter 5, the patterns are due to the nonnormality of the network.
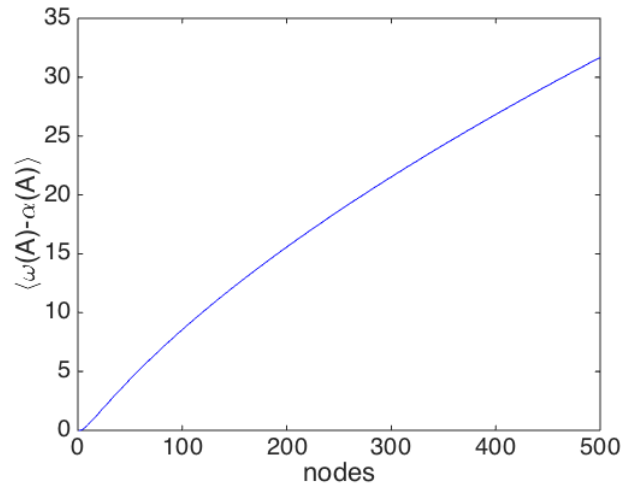

Figure D2: $\omega - \alpha$ of the nonnormal balanced network, function of the nodes; we can observe that the nonnormality increases as the number of nodes does so.
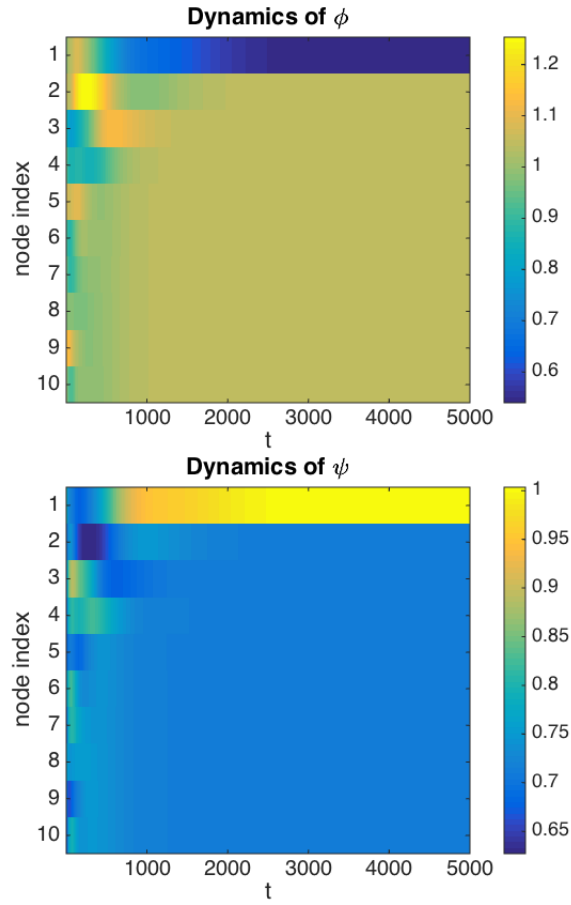
Figure D3: Turing-like patterns for the Brussellator model on a nonnormal balanced network of 10 nodes; $b = 5.9$, $c = 8$, $D_\varphi = 0.1$, $D_\psi = 0.385$ and $\varepsilon = 0.1$.

Figure D4: Dispersion relation for the Brussellator model on a nonnormal balanced network of 10 nodes; $b = 5.9$, $c = 8$, $D_\varphi = 0.1$, $D_\psi = 0.385$ and $\varepsilon = 0.1$.
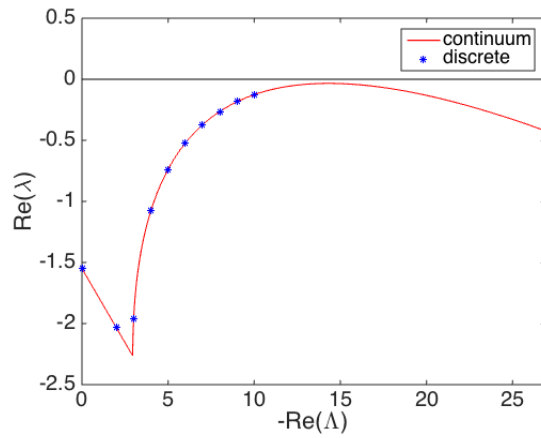
Bibliography

- [*Asllani* 2015] Asllani M., *"Reaction-Diffusion Models on a Network: Stochastic and Deterministic Pattern Formation"*, PhD Thesis in Applied Mathematics, Supervisor: Prof. Duccio Fanelli, Università degli studi dell'Insubria (2015);

- [*Asllani − Carletti* 2018a] Asllani M. & Carletti T., *"Topological Resilience in Non-Normal Networked Systems"*, Physical Review E (2018);

- [*Asllani − Carletti* 2018b] Asllani M. & Carletti T., *"Universality of Non-Normality in Real Complex Networks"*, arXiv:1803.11542 (2018);

- [*Asllani et al.* 2014] Asllani M., Challenger J., Pavone F. S., Sacconi L. & Fanelli D., *"Topology-Driven Instability: the Theory of Pattern Formation on Directed Networks"*, Nature Communication (2014);

- [*Baracca* 1980] Baracca A., *"Manuale critico di meccanica statistica"*, CULC (1980);

- [*Barletti* 2013] Barletti L., *"Appunti del corso Metodi Matematici per le Applicazioni"*, class notes, Università degli Studi di Firenze (2013);

- [*Bellone* 2004] Bellone E., *"Caos e Armonia. Storia della Fisica"*, UTET (2004);

- [*Biancalani* 2009] Biancalani Tommaso, *"Instabilità di Turing nei modelli stocastici di popolazioni"*, Master Thesis in Physics and Astrophysics, Supervisor: Prof. Duccio Fanelli, Università degli studi di Firenze (2009);

- [*Biancalani et al.* 2010] Biancalani T., Fanelli D. & Di Patti F., *"Stochastic Turing Patterns in the Brussellator Model"*, Physical Review E (2010);

- [*Biancalani et al.* 2017] Biancalani T., Jafarpour F. & Goldenfeld N., *"Giant Amplification of Noise Fluctuation-Induced Pattern Formation"*, Physical Review Letters (2017);

- [*Boland et al.* 2008] Boland R. P., Galla T. & McKane A. J., *"How Limit Cycles and Quasi-Cycles are Related in a System with Intrinsic Noise"*, Journal of Statistical Mechanics (2008);

- [*Boncinelli* 2012] Boncinelli E., *"La Scienza non ha Bisogno di Dio"*, Mondadori (2012);

- [*Bransden − Joachain* 2000] Bransden B. H. & Jaochain C. J., *"Quantum Mechanics (Second Edition)"*, Pearson (2000);

- [*Bressloff et al.* 2002] Bressloff P. C., Cowan J. D., Golubitsky M., Thomas P. J., & Wiener M. C., *"What Geometric Visual Hallucinations Tell Us about the Visual Cortex"*, Neural Computation (2002);

- [*Broido − Clauset* 2018] Broido A. D. & Clauset A., *"Scale-free Networks are Rare"*, arXiv:1801.03400 (2018);

- [*Buchanan* 2003] Buchanan M., *"Nexus: Small Worlds and the Groundbreaking Theory of Networks"*, W. W. Norton (2003);

- [*Burioni et al.* 2014] Burioni R., Casartelli M., Di Volo M., Livi R. & Vezzani A., *"Average Synaptic Activity and Neural Networks Topology: a Global Inverse Problem"*, Scientific Reports (2014);

- [*Caldarelli − Catanzaro* 2012] Caldarelli G. & Catanzaro M., *"Networks: A Very Short Introduction"*, Oxford University Press (2012);

- [*Casolo − Fumagalli* 2016] Casolo C. & Fumagalli F., *"Corso di Teoria dei Grafi e Combinatoria"*, class notes, Università degli Studi di Firenze (2016);

- [*Castets et al.* 1990] Castets V., Dulos E., Boissonade J. & De Kepper P., *"Experimental Evidence of a Sustained Standing Turing-Type Nonequilibrium Chemical Pattern"*, Physical Review Letters (1990);

- [*Conn et al.* 2000] Conn A. R., Gould N. I. M. & Toint P. L., *"Trust Region Methods"*, SIAM (2000);

- [*Davis* 1994] Davis P. J., *"Circulant Matrices: Second Edition"*, American Mathematical Society (1994);

- [*Debnath − Mikusinski* 2005] Debnath L. & Mikusinski P., *"Introduction to Hilbert Spaces with Applications (Third Edition)"*, Pearson (2005);

- [*Di Patti et al.* 2016] Di Patti F., Fanelli D. & Carletti T., *"Drift-Induced Benjamin-Feir Instabilities"*, European Physics Journal (2016);

- [*Dulos et al.* 1996] Dulos E., Boissonade J., Perraud J. J., Rudovics B. & De Kepper P., *"Chemical morphogenesis: Turing patterns in an experimental chemical system"*, Acta Biotheoretica (1996);

- [*Economou et al.* 2012] Economou A. D., Ohazama A, Porntaveetus T., Sharpe P. T., Kondo S., Basson M. A., Gritli-Linde A., Cobourne M. T. & Green J. B. A., *"Periodic Stripe Formation by a Turing Mechanism Operating at Growth Zones in the Mammalian Palate"*, Nature Genetics (2012);

- [*Elsner − Ikramov* 1998] Elsner L. & Ikramov K. D., *"Normal Matrices: an Update"*, Linear Algebra and its Applications (1998);

- [*Erdős − Rényi* 1959] Erdős P. & Rényi A., *"On Random Graphs"*, Publicationes Mathematicae (1959);

- [*Fusco et al.* 1996] Fusco N., Marcellini P. & Sbordone C., *"Analisi Matematica 2"*, Liguori (1996);

- [*Gilbert* 1959] Gilbert E. N., *"Random Graphs"*, Annals of Mathematical Statistics (1959);

- [*Girotto et al.* 2008] Girotto V., Pievani T. & Vallordigara G., *"Nati per Credere. Perché il Nostro Cervello Sembra Predisposto a Fraintendere la Teoria di Darwin"*, Codice (2008);

- [*Golub − Van Loan* 1996] Golub G. H. & Van Loan C. F., *"Matrix Computation"*, Johns Hopkins University Press (1996);

- [*Grätzer* 2011] Grätzer G, *"Lattice Theory: Foundation"*, Birkhäuser (2011);

- [*Groone et al.* 1987] Grone R., Johnson C. R., Sa E. M. & Wolkowicz H., *"Normal Matrices"*, Linear Algebra and its Applications (1987);

- [*Hardin* 1960], Hardin G., *"The Competitive Exclusion Principle"*, Science (1960);

- [*Helbing* 2009] Helbing D., *"Pattern formation, social forces, and diffusion instability in games with success-driven motion"*, European Physics Journal B (2009);

- [*Hodges* 1983] Hodges A., *"Alan Turing: the enigma"*, Walker & Company (1983);

- [*Horn − Johnson* 1985] Horn R. A. & Johnson C. R., *"Matrix Analysis"*, Cambridge University (1985);

- [*Hutchinson* 1961] Hutchinson G. E., *"The Paradox of the Plankton"*, The American Naturalist (1961);

- [*Kandel et al.* 2012] Kandel E. R., Schwartz J. & Jessel T., *"Principles of neural science"*, McGraw-Hilll Education (2012);

- [*Koch − Meinhardt* 1994] Koch A. & Meinhardt H., *"Bioogical Pattern Formation: from Basic Mechanisms to Complex Structures"*, Review of Modern Physics (1994);

- [*Kondo − Miura* 2010] Kondo S. & Miura T., *"Reaction-Diffusion Model as a Framework for Understanding Biological Pattern Formation"*, Science (2010);

- [*Lengyel − Epstein* 1992] Lengyel I. & Epstein I. R., *"A chemical approach to designing Turing patterns in reaction-diffusion systems"*, Proceeding of the National Academy of Sciences (1992);

- [*Lengyel − Epstein* 1993] Lengyel I. & Epstein I. R., *"Turing Structures in Simple Chemical Reactions"*, Accounts of Chemical Research (1993);

- [*López − Muolo* 2016] López R. C. & Muolo R., *"Estudio de la Reacción de Belousov-Zhabotinsky"*, Lab Report from the cours "Biofísica" (Biophysics) at Universidad de Granada, supervised by Professor M. J. Gálvez (2016);

- [*Macdonald−Ruuth* 2009] Macdonald C. B & Ruuth S. J., *"The Implicit Closest Point Method for the Numerical Solution of Partial Differential Equations on Surfaces"*, SIAM Journal of Scientific Computing (2009);

- [*Magnus − Winkler* 1966] Magnus W. & Winkler S., *"Hill's Equations"*, Interscience Publishers (1966);

- [*Maini et al.* 2012] Maini P. K., Woolley T. E., Baker R. E., Gaffney E. A. & Lee S. S., *"Turing's Model for Biological Pattern Formation and the Robustness Problem"*, Interfaces Focus (2012);

- [*Mattuck et al.* 2011] Mattuck A., Miller H., Orloff J. & Lewis J. *"18.03SC Differential Equations. Fall 2011. Massachusetts Institute of Technology: MIT OpenCourseWare"*, ocw.mit.edu (2011);

- [*Murray* 1988] Murray J. D., *"How the Leopard Gets its Spots"*, Scientific American (1988);

- [*Murray* 1989] Murray J. D., *"Mathematical Biology (Second Edition)"*, Springer (1989);

- [*Nakao − Mikhailov* 2010] Nakao H. & Mikhailov A., *"Turing Patterns in Network Organized Activator Inhibitor Systems"*, Nature Physics 1651 (2010);

- [*Neubert − Caswell* 1997] Neubert M. G. & Caswell H., *"Alternative to Resilience for Measuring the Responses of Ecological Systems to Perturbations"*, Ecology (1997);

- [*Neubert et al.* 2002] Neubert M. G., Caswell H. & Murray J. D., *"Transient Dynamics and Pattern Formation: Reactivity is Necessary for Turing Instabilities"*, Mathematical Biosciences (2002);

- [*Newman* 2010] Newman M., *"Networks. An introduction"*, Oxford University Press (2010);

- [*Nicolis − Prigogine* 1977] Nicolis G. & Prigogine I., *"Self-Organization in Nonequilibrium Systems: from Dissipative Structures to Order Through Fluctuations"*, Wiley (1977);

- [*Othmer − Scriven* 1971] Othmer H. & Scriven L., *"Instability and Dynamic Patterns in Cellular Networks"*, Journal of Theoretical Biology, 43:83–112 (1971);

- [*Pecora − Carroll* 1998] Pecora L. M. & Carroll T. L., *"Master Stability Functions for Synchronized Coupled Systems"*, Physical Review Letters (1998);

- [*Perko* 2001] Perko L., *"Differential Equations and Dynamical Systems (Third ed.)"*, Springer (2001);

- [*Plaza et al.* 2004] Plaza R. G., Sánchez-Garuño F., Padilla P., Barrio R. A & Maini P. K., *"The Effect of Growth and Curvature on Pattern Formation"*, Journal of Dynamics and Differential Equations (2004);

- [*Press et al.* 1986] Press W. H., Flannery B. P., Teukolsky S. A. & Vetterling W. T., *"Numerical Recipes: The Art of Scientific Computing"*, Cambridge University Press (1986);

- [*Prigogine − Lefever* 1968] Prigogine I. & Lefever R., *"Symmetry Breaking Instabilities in Dissipative Systems. II"*, Journal of Chemical Physics (1968);

- [*Prigogine − Nicolis* 1967] Prigogine I. & Nicolis G., *"Symmetry Breaking Instabilities in Dissipative Systems"*, Journal of Chemical Physics (1967);

- [*Ridolfi et al.* 2011] Ridolfi L., Camporeale C., D'Odorico P. & Laio F., *"Transient Growth Induces Unexpected Spatial Patterns in the Turing Process"*, European Physics Journal (2011);

- [*Rovinsky − Menzinger* 1992] Rovinsky A. B. & Menzinger M., *"Chemical Instability Induced by a Differential Flow"*, Physical Review Letters (1992);

- [*Rovinsky−Menzinger* 1993] Rovinsky A. B. & Menzinger M., *"Self-Organization Induced by Differential Flow of Activator and Inhibitor"*, Physical Review Letters (1993);

- [*Schrödinger* 1944] Schrödinger E., *"What is Life?"*, Cambridge University Press (1944);

- [*Strogatz* 1994] Strogatz S., *"Non Linear Dynamics and Chaos"*, Perseus Books (1994);

- [*Trefethen−Embree* 2005] Trefethen L. N. & Embree M., *"Spectra and Pseudospectra: The Behavior of Nonnormal Matrices and Operators"*, Princeton University Press (2005);

- [*Trefethen et al.* 1993] Trefethen L. N., Trefethen A. E., Reddy S. C. & Driscoll T. A., *"Hydrodynamic Stability Without Eigenvalues"*, Science (1993);

- [*Turing* 1952] Turing A., *"The Chemical Basis of Morphogenesis"*, Philosophical Transactions of the Royal Society of London. Series B, Biological Sciences, Vol. 237, No. 641 (1952);

- [*Varea et al.* 1999] Varea C., Aragón J. L. & Barrio R. A., *"Turing Patterns on a Sphere"*, Physical Review E (1999);

- [*Varga* 2004] Varga R. S., *"Geršgorin and His Circles"*, Springer-Verlag (2004);

- [*Watts − Strogatz* 1998] Watts D. & Strogatz S., *"Collective dynamics of Small-World networks"*, Nature (1998);

- [*Wilson* 1996] Wilson R., *"Introduction to Graph Theory"*, Prentice Hall (1996);

- [*Woolley et al.* 2017] Woolley T. E., Baker R. E. & Maini P. K., *"Turing's Theory of Morphogenesis: Where We Started, Where We Are and Where We Want to Go"*, in "S.B. Cooper, M.I. Soskova (eds.), The Incomputable", Springer (2017);

- [*Wright* 2002] Wright T. G., *"EigTool"*, MATLAB® ToolBox (2002);

- [*Yang et al.* 2017] Yang Y., Nishikawa T. & Motter A. E., *"Small vulnerable sets determine large network cascades in power grids"*, Science (2017);

- [*Zhabotinsky et al.* 1995] Zhabotinsky A. M., Dolnik M. & Epstein I. R., *"Pattern Formation Arising Wave Instability in a Simple Reaction-Diffusion System"*, Journal of Chemical Physics (1995).